

A STUDY OF SOLIDIFICATION IN AN ENCLOSED REGION WITH NATURAL CONVECTION IN THE MELT

**A Thesis Submitted
in Partial Fulfilment of the Requirements
for the Degree of
DOCTOR OF PHILOSOPHY**

**By
N. RAMACHANDRAN**

**to the
DEPARTMENT OF CHEMICAL ENGINEERING
INDIAN INSTITUTE OF TECHNOLOGY, KANPUR**

MARCH, 1981

CHE-2221-D-RAM-STU

I. I. T. KANPUR
CENTRAL LIBRARY

Acc. No. A 70660

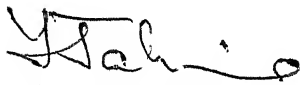
15 MAY 1982

To

Periya Mama & Mami

CERTIFICATE

This is to certify that the work presented in this thesis entitled, 'A STUDY OF SOLIDIFICATION IN AN ENCLOSED REGION WITH NATURAL CONVECTION IN THE MELT' has been carried out by Mr. N. Ramachandran under our supervision and the same has not been submitted elsewhere for a degree.



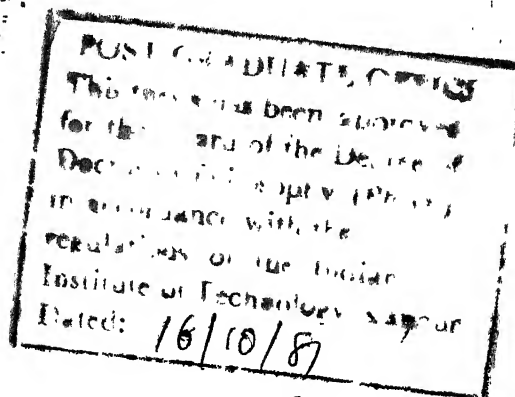
Y. JALURIA
Assistant Professor
Department of Mechanical
Engineering
Indian Institute of Technology
Kanpur-208016, India



J.P. GUPTA
Assistant Professor
Department of Chemical
Engineering
Indian Institute of Technology
Kanpur-208016, India

Date:

Date:




ACKNOWLEDGEMENTS

I am most indebted to my advisors Dr. Y. Jaluria and Dr. J.P. Gupta for recognizing a viable dissertation topic, leading ~~me over~~ many trouble spots, gently prodding me on, and spending hours critiquing and correcting a vast number of drafts.

I also thank Dr. S.M.Aeron, Dr.S.C. Mehta, Professor S.K. Gupta and Dr.G. Mukherjee of R and D Centre, SAIL, Ranchi, for providing useful comments and encouraging me at every stage of this work. I would like to thank Dr.D.P.Rao for allowing me to work in the Data Acquisition System.

My special thanks go to Shankar, Somu, Arun and Anmi for many fruitful discussions and help at various stages of this work.

I would like to acknowledge with deep gratitude the cooperation and help I have received from Messers P.N.Sharma and P.N. Mishra in the laboratory.

I would also like to thank the members of the Poopers' Club who gave me a wonderful time in my athletic endeavours which enabled me to keep my academic pursuits in proper perspective.

I would like to thank Mr. B.S. Pandey for his efficient typing, Mr.D.K. Mishra for his excellent drawings, Mr. Hari Ram for neat cyclostyling and Mr. Jai Ballabh for good ammonia printing.

This work has been carried out through the sponsorship given by my employers R and D Centre for Iron and Steel, Steel Authority of India Ltd., Ranchi, India under the 'Technical Scholar Scheme'.

N. RAMACHANDRAN
Author

CONTENTS

	List of Figures	...	ix
	Synopsis	...	xvii
	Nomenclature	...	xxi
CHAPTER			
1	INTRODUCTION	...	1
2	LITERATURE SURVEY	...	4
	2.1 Conduction-Based Solutions		4
	2.1.1 Analytical solution		4
	2.1.2 Nonanalytical solutions		5
	2.1.3 Treatment of the mold		7
	2.1.4 Heat transfer from the mold to ambient	...	7
	2.2 Thermal Convection	...	8
	2.2.1 Convection without solidi- fication	...	9
	2.2.2 Solidification with convection		9
	2.3 Experiments	...	11
3	ANALYSIS OF SOLIDIFICATION IN ONE DIRECTIONAL VERTICAL SLOT AND CIRCULAR CYLINDER	...	13
	3.1 Introduction	...	13
	3.2 Analysis	...	15
	3.2.1 Assumptions	...	15
	3.2.2 Governing equations		18
	3.2.3 Energy equations		18
	3.2.4 Momentum equation		20
	3.2.5 Continuity equation		21
	3.2.6 Non-dimensionalization		22

3.3	Solution Methodology ...	26
3.3.1	Explicit scheme	28
3.3.2	Implicit scheme	28
3.4	Vertical Cylinder ...	30
3.5	Results and Discussion	31
3.5.1	Temperature profile	31
3.5.2	Velocity profile	34
3.5.3	Effect of melt velocity	36
3.5.4	Effect of Prandtl number	37
3.5.5	Effect of Stefan number	37
3.5.6	Effect of superheat	40
3.5.7	Effect of Biot number, radiation constants	40
3.5.8	Comparison with previous work ...	40
3.6	Concluding Remarks ...	44
4	TWO DIMENSIONAL SOLIDIFICATION INSIDE A RECTANGULAR ENCLOSURE ...	45
4.1	Introduction ...	45
4.2	Formulation ...	47
4.2.1	Boundary conditions	47
4.2.2	Assumptions ...	49
4.2.3	Governing equations	49
4.2.4	Non-dimensionalization	54
4.3	Solution Methodology ...	59
4.3.1	Vorticity and energy equations ...	60
4.3.2	Stream function equation	61
4.3.3	Vorticities at boundaries	62
4.3.4	Moving boundary equation	63
4.3.5	Choice of grid system	63
4.3.6	Computational steps	65

	4.4 Results and Discussion ...	68
	4.4.1 Thermal and fluid flow in melt-without solidification	68
	4.4.2 Thermal and fluid flow in melt-with solidification, top and bottom of the enclosure adiabatic, mold wall at a constant temperature	73
	4.4.3 Thermal and fluid flow in melt-with solidification, top and bottom surface adiabatic, and, convection and radiation at the mold outer surfaces	87
	4.4.4 Thermal and fluid flow in melt-with solidification, bottom surface adiabatic, and, convection and radiation at the top surface and the mold outer surfaces ...	89
	4.5 Conclusion ...	105
5	EXPERIMENTS ...	107
	5.1 Introduction ...	107
	5.2 Experimental Apparatus ...	109
	5.2.1 Test cell for one dimensional case ...	109
	5.2.2 Test cell for two dimensional case ...	111
	5.2.3 Temperature measurements	112
	5.3 Experimental Procedure ...	114
	5.4 Results ...	116
	5.4.1 Two dimensional experiments	116
	5.4.2 One dimensional case	127
	5.5 Conclusion ...	134
6	CONCLUSIONS AND RECOMMENDATIONS	135
	6.1 Summary and Conclusions	135
	6.2 Recommendations ...	139

	REFERENCES	...	143
APPENDIX			
I	SIMPLIFICATION OF MOMENTUM EQUATION		148
II	RADIATIVE BOUNDARY CONDITION		150
III	PROPERTIES OF STEEL	...	151
IV	MOVING BOUNDARY EQUATION	...	152
V	COORDINATE TRANSFORMATION	...	154
VI	SECOND UPWIND DIFFERENCING METHOD		158
VII	ADI ALGORITHM FOR VORTICITY EQUATION		159
VIII	PROPERTIES OF WAX	...	161

LIST OF FIGURES

FIGURE		Page
3.1	Vertical parallel plates and circular cylinder infinite in x-direction	16
3.2	Temperature distribution in the three regions for the boundary condition of first kind ($Pr=0.15$; $Ste=5.0$; $\phi=0.5$ and $Gr=3000$) ...	32
3.3	Temperature distribution in the three regions, for the boundary condition of third kind ($Pr=0.15$; $Ste=5.0$; $\phi=0.5$; $Bi_1=2.0$ and $Gr=3000$) ...	33
3.4	Vertical velocity distribution in the melt for the boundary condition of first kind ($Pr=0.15$; $Ste=5.0$; $\phi=0.5$ and $Gr=3000$) ...	35
3.5	Dependence of interface location on the Prandtl number for the boundary condition of third kind ($Pr=0.15$ to 15.0 ; $Ste=1.0$; $\phi=0.7$ and $Bi_1=2.0$)	38
3.6	Dependence of interface movement on Stefan number for the boundary condition of third kind for vertical parallel plates ($Ste=1.0$ to 80.0 ; $Pr=0.5$; $\phi=0.7$ and $Bi_1=2.0$) ...	39
3.7	Dependence of interface movement on the Biot number and the superheat for parallel plates ($Bi_1=0.02-2.0$; $\phi=0.25$ to 1.0 ; $Pr=0.15$ and $Ste=1.0$)	41

3.8	Dependence of interface movement on the Radiation constant for parallel plates ($Rc_1=0.05-10$; $\phi=0.5$; $Pr=0.15$ and $Ste = 1.0$) ...	42
3.9	Comparison of the thickness of the solid formed with time, with literature ...	43
4.1	Rectangular enclosure infinite in z-direction ...	48
4.2	(a) Cartesian grid system (b) Grid system for present work ...	64
4.3	Flow chart for the computation cycle	67
4.4	Streamlines and isotherms for different Rayleigh numbers at $t^* = 0.027$ - Without solidification, top and bottom surfaces adiabatic, sides at a constant temperature ($Ra = 10^3$, 10^6 and 10^8)	70
4.5	Streamlines and isotherms for different Rayleigh numbers at $t^* = 0.027$ -Without solidification, bottom surface adiabatic, top surface convecting and radiating, sides at a constant temperature ($Ra = 10^3$ and 10^6) ...	71
4.6	Comparison of the streamlines of present work with literature -without solidification ...	72
4.7	Temperature distributions in the three regions, at different x^* , for constant temperature at the outer surface of the mold and adiabatic at top and bottom of the enclosure ($Ra=5 \times 10^3$; $Pr=0.98$; $Ste=0.5$ and $\phi=1.0$)	74

FIGURE		Page
4.8	Vertical velocity distribution in the melt at different x^* ($Ra=5 \times 10^3$; $Pr=0.98$; $Ste=0.5$ and $\phi=1.0$)	75
4.9	Streamline pattern in the melt for $Ra=5 \times 10^3$ and $t^*=0.27$, for constant temperature at the mold surface, adiabatic at top and bottom of the enclosure ($Pr=0.98$; $Ste=0.5$ and $\phi=1.0$)	77
4.10	Isotherm pattern in the melt for $Ra=5 \times 10^3$ and $t^*=0.27$, for constant temperature at mold outer surface, adiabatic at top and bottom of the enclosure ($Pr=0.98$; $Ste=0.5$ and $\phi=1.0$)	79
4.11	Streamline pattern in the melt for $Ra=5 \times 10^5$ and $t^*=0.03$ for constant temperature at mold surface, adiabatic at top and bottom of the enclosure ($Pr=0.98$; $Ste=0.5$ and $\phi=1.0$)	80
4.12	Dependence of the interface movement on Rayleigh number at different time, for constant temperature at mold surface, adiabatic at top and bottom of the enclosure ($Ra=5 \times 10^2$, 5×10^3 and 5×10^5 ; $Pr=0.98$; $Ste=0.5$ and $\phi=1.0$)	81
4.13	Interface movement at various time intervals, for L/D ratios of 2.0 and 10.0, for constant temperature at the mold surface, adiabatic at the top and bottom of the enclosure ($L/2Y_0=1.1$ and 5.5 ; $Ra=5 \times 10^3$; $Pr=0.98$; $Ste=0.5$ and $\phi=1.0$)	82

FIGURE

Page

- 4.14 Dependence of interface movement on Prandtl number at different time, for constant temperature at the mold surface, adiabatic at top and bottom of the enclosure
($Pr=0.1, 10$ and 100 ; $Ra=5 \times 10^3$; $Ste=0.50$ and $\phi=1.0$) ... 84
- 4.15 Dependence of interface movement on Stefan number at various time intervals, for constant temperature at the mold surface, adiabatic at top and bottom of the enclosure
($Ste=0.5, 5.0$ and 1.0 ; $Ra=5 \times 10^3$; $Pr=0.98$ and $\phi=1.0$) ... 85
- 4.16 The effect of superheat on solid formed, for constant temperature at the mold surface, adiabatic at top and bottom of the enclosure
($\phi=0.67$ and 2.33 ; $Ra=5 \times 10^3$; $Pr=0.98$ and $Ste=0.5$) ... 86
- 4.17 Temperature profiles at the center line of the enclosure and mold outer surfaces at different times - Top and bottom of the enclosure adiabatic, mold surface convecting and radiating
($Ra=10^3$; $Bi_1=1.0$; $Re_1=0.01$; $Pr=1.0$; $Ste=0.5$ and $\phi=1.0$) ... 88
- 4.18 Velocity profiles at the center line of the enclosure for different times - Top and bottom surfaces adiabatic, mold surface convecting and radiating
($Ra=1 \times 10^3$; $Bi_1=1.0$; $Re_1=0.01$; $Pr=1.0$; $Ste=0.5$ and $\phi=1.0$) ... 90

FIGURE

Page

- 4.19 Dependence of interface movement on Biot number and Radiation constant - Top and bottom surfaces adiabatic, mold surface convecting and radiating ($Bi_1=5$ to 100 ; $Re_1=5$ to 5000 ; $Ra=1 \times 10^3$; $Pr=1.0$; $Stc=0.5$ and $\phi=1.0$) ... 91
- 4.20 Dependence of interface movement on Rayleigh number at different times - Bottom surface adiabatic, top surface and mold outer surfaces convecting and radiating ($Ra=10^3$, 10^4 and 10^5 ; $Pr=0.01$; $Stc=0.5$; $Bi_1=1.0$; $Re_1=0.01$ and $\phi=1.0$) 93
- 4.21 Variation of interface heat transfer rate with time for different Rayleigh numbers ($Ra=10^2$, 10^3 , 10^4 , 10^5 and 10^6) 95
- 4.22 Dependence of interface movement on Radiation constant at different times - Bottom surface adiabatic, top surface and mold surface convecting and radiating ($Re_1=1.0$ and 5.0 ; $Ra=10^4$; $Pr=0.01$; $Stc=0.5$ and $\phi=1.0$) ... 97
- 4.23 Dependence of interface movement on Biot number at different times - Top surface and mold outer surfaces convecting and radiating, bottom surface adiabatic ($Bi_1=0.5$ and 2.0 ; $Ra=10^3$, $Pr=1.0$; $Stc=0.5$ and $\phi=1.0$) ... 98

FIGURE

Page

4.24	Streamline pattern for $Ra=1 \times 10^4$ and $t^*=0.06$ - Bottom surface adiabatic, top surface and mold outer surfaces convecting and radiating ($Pr=1.0$; $Bi_1=1.0$ and $Re_1=0.01$)	99
4.25	Streamline pattern for $Ra=1 \times 10^4$ and $t^*=0.30$ - Bottom surface adiabatic, top surface and mold outer surfaces convecting and radiating ($Pr=1.0$; $Bi_1=1.0$ and $Re_1=0.01$)	100
4.26	Streamline pattern for $Ra=1 \times 10^5$ and $t^*=0.06$ - Bottom surface adiabatic, top surface and mold outer surfaces convecting and radiating ($Pr=1.0$; $Re_1=0.01$ and $Bi_1=1.0$)	101
4.27	Isotherm pattern in melt for $Ra=1 \times 10^4$ and $t^*=0.06$ - Bottom surface adiabatic top surface and mold outer surfaces convecting and radiating ($Pr=1.0$; $Re_1=0.01$ and $Bi_1=1.0$)	103
4.28	Isotherm pattern in melt for $Ra=1 \times 10^5$ and $t^*=0.06$ - Bottom surface adiabatic, top surface and mold outer surfaces convecting and radiating ($Pr=1.0$; $Bi_1=1.0$ and $Re_1=0.01$)	104
5.1	Diagrammatic sketch of the apparatus	110
5.2	(a) Photograph of the experimental set up (b) Photograph of thermo-couple assembly ...	113
5.3	Variation of temperature with time for initial temperature 72°C and height $=3.5\text{cm}$	117

FIGURE

Page

5.4	Variation of temperature with time for initial temperature 82°C and height 3.5cm	...	118
5.5	Variation of temperature with time for initial temperature 90°C and height 3.5 cm	...	119
5.6	Variation of solid thickness with time for initial temperature 72°C and height 3.5 cm	...	121
5.7	Variation of solid thickness with time for initial temperature 82°C and height 3.5 cm	...	122
5.8	Variation of solid thickness with time for initial temperature 90°C and height 3.5 cm	...	123
5.9	Variation of temperature with time for initial temperature 84°C and height 5 cm	...	124
5.10	Variation of temperature with time for initial temperature 84°C and height 6 cm	...	125
5.11	Variation of solid thickness with time for initial temperature 84°C and heights 5 cm and 6 cm	...	126
5.12	Variation of temperature with time for one dimensional case, initial tempera- ture of wax 65°C	...	128
5.13	Variation of temperature with time for one dimensional case, initial temperature 70°C	...	129

FIGURE		Page
5.14	Variation of temperature with time for one dimensional case, initial temperature 77°C ...	130
5.15	Variation of solid thickness with time for one dimensional case, initial temperature 65°C ...	131
5.16	Variation of solid thickness with time for one dimensional case, initial temperature 70°C ...	132
5.17	Variation of solid thickness with time for one dimensional case, initial temperature 77°C ...	133

SYNOPSIS

Heat conduction problems with phase change have been studied extensively for over a century. These problems are encountered in a wide range of situations, encompassing such diverse applications as casting of metals and alloys, storage of thermal energy, spacecraft thermal design, drying of foodstuffs etc. In modern foundry technology, the prediction of the solidification rate and the temperature distribution during the solidification process is very important, in order to control the fundamental parameters, such as stripping time for static casting and withdrawal rates for continuous casting, as well as the incidence of casting defects. A series of analytical solutions have been reported in the literature, starting with the well known Neumann solution. Most of the investigators have so far, considered only conduction in the melt, neglecting the natural convection effects, which arise due to buoyancy. The study of natural convection in the melt is very important as it may affect the process in the following ways:

- (i) The motion in the melt may modify the heat transfer rate at the melt-solid interface, and hence affect the gross solidification rate.
- (ii) The convective motion in the melt may influence the structure of the solid formed.
- (iii) The distribution of the solutes in the multi-component

system may be affected by the bulk motion in the melt.

(iv) The velocities in the melt would affect the rate at which non-metallic inclusions can float to the surface.

The present work has been divided into three parts:

- (i) Computation of the solidification rate and the temperature and velocity distributions in a one dimensional solidification process.
- (ii) Computation of the flow pattern, solidification rate and the temperature and velocity distributions during solidification in a two dimensional rectangular enclosure.
- (iii) Experimental verification of the analytical results obtained in (i) and (ii).

In the one dimensional problem, equations have been written to study the solidification taking into account the heat transfer in the melt, in the solid formed and in the mold. Analysis has also been carried out to determine the velocity distribution that arises due to thermal gradients. The equations are solved for different boundary conditions, such as constant wall temperature and convective and radiative heat transfer at the outer surface of the mold. Solidification between infinite parallel plates and inside an infinite vertical cylinder have been considered. The temperature and the velocity distributions in the melt are obtained, along with the rate of movement of the solidification

front for various non-dimensional parameters such as the Prandtl number, Biot number, Stefan number etc. The computed results are compared with the results of other investigators for which comparison could be made.

In the second part, the natural convection arising due to the thermal gradients during solidification in a rectangular enclosure has been studied. The two dimensional equations have been solved, initially without considering the solidification as a check on the numerical scheme and later, including the solidification. For the melt region equations for the conservation of mass, momentum and energy are written. These equations, coupled with the energy transfer equations for the solid region and the mold through the boundary conditions at the melt-solid and solid-mold interface, are solved simultaneously for different boundary conditions. The boundary conditions considered are:

- (i) The top and the bottom surfaces of the enclosure are adiabatic, whereas the outer surfaces of the mold are kept at a constant temperature.
- (ii) The top and the bottom surfaces of the enclosure are adiabatic while the outer surfaces of the mold exchange energy by convection and radiation.
- (iii) The top surface and the mold outer surfaces exchange energy by convection and radiation,

the bottom surface of the enclosure
being kept adiabatic.

The non-linear, coupled equations are non-dimensionalized and solved numerically using the Alternating Direction Implicit Technique. The results are computed for various dimensionless parameters, such as Rayleigh number, Prandtl number, Stefan number, aspect ratios, Biot number etc. For these boundary conditions, the temperature profiles, the velocity profiles and the rate of interface movement are obtained.

Experiments were carried out, using paraffin wax as the solidifying material. The experimental arrangement consists of a rectangular Plexiglas tank with two aluminium plates inserted vertically, thus dividing it in three compartments. The molten paraffin wax is poured into the central compartment while the end compartments are used for circulating water at a constant temperature. The temperature of the paraffin wax is monitored by thermocouples, the output of which has been recorded by a Hewlett Packard Data Acquisition System. The thermocouples are prepositioned at given horizontal and vertical locations. From the temperature vs time plot, the position of the interface at various time intervals is found. The experiments are conducted for different aspect ratios, and superheat of wax. The results are then compared with the theory.

NOMENCLATURE

Bi_1	Biot number at the mold outer surface = $h_1 d/k_m$;
Bi_2	Biot number at the top surface of the enclosure = $h_2 L/k_1$;
C_p	specific heat [J/Kg °K];
d	thickness of the mold [m];
d_p	diameter of non-metallic inclusions [m];
D	width of the enclosure [m];
f	vertical velocity of the melt when $Gr=1$, [m/s];
h_1	heat transfer coefficient at the mold outer surface [J/s m ² °K];
h_2	heat transfer coefficient at the top surface of the enclosure [J/s m ² °K];
g	gravitation constant [9.8 m/s ²];
Gr	Grashof number = $(g\beta(T_i - T_c)Y_o^3 / \nu^2)$;
k	thermal conductivity [J/s m °K]
L	height of the enclosure [m];
L_q	latent heat of solidification [J/Kg];
p	pressure [N/m ²]; p_a hydrostatic pressure [N/m ²];
p_d	dynamic pressure [N/m ²];
Pr	Prandtl number = ν/α ;
Q	heat transferred at the interface [J];
Q_o	superheat present in the melt = $\rho C_p L Y_o (T_i - T_c)$, [J];
r	radial coordinate measured from the center of the cylinder [m];
R_o	inner radius of the vertical cylinder [m];
Ra	Rayleigh number = $Gr.Pr$;
Rc_1	radiation constant at the mold outer surface = $(\epsilon_1 \sigma d(T_i - T_c)^3)/k_m$;

Re_2	radiation constant at the top surface of the enclosure = $(\epsilon_2 \sigma L(T_i - T_c)^3)/k_1$;
Ste	Stefan number = $L_q/C_p(T_i - T_c)$;
t	time [s];
t^*	dimensionless time = $\nu t/Y_0^2$ or $\alpha t/D^2$;
T	temperature [K];
\bar{T}	average temperature in the melt [K];
T_c	mold outer surface temperature or the ambient temperature as the case may be [K];
T_c^*	dimensionless temperature = $T_c/(T_i - T_c)$;
T_i	initial temperature [K];
T_l	temperature in the melt [K];
T_m	temperature in the mold [K];
T_s	temperature in the solid [K];
T_l^*	dimensionless temperature in the melt = $(T_l - T_c)/(T_i - T_c)$;
T_m^*	dimensionless temperature in the mold = $(T_m - T_c)/(T_i - T_c)$;
T_s^*	dimensionless temperature in the solid = $(T_s - T_c)/(T_i - T_c)$;
T_{sat}	solidification temperature [K];
u	velocity in the x-direction [m/s];
u^*	dimensionless velocity in the x direction = $uD^2/\alpha_1 L$;
u_t	terminal rising velocity of non-metallic inclusions [m/s];
v	velocity in the y direction [m/s];
v^*	dimensionless velocity in the y direction = vD/α_1 ;
x	vertical coordinate measured from the bottom of the enclosure [m];

x^*	dimensionless vertical coordinate = x/L ;
y	horizontal coordinate measured from the center of the enclosure [m];
y_l^*	dimensionless horizontal coordinate in the melt = y/Y' ;
y_m^*	dimensionless horizontal coordinate in the mold = $(y-Y_0)/(D-Y_0)$;
y_s^*	dimensionless horizontal coordinate in the solid = $(y-Y')/(Y_0-Y')$;
Y'	half width of the melt region [m];
Y_0	distance from the center line to solid-mold interface [m];
z	coordinate measured from the center of the enclosure [m];

Greek Symbols

α	thermal diffusivity [m^2/s];
β	temperature coefficient of cubical expansion [K^{-1}] ;
δ	relative width of melt region = Y'/Y_0 ;
δ_m	relative width of mold region = D/Y_0 ;
ε_1	emissivity at the mold outer surface;
ε_2	emissivity at the top surface of the enclosure;
μ	coefficient of viscosity [$Kg/m\ s$];
ν	kinematic viscosity = μ/ρ , [m^2/s];
ρ	density [Kg/m^3];
ρ_p	density of non-metallic inclusions [Kg/m^3];
ρ_{sat}	density of the melt at the average temperature [Kg/m^3];

σ	Stefan-Boltzman constant [5.67×10^{-8} J/s m ² K ⁴];
ϕ	dimensionless temperature $=(T_i - T_{\text{sat}})/(T_{\text{sat}} - T_c)$;
ψ	stream function [m ² /s];
ψ^*	dimensionless stream function $= \psi D / \alpha_1 L$;
$\bar{\psi}$	normalized stream function $= \psi / \psi_{\text{max}}$;
ψ_{max}	maximum stream function [m ² /s];
Ω_{opt}	optimum relaxation factor;
ω	vorticity [s ⁻¹]
ω^*	dimensionless vorticity $= \omega D^3 / \alpha_1 L$;

Superscript

k	iteration number;
*	dimensionless quantities;

Subscript

i	grid point in x direction;
j	grid point in y direction;
l	melt;
m	mold;
n	time;
s	solid;
w	boundary;

CHAPTER 1

INTRODUCTION

Many processes involving phase change are encountered in chemical, food and metallurgical industries as well as in the fields of cryobiology and space technology. The applications of solidification or melting include, casting of metals and alloys, the production of chemicals as prills or flakes, the freezing and destruction of tumorous brain tissue, spacecraft thermal design and storage of thermal energy, etc. The prediction of solidification rate and temperature distribution during the solidification process is very important in modern foundry technology in order to control the fundamental parameters such as stripping times for static casting and withdrawal rates of continuous casting, as well as the incidence of casting defects. Furthermore, solidification rate and temperature gradients, in the melt, the solid formed and the mold encompassing them, have a strong influence on the final properties of the cast piece and on the possibility of damage to the mold surface. Solidification rate and temperature gradients, however, are controlled by the direction and the rate at which heat is removed from the melt.

The presence of temperature variations in the melt will, in most cases, produce natural convection currents.

Under these conditions, the conduction problems in the solid and the mold have to be solved simultaneously with the natural convection flow and heat transfer in the melt. Historically, the possible existence of natural convection in the melt has largely gone untreated in the heat transfer literature. Therefore, many of the conduction-based phase change solutions developed by numerous investigators over a century do not fully reflect the physical reality. The inclusion of natural convection in the melt is very important as it affects the process of solidification in the following ways.

- (i) the bulk motion in the melt may modify the rate of heat transfer at the melt-solid interface and hence affect the actual, gross solidification rate.
- (ii) convective motion may influence the structure of the solid formed, in particular the transition from columnar to equiaxed orientation, in case of solidification of metals,
- (iii) convection in the melt would affect the distribution of solutes in the multicomponent systems,
- (iv) velocities in the melt would affect the rate at which non-metallic inclusions

can float to the surface, for ingot casting of metals.

The objective of the present work is to study the thermal and fluid flow fields developed during the solidification, along with the movement of the melt-solid interface in an enclosed region.

A brief review of literature on solidification and fluid flow in enclosed regions is given in Chapter 2. In Chapter 3 the temperature and velocity field developed during the solidification in one dimensional vertical slot and vertical cylinder are discussed. The dependence of solidification rate on various dimensionless parameters is also studied for the one dimensional solidification. In Chapter 4, the two dimensional solidification in rectangular enclosures with the natural convection in the melt has been discussed. Streamline and isotherm patterns are presented along with the position and shape of the interface at various times, for different boundary conditions. The experimental technique, apparatus and procedure are described in Chapter 5. The comparison of the experimental results with the theory is also presented in Chapter 5. The conclusions and recommendations for the future work are given in Chapter 6.

CHAPTER 2

LITERATURE SURVEY

An examination of the literature on phase change reveals no comprehensive or unified treatment of the combined thermal and fluid flow phenomena that occurs during solidification. The phase change problems discussed in the literature can be broadly divided into two categories: (i) Problems in which the conduction in the solid phase alone is considered assuming the melt to be at saturation temperature. (ii) Problems in which the superheat in the melt is considered. This superheat gives rise to buoyancy forces, which in turn produce convective flows.

2.1 CONDUCTION-BASED SOLUTIONS:

2.1.1 Analytical Solutions: Analytical and closed form solutions of the pure conduction problems with solidification have been obtained for a few idealized situations. The simplest case is the solidification of a semi-infinite medium with a constant surface temperature, known as the Stefan's problem. If the heat conducted into the solid alone is considered, the solidification time can be obtained by applying Chvorinov's rule discussed by Cole (1969). Carslaw and Jaeger (1959) have discussed the problem, when both

the solid and the melt are assumed to be semi-infinite, the melt being at a temperature different from the solidification temperature. The solution to the above problem has been developed by Franz Neumann (1912) for the surface of the semi-infinite solid being maintained at a temperature lower than the solidification temperature. Tien (1965) applies the condition, that the surface temperature is time dependent, and suggests that the solidification thickness increases almost linearly with the time whereas the rate of solidification first increases and then decreases in a complicated manner.

2.1.2 Nonanalytical Solutions: There are other methods which are less exact than the Neumann solution, and these generally require the use of a computer. A contour integral approach used by Boley (1964), graphical method suggested by Sarjant and Slack (1954), analog methods, applying electrical analogs to the heat flow, used by Paschkis (1945), and isotherm migration method discussed by Dix and Cizek (1970) are some of the non-analytical methods reported in the literature.

Another approximate but elegant method to solve the conduction problems is proposed by Goodman (1958), employing a heat balance integral technique. In the integral method treated by Hrycak (1963), the Neumann conditions are applied, but with an assumed temperature distribution which is linear

in the solid and parabolic in the melt. The heat flow at the surface of the solid, is removed from the system by convective flow to the ambient fluid. When the integral equation is specified, the equation can be solved using a computer. Hills and Moore (1967) have used the integral method by assuming polynomial series for the temperature and the thickness of the solid formed. A generalized solution for the melting of a semi-infinite solid, initially at the melting temperature and subjected to a non-linear boundary condition at the surface of the solid, has been discussed by Özisik and Mody (1975), by applying the integral method.

While Goodman (1958) restricts the approximation of the temperature distribution inside the solid phase to a cubic polynomial, Megerlin (1968) extends the method to any ordered polynomial and suggests that as the order of the polynomial approximation is increased, the solution asymptotically approaches the exact solution. Sparrow and Shamsunder (1974) have applied Megerlin's technique to the problem of the thermal energy storage in which the heat conduction equation written for the cylindrical coordinate has been solved for the convective boundary condition.

The other scheme which has created considerable interest in solving the heat conduction equation is the numerical techniques. Goodling and Khader (1974) have applied an implicit numerical scheme to solve the inward solidification problem for slabs, cylinders and spheres with a mixed

radiative and convective boundary condition at the outer surface of the solid.

2.1.3 Treatment of the Mold: The previous solutions generally ignore the heat transfer in the mold and in most of the cases, the surface of the solid has always been assumed at some constant temperature. In real systems there is a mold that plays an important role in dissipating the heat to the environment.

In a simple case, the mold is assumed to be thick enough (semi-infinite) that no temperature rise occurs on its external surface, and initially, the mold is kept at a particular temperature. In addition the semi-infinite melt is assumed to be initially at its freezing temperature, thereby neglecting the superheat. A solution for the above mentioned problem has been given by Schwartz (1933) and Ruddle (1957).

2.1.4: Heat Transfer from the Mold to Ambient: Heat transfer from the external surface of the mold determines the rate at which finite castings solidify and this has been treated in several papers. Kosky (1975) has treated this problem using the concept of Biot modulus. Bi is the ratio of the heat transfer coefficient at the surface of the mold to the thermal conductivity at the mold and is, thus, a measure of the relative magnitude of the surface convection and internal conduction resistance to heat transfer. (A low Biot number

implies no internal conduction resistance, so that the temperature is uniform throughout the solid.) Szekely and Ludely (1966) have considered the surface flux as a mixture of convection and radiation from the surface of the solidifying melt. An arbitrary flux at the surface is treated by Hamil and Bankoff (1963), using the integral method. Garcia and Prates (1978) have developed a model for the unidirectional solidification of the metals in the molds cooled by fluids such as air and water. Their model permits the measurement of the Newtonian heat transfer coefficient at the metal/mold interface, and it differs from other analytical models in the sense that it is more general in application and easier to manipulate, while retaining the advantage and convenience over numerical techniques.

2.2 THERMAL CONVECTION:

The movement of a fluid in free convection results from buoyancy forces imposed on the fluid, when its density is increased locally as a result of the cooling process. The two main sources of the convective flow, that can be considered are: (i) the temperature difference between the hot fluid and some colder wall, either the melt-solid interface or, more generally any cold vertical wall immersed in the hot fluid. (ii) the heat loss at the top free surface of the fluid exposed to the environment. Radiation and convection to the ambient will locally cool the melt near

the top surface, and the heavier fluid then moves downward, displacing the warmer fluid below.

2.2.1 Convection without Solidification: Numerous investigators have considered the presence of natural convection of the fluid, in an enclosed region but without solidification. A study of these investigations is helpful to understand the flow pattern that may arise with solidification. Eckert and Carlson (1961) have provided very useful information on the temperature profiles and the circulation pattern developed by an air layer, enclosed between two isothermal vertical plates. Elder (1965) has analysed the temperature and the velocity profiles of the fluid enclosed in a narrow slot and has arrived at the criteria for the establishment of secondary and tertiary flows. The application of the finite-difference numerical techniques has been pioneered by Wilkes and Churchill (1966) who have studied the steady state and transient behaviour of the fluids enclosed in rectangular cavities for various boundary conditions. In a subsequent work Torrence and Rockett (1968) have made the transient analysis for the fluid in a rectangular enclosure heated from below, for high Rayleigh numbers, whereas the work by Elder (1966), De Vahl Davis (1968) and Newell and Schmidt (1970) has concerned with the steady state systems.

2.2.2 Solidification with Convection: Although the natural convection heat transfer and solidification have been

extensively studied individually, their combined occurrence has so far received little attention. Tillier (1962) has recognised the role of convection in the early stage of solidification. Ostrach and Kroger (1974) have considered the role of natural convection in the analysis of the steady state phase change problem associated with continuous casting. Seki, Fukusako and Sugawara (1977) have investigated the effects of the natural convection in the problem of freezing or melting of water in horizontal layers, using linear perturbation technique.

While the works mentioned above represent the effects of fluid motion, the first attempt to study the exact nature of the fluid motion has been made by Szekely and Stanek (1970). They have developed explicit expressions for the temperature and the velocity distribution in the fluid. However, since the relevant energy equation does not contain any velocity terms, the heat transfer process is not affected by buoyancy and conduction is the only transport mechanism. The only investigation which takes into account the role of the natural convection in the energy transport is that of Sparrow, Patankar and Ramadhyani (1977). They have carried out an analysis for the two dimensional melting in a cylindrical enclosure, taking into account the natural convection induced by temperature differences in the melt. Their results decisively differ from those of the earlier conduction solutions.

2.3 EXPERIMENTS:

In addition to the above mentioned investigations, there appears to be a greater awareness in other literature, particularly metallurgy, of the role of natural convection in phase change problems. Experiments have been conducted by many investigators to understand the role of the natural convection in modifying the structure of the solid formed, and distribution of the solute in the multicomponent system. In an experimental study Cole and Bolling (1965) have shown that the structure of the casting can be significantly changed by eliminating the natural convection effects. An attempt to know the quantitative effect of the natural convection has been made by Szekely and Chhabra (1970) who studied the controlled solidification of Lead under conditions of unidirectional heat flow within the system. The observed shape and position of the melt-solid interface agreed reasonably with the predicted results after giving consideration to the heat transferred by natural convection from the melt to the solid. The experiments have been performed for both steady state and transient cases. Sparrow and Ramsey (1978) have conducted experiments to provide definitive information about the heat transfer processes which occur when the solid is melted by a vertical, cylindrical heat source embedded within the solid. The role of natural convection has been studied by taking photographs of the melt-solid interface at various time intervals. Recently Sparrow, Ramsey and

• Kemink (1979) have performed experiments for freezing n-eicosane, a paraffin, under conditions where the melt is either above or at the fusion temperature, the freezing material being housed in a cylindrical containment vessel. Interesting results have been obtained when the melt is superheated, for the boundary conditions considered by the authors. The other experiments intended to clarify the interaction of the natural convection and the phase change in one dimensional geometries are reported by Heertjes, Jongenelen, and de Leeuw den Boutor (1970), and Chiesa and Guthrie (1974).

CHAPTER 3

ANALYSIS OF SOLIDIFICATION IN ONE DIMENSIONAL VERTICAL SLOT AND CIRCULAR CYLINDER

3.1 INTRODUCTION:

The mathematical modelling of the solidification of the melt, in molds of finite dimensions is very complex. The solution of the equations, to understand the thermal and fluid flow phenomena, is complicated since in a multi-dimensional system the thermal and momentum equations are nonlinear and coupled, and have to be solved simultaneously along with the moving boundary equation, as the solidification proceeds. Solidification in one dimensional, vertical, narrow slot (or vertical cylinder) represents the realistic situation, when the height of the mold is very large compared to the width, i.e., molds of very high aspect ratios. Because of the one dimensional approximation, the thermal and the momentum equations are decoupled and conduction is the only mode of heat transfer. Even for such a simplified system analytical closed form solution is not possible as the heat conduction equations for the melt, solid and the mold have to be solved simultaneously along with the moving boundary equation.

In the present chapter, an analysis is carried out to study the transient thermal characteristics of solidification,

accompanied by natural convection flow, in a vertical slot and in a vertical cylinder. The solution is facilitated by suitable coordinate transformations that immobilize the moving interface between the melt and the solid. Consideration has been given to the energy conducted through and stored in the mold, solid and the melt regions. The problem has been studied for various boundary conditions at the mold surface. These are:

- [i] constant wall temperature;
- [ii] convection from the mold to ambient, and
- [iii] radiation from the mold to ambient.

The governing coupled equations for the melt, solid and the mold regions are solved using an implicit, finite-difference scheme to obtain the time dependent temperature and velocity distributions. The effect of various non-dimensional parameters such as Prandtl number, Stefan number, Biot number etc., on the rate of solidification has also been studied. It has been shown that in case of liquid metals, the velocity of the melt that arises due to thermal gradients is sufficient to float up any non-metallic inclusion of dimensions found in practical applications.

Though the analysis has been made for the parallel plates and the circular cylinder, only the parallel plates equations are discussed in detail; however a brief idea about the governing equations for the circular cylinder and their differences from the equations of the parallel plates

have been discussed in section 3.4.

3.2 ANALYSIS:

A schematic diagram of the vertical parallel plates and the circular cylinder is shown in Figure 3.1. The width of the rectangular slot is $2Y_0$ and the inner diameter of the cylinder is $2R_0$. The slot is extended to infinity in both the x and z directions, whereas axisymmetry is assumed for the circular cylinder which is extended to infinity in the x -direction. The thickness of the mold is d . At time $t=0$, the mold is kept at a temperature T_c , the ambient temperature. At this time, melt at an initial temperature T_i is poured into the mold. As a result, thermal gradients are set up and a thin crust of solid is formed at the inner surface of the mold. An inward movement of the melt-solid interface also starts. The transient temperature profile developed in the melt changes the local density of the melt giving rise to buoyancy forces, which in turn cause natural convection in the melt.

3.2.1 Assumptions: The following assumptions are made for the analysis:

[1] The physical properties such as thermal conductivity, specific heat and density are assumed to be independent of the temperature for the melt, the solid and the mold with the exception of the density of the melt contributing to the buoyancy forces. This assumption is well justified, as

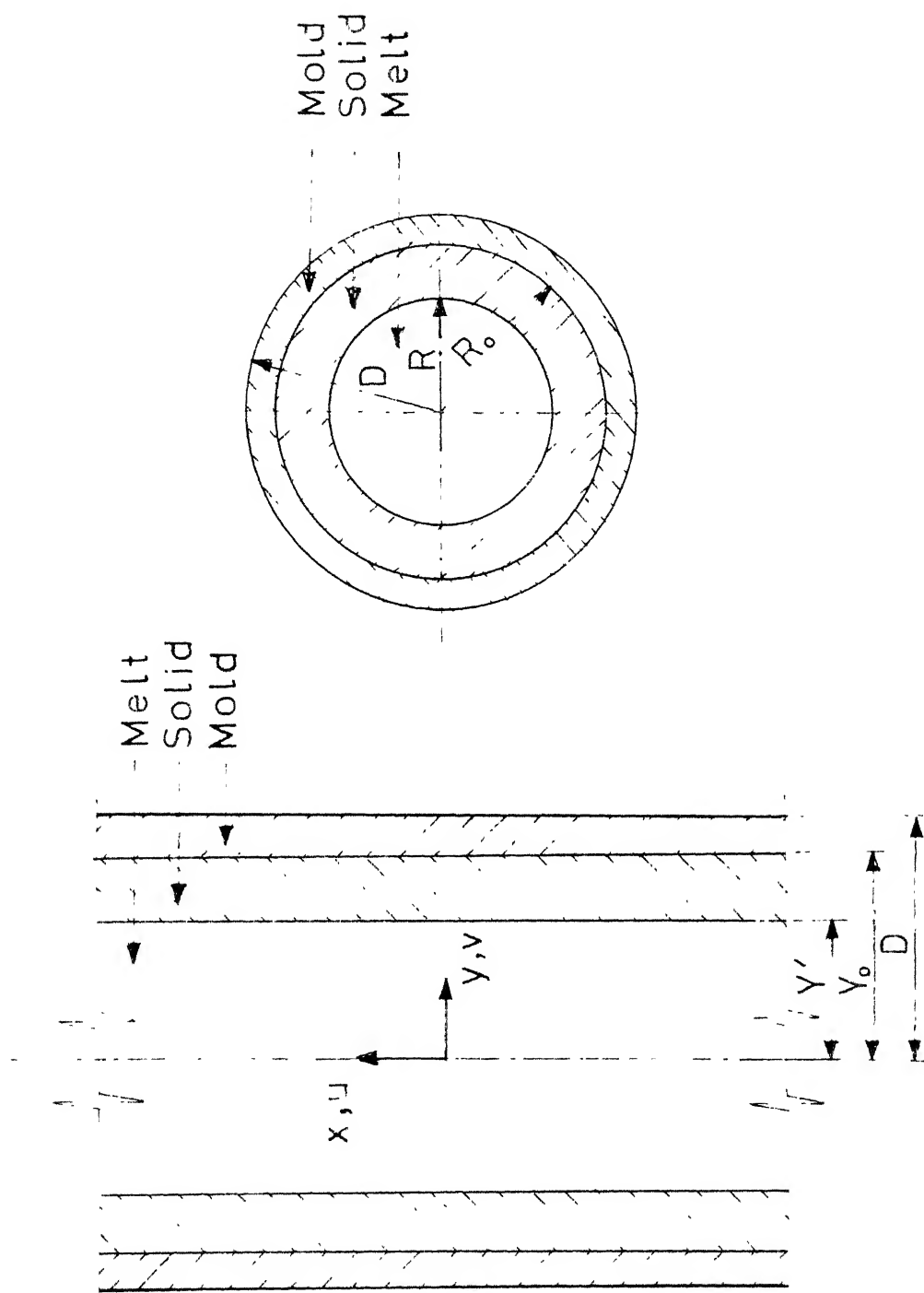


Fig.3.1 Vertical parallel plates and circular cylinder infinite in x-direction

long as the temperature variation is not high.

[ii] The melt is considered to be Newtonian. This assumption is also valid as in most of the practical applications, the fluid is Newtonian.

[iii] The vertical slot is considered to be narrow so that the heat transfer can occur only in the y-direction. An immediate consequence of this assumption is that only the vertical velocity component u predominates, leaving the horizontal velocity component v negligible, since parallel flow arises for this configuration. The problem becomes unidirectional and hence the solid front can move only in the y-direction, parallel to the mold.

Because of this assumption the momentum and the energy equations are decoupled and conduction becomes the only mode of heat transfer in cooling the melt. Batchelor (1954) has discussed that the heat transferred between two fixed, vertical plates can be assumed to be by conduction provided

$$Ra \leq 500 \qquad (3.2.1)$$

where Ra is the Rayleigh number. Though the above relation is very approximate, it gives an idea about the mode of heat transfer.

[iv] The convective flow developed in the melt is assumed to be laminar. The criterion for the onset of turbulent natural convection has been discussed by Cole (1969)

who puts the laminar range as $0 < Ra < 10^8$; the assumption is quite valid since the present investigation is well within the range.

[v] Time taken to pour the melt into the mold is small and neglected in calculations, so that solidification starts only after the pouring is complete.

[vi] Solidification is assumed to occur at a constant temperature.

3.2.2 Governing Equations: The problem can be stated mathematically, by the use of the following equations.

- (i) Equation of continuity in the melt.
- (ii) Momentum equation in the melt.
- (iii) Energy equations in the melt, the solid and the mold.

The equations are written for only one half of the slot as they are valid for the other half also, due to symmetry.

3.2.3 Energy Equations: The energy equations are:

Melt:

$$\frac{\partial T_l}{\partial t} = \alpha_l \frac{\partial^2 T_l}{\partial y^2} \quad (3.2.2a)$$

Solid:

$$\frac{\partial T_s}{\partial t} = \alpha_s \frac{\partial^2 T_s}{\partial y^2} \quad (3.2.2b)$$

Mold:

$$\frac{\partial T_m}{\partial t} = \alpha_m \frac{\partial^2 T_m}{\partial y^2} \quad (3.2.2c)$$

where T_l , T_s and T_m are the temperatures of the melt, the solid and the mold respectively.

The initial and the boundary conditions for these equations can be written as:

in the melt,

$$t = 0: \quad T_l = T_i \quad (3.2.3a)$$

$$y = 0: \quad \frac{\partial T_l}{\partial y} = 0 \text{ (because of symmetry)} \quad (3.2.3b)$$

$$y = Y': \quad T_l = T_{sat} \quad (3.2.3c)$$

where T_{sat} = solidification temperature

and,

$$k_s \frac{\partial T_s}{\partial y} - k_l \frac{\partial T_l}{\partial y} = \rho L_q \frac{dY'}{dt}. \quad (3.2.3d)$$

in the solid,

$$y = Y': \quad T_s = T_{sat} \quad (3.2.3e)$$

$$y = Y_0:$$

At the melt-solid interface the heat released by the solid should be conducted through the mold. Hence,

$$k_s \frac{\partial T_s}{\partial y} = k_m \frac{\partial T_m}{\partial y} \quad (3.2.3f)$$

in the mold,

$$t = 0: \quad T_m = T_c \quad (3.2.3g)$$

$$y = Y_0: \quad T_m = T_s \quad (3.2.3h)$$

$$y = D:$$

Boundary condition of first kind,

$$T_m = T_c = \text{constant}$$

(or)

Boundary condition of third kind,

$$-k_m \frac{\partial T_m}{\partial y} = h_1 (T_m - T_c)$$

(or)

Boundary condition of fourth kind,

$$-k_m \frac{\partial T_m}{\partial y} = \epsilon_1 \sigma (T_m^4 - T_c^4) \quad (3.2.3i)$$

3.2.4 Momentum Equation:

Since the horizontal velocity $v(x,t)$ is negligible in comparison with the vertical velocity $u(y,t)$, the momentum equation for the u -component can be written as:

$$\rho \frac{\partial u}{\partial t} = \mu \frac{\partial^2 u}{\partial y^2} - \rho g - \frac{\partial p}{\partial x} \quad (3.2.4)$$

The first term on the RHS is due to momentum diffusion whereas the second and the third terms are due to body forces and the pressure respectively.

The second and the third terms can be combined into a single term, the details of which are discussed in Appendix I. Thus,

$$\rho \frac{\partial u}{\partial t} = \mu \frac{\partial^2 u}{\partial y^2} + \rho g (T - \bar{T}) \quad (3.2.5)$$

The temperature \bar{T} is an average temperature in the melt, the value of which is found in such a way that the conservation

of mass is satisfied.

The initial and the boundary conditions for this equation can be written as:

$$u = 0, \quad \text{at} \quad t = 0 \quad (3.2.6a)$$

$$-\frac{\partial u}{\partial y} = 0, \quad \text{at} \quad y = 0 \quad (3.2.6b)$$

$$\text{and} \quad u = 0 \quad \text{at} \quad y = Y' \quad (3.2.6c)$$

3.2.5 Continuity Equation: The continuity equation for the melt is written as:

$$\frac{\partial(\rho u)}{\partial x} = 0 \quad (3.2.7)$$

since the velocity components v and w are neglected in **comparison** with the u -component velocity. Apart from the assumption (i) if we also assume that there is no change of volume during solidification then the above equation becomes,

$$-\frac{\partial u}{\partial x} = 0 \quad (3.2.8)$$

Thus, the density of the melt is assumed to be constant in the continuity equation, whereas it is assumed to vary with the temperature in the equation of motion. This kind of treatment is very common in natural convection studies and it has been discussed by Schlichting (1969).

With these simplifying assumptions, which are thought to be reasonable at least as a first approximation, the equation of continuity may be stated by expressing the fact

that there is no net motion of fluid across any horizontal section, i.e.

$$\int_0^{Y'} u dy = 0 \quad (3.2.9)$$

Equation (3.2.9) is a modified form of continuity equation, which can be used directly in the computation and has been discussed in the section 3.3.2.

3.2.6 Non-dimensionalization: Since the analytical closed form solution is not possible, the problem is solved by adopting numerical techniques. The problem can be solved with less complication, if the moving boundary is immobilized. To facilitate this, a transformation of the variables is carried out. The other purpose of the transformation is to introduce dimensionless variables and parameters.

The non-dimensional variables for the melt are:

$$\begin{aligned} y_1^* &= y/Y'(t) \\ T_1^* &= (T_1 - T_c)/(T_i - T_c) \\ u^* &= u Y_o / v \end{aligned} \quad (3.2.10)$$

For the solid,

$$\begin{aligned} y_s^* &= (y - Y'(t))/(Y_o - Y'(t)) \\ T_s^* &= (T_s - T_c)/(T_i - T_c) \end{aligned} \quad (3.2.11)$$

and for the mold,

$$\begin{aligned} y_n^* &= (y - Y_o)/(D - Y_o) \\ T_n^* &= (T_n - T_o)/(T_i - T_o) \end{aligned} \quad (3.2.12)$$

The dimensionless time is defined as,

$$t^* = \nu t / Y_o^2 \quad (3.2.13)$$

Because of the transformation, the dimensions for the domains of the melt, the solid and the mold become unity, and do not change with time. This simplification, however, results in greater complexity in the governing equations as shown below.

By substituting these dimensionless variables in the governing equations (3.2.2a) - (3.2.2c) we get,

Melt:

$$\frac{\partial T_1^*}{\partial t^*} - \frac{\partial T_1^*}{\partial y_1^*} \frac{y_1^*}{\delta(t^*)} \frac{d\delta}{dt^*} = \frac{1}{Pr} \frac{1}{\delta^2(t^*)} \frac{\partial^2 T_1^*}{\partial y_1^{*2}} \quad (3.2.14a)$$

where,

$$\delta(t^*) = Y'(t)/Y_o$$

and, $Pr = \text{Prandtl number}$

Solid:

$$\frac{\partial T_s^*}{\partial t^*} + \frac{\partial T_s^*}{\partial y_s^*} \frac{y_s^* - 1}{(1 - \delta(t^*))} \frac{d\delta}{dt^*} = \frac{\alpha_s}{\alpha_l} \frac{1}{Pr} \frac{1}{(1 - \delta(t^*))^2} \frac{\partial^2 T_s^*}{\partial y_s^{*2}} \quad (3.2.14b)$$

and,

Mold:

$$\frac{\partial T_n^*}{\partial t^*} = \frac{\alpha_n}{\alpha_1} \frac{1}{Pr} \left(\frac{1}{\delta_n} - 1 \right)^2 \frac{\partial^2 T_n^*}{\partial y_{n1}^{*2}} \quad (3.2.14c)$$

where,

$$\delta_n = D/Y_o$$

The extra terms found in the LHS of equations (3.2.14a) and (3.2.14b) represent the convection associated with the immobilization of the moving boundary. An observer sitting on the immobilized melt-solid interface sees a mass moving towards (or away) from him.

The boundary and the initial conditions become:

in the melt

$$T_1^* = 1 \quad \text{at } t^* = 0 \quad (3.2.15a)$$

$$\frac{\partial T_1^*}{\partial y_{11}^*} = 0 \quad \text{at } y_{11}^* = 0 \quad (3.2.15b)$$

$$T_1^* = \frac{1}{1 + \phi} \quad \text{at } y_{11}^* = 1 \quad (3.2.15c)$$

where, $\phi = (T_i - T_{sat}) / (T_{sat} - T_c)$

= Constant

and,

$$\frac{k_s}{k_1} \frac{1}{(1-\delta(t^*))} \frac{\partial T_s^*}{\partial y_s^*} - \frac{1}{\delta(t^*)} \frac{\partial T_1^*}{\partial y_{11}^*} = Pr.Stc. \frac{d\delta}{dt^*} \quad (3.2.15d)$$

where, $Sto = Lq/[C_p(T_i - T_c)]$

= Stefan number

in the solid,

$$T_s^* = 1/(1+\phi) \text{ at } y_s^* = 0 \quad (3.2.15e)$$

$$\frac{k_s}{k_l} \frac{(\phi_l - 1)}{(1 - \delta(t))} \frac{\partial T_s^*}{\partial y_s^*} = - \frac{\partial T_l^*}{\partial y_l^*} \text{ at } y_c^* = 1 \quad (3.2.15f)$$

in the mold,

$$T_m^* = 0 \quad \text{at } t^* = 0 \quad (3.2.15g)$$

$$T_m^* = T_s^* \quad \text{at } y_m^* = 0 \quad (3.2.15h)$$

At $y_m^* = 1$,

$$\frac{\partial T_m^*}{\partial y_m^*} = - Bi_l T_m^*,$$

for the boundary condition of third kind, where

$$Bi_l = \frac{h_l d}{k_m}$$

= Biot number at the mold outer surface

(or)

$$\frac{\partial T_m^*}{\partial y_m^*} = - Re_l [(T_c^* + T_m^*)^4 - T_c^{*4}] ,$$

for the boundary condition of fourth kind, where,

$$Re_l = \frac{\epsilon_l \sigma d (T_i - T_m)^3}{k_m}$$

= Radiation constant

$$\text{and } T_c^* = T_c / (T_i - T_c) \\ (\text{or})$$

(3.2.15i)

$$T_\infty^* = 0$$

for the boundary condition of first kind

The momentum equation gets transformed to:

$$\frac{\partial u^*}{\partial t^*} - \frac{\partial u^*}{\partial y_1^*} \frac{y_1^*}{\delta(t^*)} \frac{d\delta}{dt^*} = \frac{1}{\delta^2(t^*)} \frac{\partial^2 u^*}{\partial y_1^{*2}} + Gr (T_1^* - T^*) \quad (3.2.16)$$

where,

$$Gr = \frac{g \beta (T_i - T_c) Y_0^3}{\nu^2} \\ = \text{Grashof number}$$

The initial and the boundary conditions become,

$$u^* = 0 \quad \text{at } t^* = 0 \quad (3.2.17a)$$

$$\frac{\partial u^*}{\partial y_1^*} = 0 \quad \text{at } y_1^* = 0 \quad (3.2.17b)$$

$$u^* = 0, \quad \text{at } y_1^* = 1 \quad (3.2.17c)$$

By applying the same non-dimensional parameters, the continuity equation (3.2.9) can be transformed to

$$\int_0^1 u^* dy_1^* = 0 \quad (3.2.18)$$

3.3 SOLUTION METHODOLOGY:

The equations (3.2.14) - (3.2.18) have been solved by numerical techniques. As a first step, the thickness of the

solid formed, $(1-\delta)$, was obtained from the moving boundary equation (3.2.15d). Equation (3.2.15d), when written in finite-difference form, reduced to cubic polynomial, which was solved using Chebyshev approximation technique discussed by Carnahan, Luthur and Wilkes (1969).

At time $t^* = 0$, the starting difficulties were avoided by assuming a very small thickness of the solid, in this case taken as $0.0001 Y_0$. The temperature profile in the solid was assumed to be linear at time $t^* = 0$, which has been supported by Schlichting (1969). Verification of this assumption was also made with Neumann's solution, which one can expect to be valid at the initial stages. The initial solid thickness calculated by the present scheme was compared with the Neumann's solution and agreement to within 0.1 per cent was obtained. The initial thickness of the solid layer, due to chilling, was also varied to ascertain that it does not affect the numerical results significantly.

The second step involved in the computation is the simultaneous solution of Eqs (3.2.14a) - (3.2.14c). The equations were solved using the finite-difference technique. The melt, the solid, and the mold regions were divided separately into 10 grid spacings each, along the y-axis, each grid being of length 0.1. The partial derivatives of the equations were replaced by their finite-difference approximations, which convert the governing partial differential

equations into a set of simultaneous algebraic equations.

3.3.1 Explicit Scheme: The finite-difference explicit scheme, discussed by Carnahan, Luther and Wilkes (1969) when tried, was found to be unstable. The instability is due to very small domain in the solid region, in the beginning of the solidification, which has restricted the time step to an unreasonably small value.

3.3.2 Implicit Scheme: The implicit scheme, which is found to be suitable for this problem, and more accurate than the explicit scheme, overcomes the difficulties encountered in the explicit scheme, at the cost of a somewhat more complicated calculational procedure. It consists of representing a derivative $\partial T_1^* / \partial y_1^*$ by a finite - difference form, evaluated at the advance point of time t_{n+1}^* instead of t_n^* as in the explicit scheme.

As an example, Eqn.(3.2.14a) can be written as

$$\begin{aligned} \frac{T_{1,j,n+1}^* - T_{1,j,n}^*}{\Delta t^*} &= \frac{T_{1,j+1,n+1}^* - T_{1,j,n+1}^*}{\Delta y^*} \frac{y_{1,j}^*}{\delta_{n+1}} \frac{\delta_{n+1} - \delta_n}{\Delta t^*} \\ &+ \frac{1}{Pr} \frac{1}{\delta_{n+1}^2} \frac{T_{1,j-1,n+1}^* - 2T_{1,j,n+1}^* + T_{1,j+1,n+1}^*}{(\Delta y^*)^2} \end{aligned} \quad (3.3.1)$$

This can be simplified to,

$$\begin{aligned}
 & - \lambda \nabla_1 T_{1,j-1,n+1}^* + (1 + 2 \lambda \nabla_1 + \varepsilon_1 \lambda \Delta y^*) T_{1,j,n+1}^* \\
 & - (\lambda \varepsilon_1 \Delta y^* + \lambda \nabla_1) T_{1,j+1,n+1}^* = T_{1,j,n}^* \quad (3.3.2)
 \end{aligned}$$

where $\lambda = \Delta t^* / (\Delta y^*)^2$

$$\varepsilon_1 = \frac{y_{1,j}^*}{\delta_{n+1}} \frac{\delta_{n+1} - \delta_n}{\Delta t^*}$$

and $\nabla_1 = \frac{1}{Pr} \frac{1}{\delta_{n+1}^2}$

Equation (3.3.2) represents a set of simultaneous, algebraic equations forming a tridiagonal matrix.

The tridiagonal matrices, thus formed for the melt, the solid and the mold, were first solved by the conventional Gauss elimination method. One of the major disadvantages of the Gauss elimination method is the accumulation of the round-off errors, especially at higher time steps. In view of this, this method was only used to solve the equation of the melt region. For the solid and the mold regions, the governing equations along with their linear boundary conditions were written in a matrix form and the matrix was inverted using the maximum pivot strategy. In case of the radiative boundary condition (Eqn.(3.2.15i)) which is non-linear, simplification has been made to bring it to a linear form, as discussed in Appendix II.

Interestingly, though the computational time involved in matrix inversion using maximum pivot strategy is much more

than solving the tridiagonal matrix using Gauss elimination technique, the former allows the use of higher time step with reasonably good accuracy. Hence, the computation time lost in the matrix inversion can be compensated by using large time steps. The Δt^* used in the computation is 0.01, in which case a CPU time of 1 minute is needed for 70 per cent solidification on a DEC 1090 computer.

The momentum equation (3.2.16) which is similar to the energy equation (3.2.14a) has been solved by the Gauss elimination technique. The important point here is that the quantity \bar{T}^* in Eqn.(3.2.16) is fictitious and has to be adjusted iteratively for each time step, in such a way that the continuity equation (3.2.18) is satisfied.

3.4 VERTICAL CYLINDER:

The analysis has also been done for the vertical cylinder. The governing equations are:

Energy equation:

$$\frac{\partial T_k}{\partial t} = \frac{\alpha_k}{r} \cdot \frac{\partial}{\partial r} \left(r \frac{\partial T_k}{\partial r} \right) \quad (3.4.1)$$

where $k = l$, for the melt
 s , for the solid
 m , for the mold

Momentum equation:

$$\frac{\partial u}{\partial t} = \frac{v}{r} \cdot \frac{\partial}{\partial r} \left(r \frac{\partial u}{\partial r} \right) + g\beta(T - \bar{T}) \quad (3.4.2)$$

The assumptions, boundary conditions, non-dimensionalization and the method of solving these equations are the same as those for the parallel plate case, except for the slight change in the governing equation, due to the introduction of an additional term in the r -coordinate.

3.5 RESULTS AND DISCUSSION:

The presentation of the results is mainly from two view points.

- (i) The study of the temperature and velocity profiles.
- (ii) Dependence of the interface movement with time on various non-dimensional parameters.

3.5.1 Temperature Profile: Figures 3.2 and 3.3 indicate the temperature profiles obtained for the melt, the solid and the mold regions, with dimensionless time as parameter, for the constant wall temperature and the convective boundary condition respectively. The curves lying above the solidification temperature represent the melt region whereas those lying below the solidification temperature, but before the melt-solid interface represent the solid region. This type of representation is logical as it gives an idea about the position of the melt-solid interface at a particular time. The dotted lines shown in Figure 3.2, indicate the temperature profiles for the cylindrical case. In the figures 3.2 and 3.3, for the non-dimensional parameters considered, the

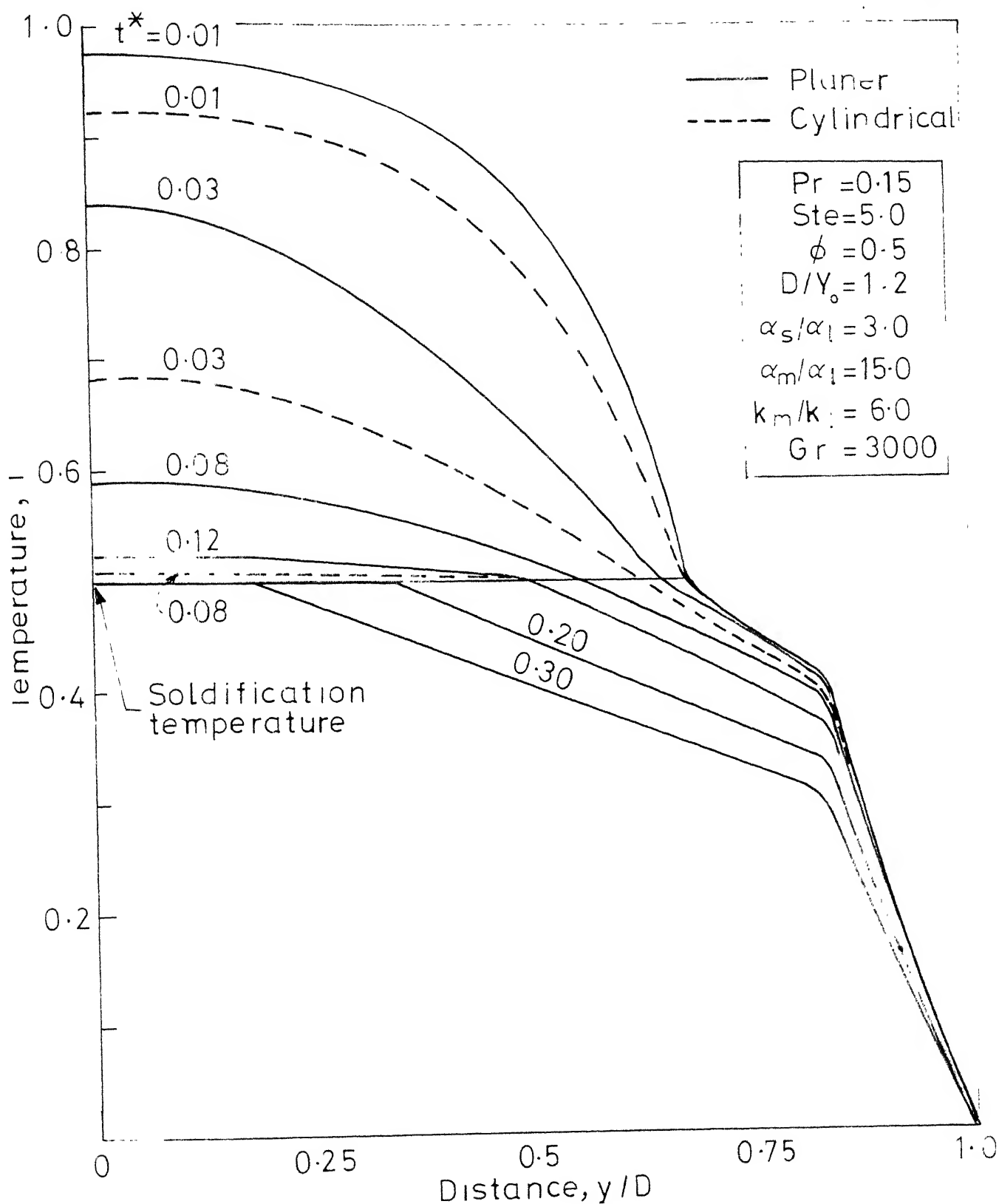


Fig. 3.2 Temperature distribution in the three regions for the boundary condition of

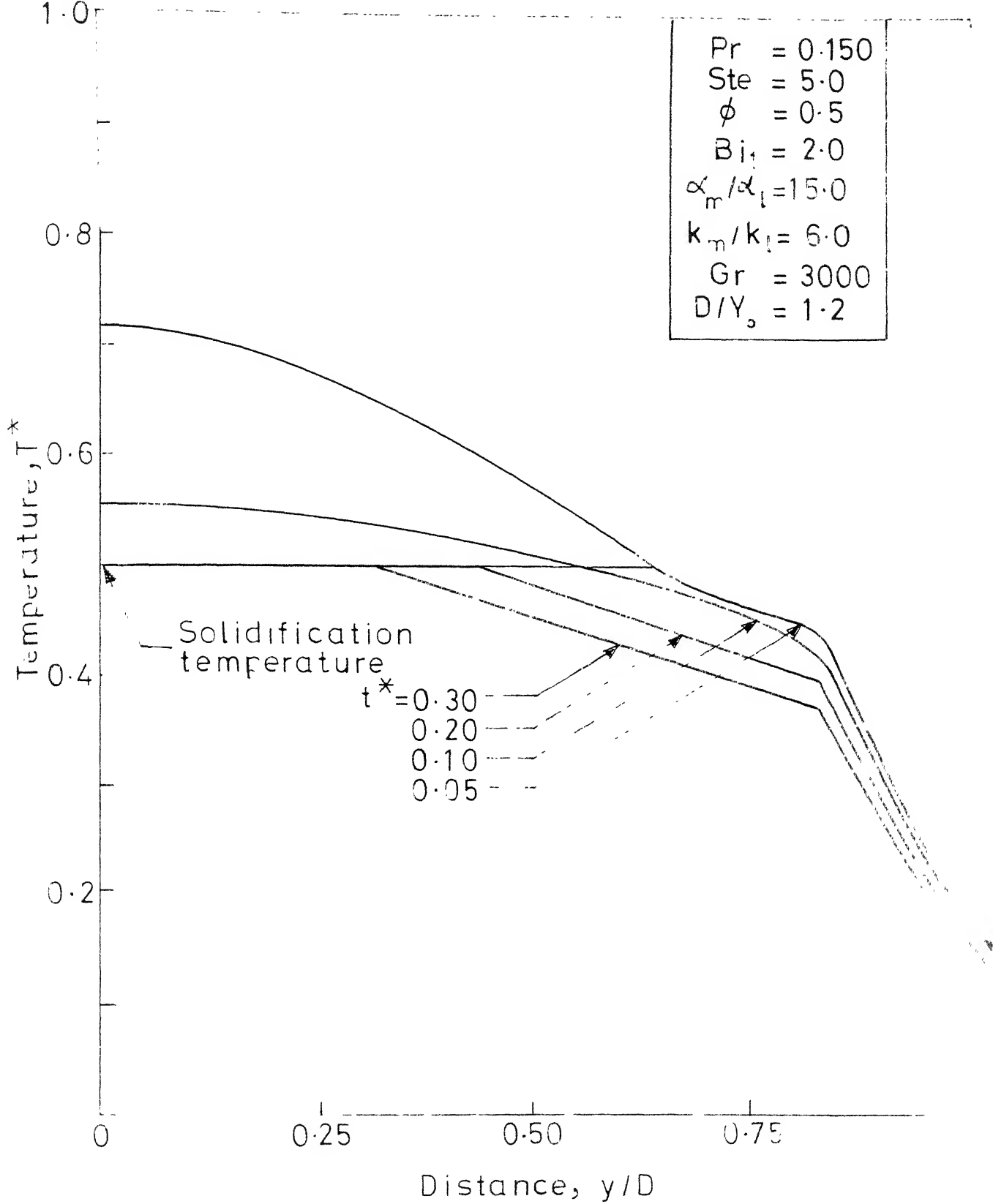


Fig. 3.3 Temperature distribution in the three regions for the boundary condition of third kind

temperature profiles for the solid and the mold are linear. This is due to very high thermal diffusivities of the solid and the mold, which lead to insignificant storage terms in their energy equations. It is seen from Figure 3.2 that the temperature decays at a faster rate in the cylindrical case than that in the planer case, resulting in a more rapid solidification. This fact is better observed from Figure 3.5, where the thickness of the solid formed can be compared for the planer case with that for the cylindrical case.

3.5.2 Velocity Profile: The time dependent velocity distribution in the melt is plotted in Figure 3.4. A point which can be immediately understood from Figure 3.4 is that, certain amount of time is required for the development of the velocity field. At a given value of y/D , the maximum velocity is reached at some intermediate time. At larger times as the solidification proceeds, the velocity field decreases.

An examination of Figures 3.2 and 3.4 indicates that for low Prandtl number the fluid motion decays more slowly as compared to the thermal field. This suggests, that appreciable fluid motion can persist even after most of the superheat has been removed from the system. This behaviour is inherently associated with the low Prandtl number fluids (e.g. liquid metals), with the physical fact that the molten metals can transmit heat much faster than they are able to transfer momentum.

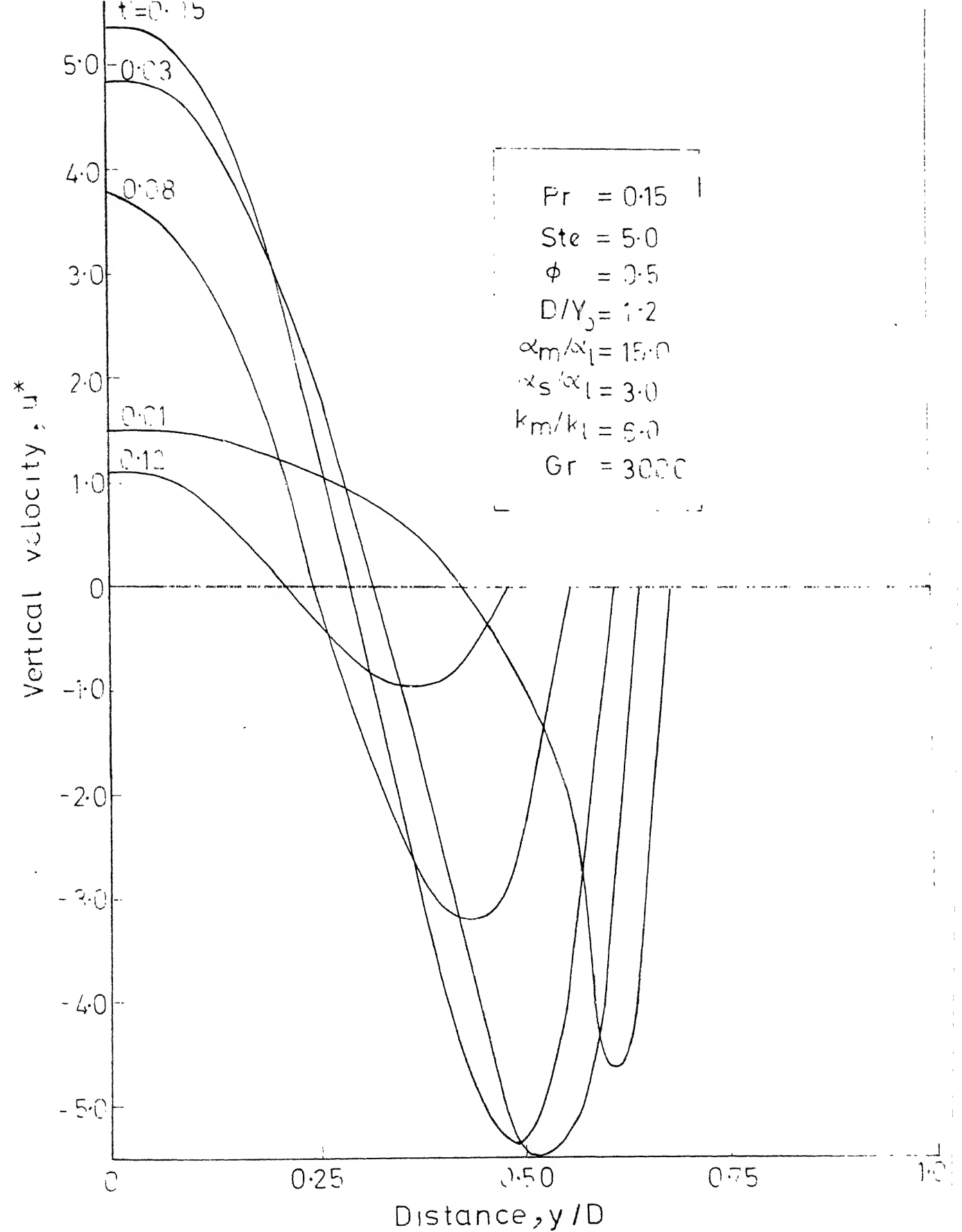


Fig.3-4 Vertical velocity distribution in the melt for the boundary condition of first kind

The velocity profiles are symmetric about $y=0$ and the total upward flow equals the total downward flow, so that an enclosed region is simulated.

Inspection of Eqn.(3.2.16) suggests that the melt velocity varies with the Grashof number as,

$$u^*(y^*, t^*) = Gr. f(y^*, t^*) \quad (3.5.1)$$

where, $f(y^*, t^*)$ = velocity of the melt when

$$Gr = 1$$

This has been verified by computing the velocity $u^*(y^*, t^*)$ for different Grashof numbers. Thus one can expect higher velocities at higher Grashof numbers. The width of the slot Y_0 , plays an important role in the magnitude of Grashof number as it is raised to its third power in the definition. This suggests, in the case of larger slots, the natural convection developed can be significant even if the superheat of the melt is low.

3.5.3 Effect of Melt Velocity: The effect of melt velocity can be understood by calculating the distance travelled by inclusions in the melt. Figure 3.4 represents the velocity distribution for the typical case of ingot casting of steel (properties in Appendix III) in a slot of 1.0 cm width.

From the figure, the maximum velocity of the melt u^* is found to be 5.35, which is equal to 1.02×10^{-5} m/sec in absolute values. In this case a superheat of 400°C is assumed which is hypothetical. In actual case the superheat will be about 20°C and the mold width is 1 m. However, for the actual case the velocity u^* is much more than 5.35 as the Rayleigh number is 6×10^8 . The calculations are not shown for this case as it runs contrary to the assumption (iii) of Sec. 3.2.1.

If we assume that the molten steel contains non-metallic inclusions of average diameter 2.0 microns then the terminal rising velocity is calculated by the Stoke's law:

$$u_t = \frac{(\rho_p - \rho) g d_p^3}{18\mu} \quad (3.5.2)$$

where,

ρ_p = density of the particle = $3.0 \times 10^3 \text{ kg/m}^3$

ρ = density of the melt

d_p = diameter of the particle

Thus,

$$u_t = 1.4 \times 10^{-6} \text{ m/sec}$$

This value is much smaller than the maximum velocity

of the melt, which implies that the particles would move along with the buoyancy induced flow that arises due to the temperature gradient in the melt.

3.5.4 Effect of Prandtl Number (Pr): The thickness of the solid formed with respect to time, with Prandtl number as the parameter is shown in Figure 3.5. The rate of solidification is found to increase with a decrease in the Prandtl number. This is expected as fluids with a low Prandtl number, have a higher thermal diffusion, resulting in large heat transfer and hence a faster solidification. It is seen from Figure 3.5 that the rate of solidification is linear at larger times. At large times, most of the superheat has been removed from the melt and the melt temperature reaches approximately the solidification temperature. In such circumstances only the latent heat is to be removed. Hence the rate of heat liberated at the melt-solid interface is approximately constant. The heat extracted through the outer surface of the mold to the ambient also remains constant as the storage terms in heat conduction equation is very small. This can be seen from Figure 3.3, which shows the temperature gradient to be almost constant with time. Since the heat liberated at the interface as well as the heat removed at the mold surface remain constant, the interface growth rate is linear at larger times.

3.5.5 Effect of Stefan Number (Ste): The effect of Stefan number on solidification is shown in Figure 3.6, in terms of

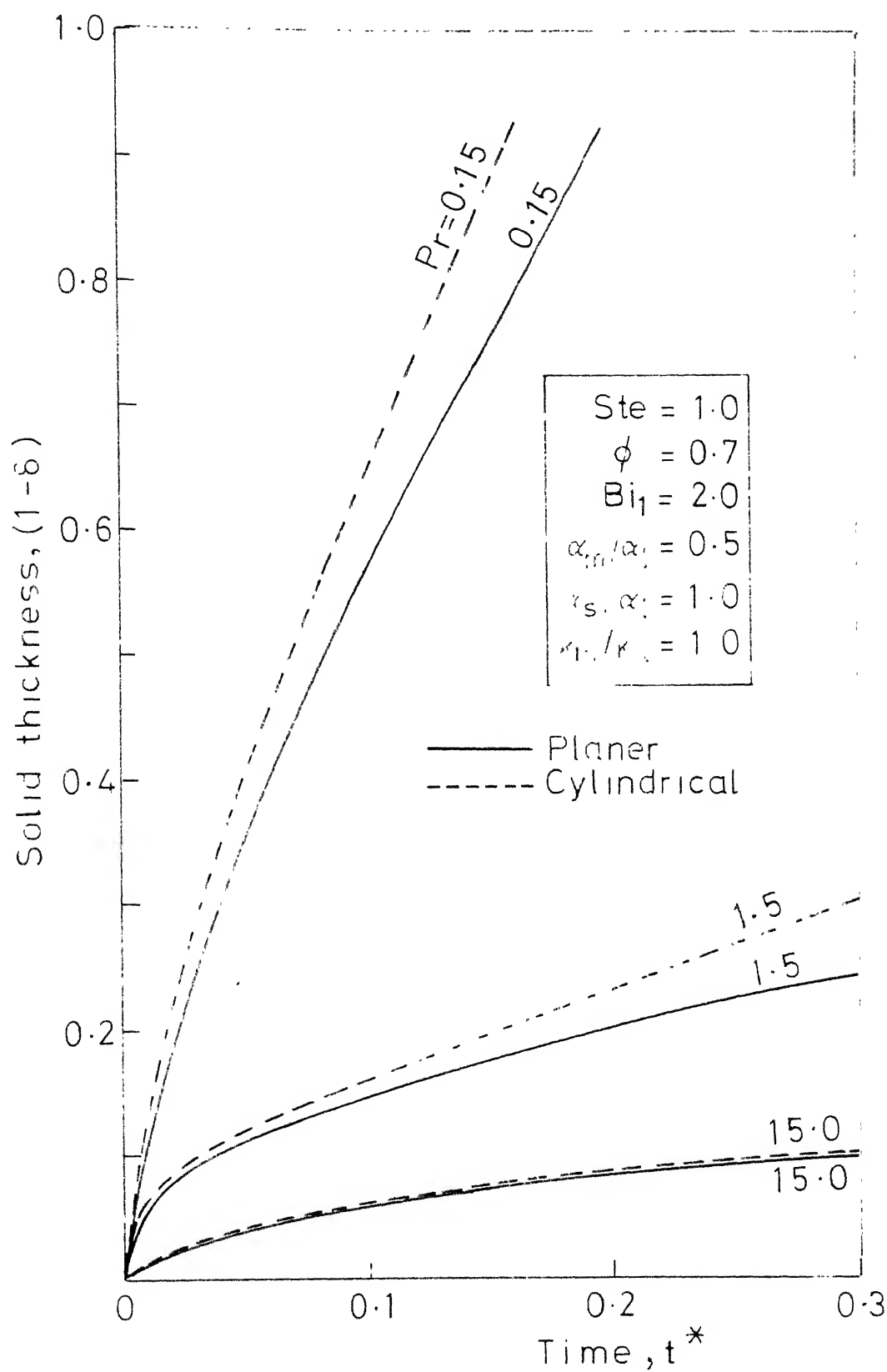


Fig. 3.5 Dependence of interface location on the Prandtl number for the boundary condition of third kind

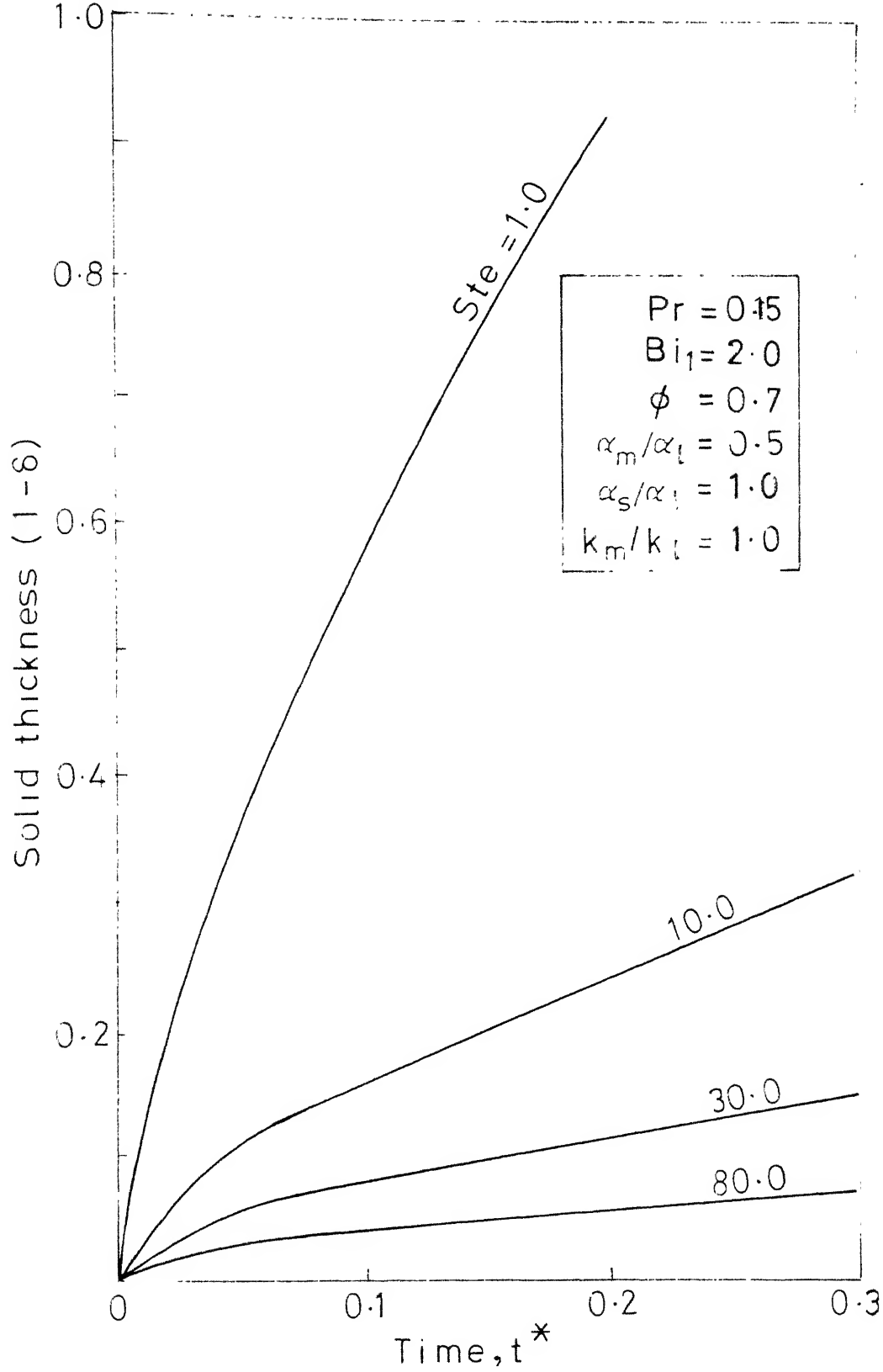


Fig. 3.6 Dependence of interface movement on Stefan number for the boundary condition of third kind for vertical parallel plates

the dependence of the thickness of the solid formed on time elapsed. It is found that the solidification proceeds at a faster rate when Ste is small. This is true as small Ste implies little latent heat and hence a faster solidification rate.

3.5.6 Effect of Superheat (ϕ): The movement of the solid front with time, with ϕ as a parameter is shown in Figure 3.7. It is seen from Figure 3.7, that the rate of movement of the solid front decreases with increase in ϕ values. This is reasonable as physically a high superheat (or large ϕ) implies more heat load and hence the decrease in solidification rate.

3.5.7 Effect of Biot number, Radiation Constants: The importance of Biot number Bi_1 , and the radiation constant Rc_1 can be understood from Figure 3.7 and 3.8 respectively. The thickness of the solid formed at various times is found to increase with Bi_1 (or Rc_1), as a high value of Bi_1 (or Rc_1) would imply a high convective (or radiative cooling), leading to rapid solidification as observed.

3.5.8 Comparison with Previous Work: Figure 3.9 shows the results computed by Szekely and Stanek (1970), Neumann (1912) and the present work (Ramachandran, Jaluria and Gupta (1981a)), for a typical case of solidification of steel. The solution has been computed neglecting the resistance offered by the

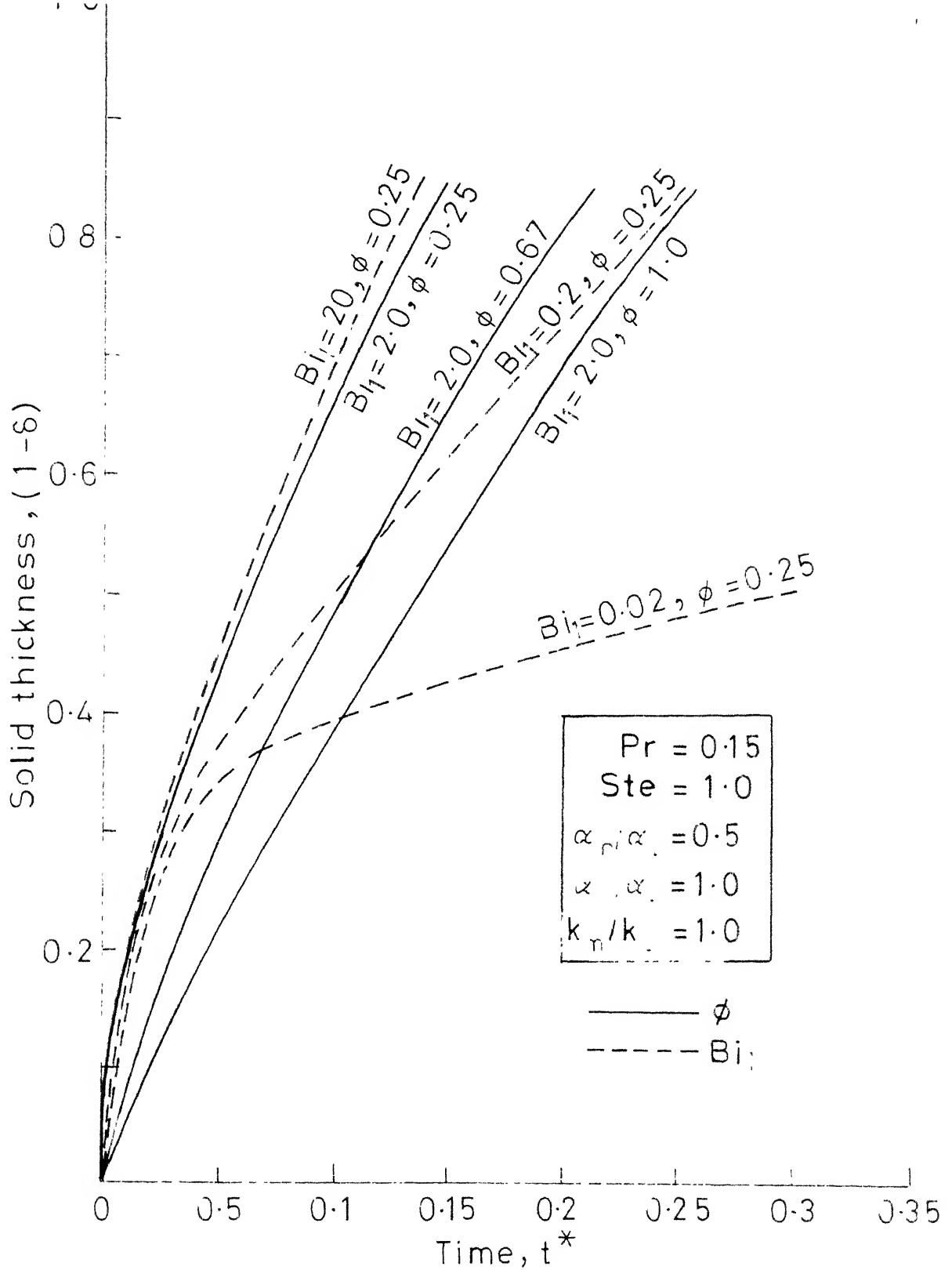


Fig.3.7 Dependence of interface movement on the Biot number and the superheat for parallel plates

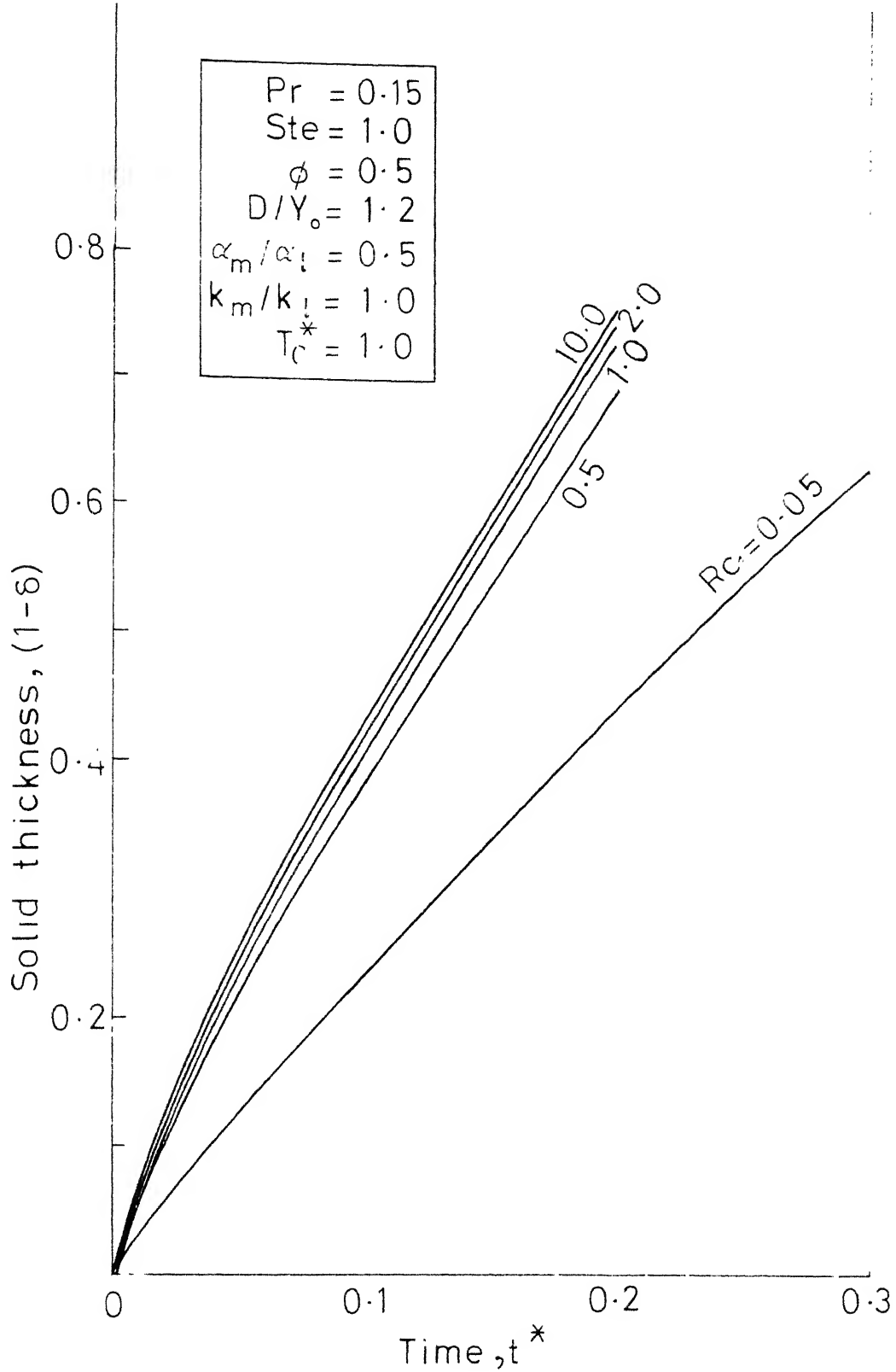


Fig. 3.8 Dependence of interface movement on the Radiation constant for parallel plates

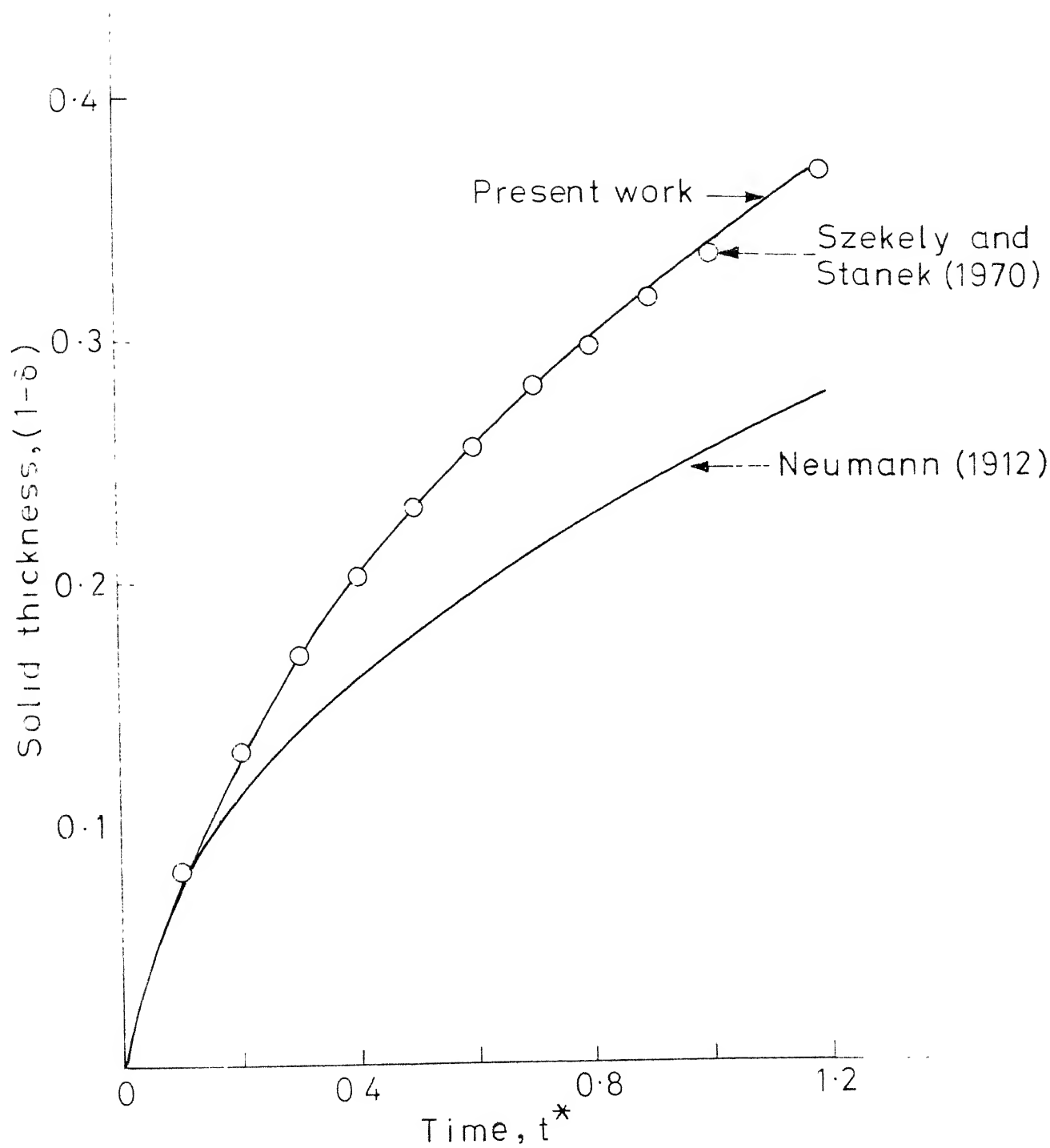


Fig. 3-9 Comparison of the thickness of the solid formed with time, with literature

mold. The results are in good agreement with Szekely and Stanek (1970) who assumed a linear temperature distribution in the solid and neglected the effect of mold. The solution predicted by Neumann shows a decrease in solidification rate as Neumann assumed semi-infinite behaviour in the solid and in the melt.

3.6 CONCLUDING REMARKS:

An analysis has been carried out for the heat conduction problem during solidification between parallel plates and in a vertical cylinder. The heat conducted through the melt, the solid and the mold as well as the velocity field generated in the melt due to thermal gradients, have been considered. The effects of various non-dimensional parameters on the solidification rate have also been studied.

The one dimensional analysis is valid only when the height of the mold is very large compared to its width. Chapter 4 describes analysis for the two dimensional solidification, for which the height to the width ratio is small.

CHAPTER 4

TWO DIMENSIONAL SOLIDIFICATION INSIDE A RECTANGULAR ENCLOSURE

4.1 INTRODUCTION:

The solidification of melt in enclosures of finite dimensions has not been extensively studied in the literature, since the mathematical formulations and their solutions are extremely difficult and many simplifying assumptions have to be made. Many of the solutions available now are conduction-based and they do not physically reflect the reality. The most important terms in the equations which define the two dimensional solidification problem are the convective terms which make the equations non-linear and rule out the possibility of any analytical solutions. Even to solve the equations numerically, special formulations are needed as non-linear derivatives lead the problem to a numerical instability. In most of the cases the convective terms cannot be neglected as internal thermal flows of varying degrees are almost always present in the melt, since even slight temperature differences in the melt can give rise to buoyancy forces which in turn can produce sizable convective flow. The flow thus developed is important in determining the shape of the interface, solidification time and the solute distribution. Further the accounting of natural convection exposes the differences between solidification and melting problems whose conduction-based solutions

are interchangeable. Thus the problem involves the solution of nonlinear, coupled, simultaneous equations written for the thermal and flow field in the melt and the energy equations written for the solid and the mold.

In the present chapter an analysis is made to understand quantitatively the thermal and flow field developed during solidification in a rectangular enclosure. Two dimensional equations describing the temperature and flow field are written. Consideration has also been given to the heat conducted and stored in the solid and the mold. The rate of interface movement which is unknown a priori is calculated by solving the heat balance equation at the melt-solid interface. The problem is solved for various boundary conditions.

The coupled partial differential equations are non-dimensionalised and solved numerically using Alternating Direction Implicit technique and Successive Over-Relaxation method. The equations are solved, initially without considering solidification, as a check on the numerical scheme and later including solidification. The results are computed for various dimensionless parameters such as Rayleigh number, Prandtl number, Stefan number, aspect ratio etc. The significance as well as the effect of these parameters on solidification are discussed. The temperature and velocity profiles are also obtained along with the rate of interface movement.

4.2 FORMULATION:

Consider a rectangular enclosure of width $2Y_0$, mold thickness d and height L . The enclosure is extended to infinity in the z -direction as shown in Figure 4.1.

Initially, the mold is kept at a temperature T_c which is below the solidification temperature T_{sat} . At time $t=0$, the melt at temperature $T_i(>T_{sat})$ is poured into the enclosure. Immediately, a thin crust of solid is formed at the inner surface of the mold and an inward movement of solid front starts. Because of the thermal gradients set up in the melt, convection currents start in the melt.

4.2.1 Boundary Conditions: The following cases are considered:

CASE I: The top and bottom surfaces of the enclosure are kept adiabatic whereas the outer surfaces of the mold are kept at a constant temperature.

CASE II: The top and bottom surfaces of the enclosure are kept adiabatic while the outer surfaces of the mold exchange energy by convection and radiation with the surroundings which is at a temperature T_c .

CASE III: The top surface of the enclosure and the mold outer surfaces exchange energy by convection and radiation with the surroundings, the bottom surface being kept adiabatic.

4.2.2 Assumptions: The following assumptions are made in the formulation of the problem:

- (i) The physical properties such as density, thermal conductivity, specific heat etc. are assumed to be independent of temperature for the melt, the solid and the mold with the exception of the density of the melt which contributes to buoyancy forces.
- (ii) The fluid flow developed in the melt due to thermal gradients is assumed to be laminar.
- (iii) The melt is assumed to be Newtonian.
- (iv) The contact between the solid formed and the mold is assumed to be perfect so that no contact resistance is introduced.

4.2.3 Governing Equations: The equations are written for one half of the enclosure because of the symmetry at $y=0$. The problem may now be stated by expressing the continuity, momentum and the energy equations in the melt, and the energy equation in the solid and the mold together with the appropriate initial and boundary conditions. Thus in the melt, Continuity equation:

$$\frac{\partial u}{\partial x} + \frac{\partial v}{\partial y} = 0 \quad (4.2.1)$$

Momentum equations:

in x-direction,

$$\frac{\partial u}{\partial t} + u \frac{\partial u}{\partial x} + v \frac{\partial u}{\partial y} = g\beta(T - T_{sat}) + \nu \left(\frac{\partial^2 u}{\partial x^2} + \frac{\partial^2 u}{\partial y^2} \right) - \frac{1}{\rho} \frac{\partial p}{\partial x} \quad (4.2.2)$$

in y-direction,

$$\frac{\partial v}{\partial t} + u \frac{\partial v}{\partial x} + v \frac{\partial v}{\partial y} = \nu \left(\frac{\partial^2 v}{\partial x^2} + \frac{\partial^2 v}{\partial y^2} \right) - \frac{1}{\rho} \frac{\partial p}{\partial y} \quad (4.2.3)$$

The first term in the RHS of Eqn.(4.2.2) is obtained by combining the vertical pressure gradient and body force terms, and applying Boussinesq model described in Appendix I.

The pressure terms appearing in Eqn (4.2.2) and (4.2.3) can be eliminated by differentiating them with respect to y and x, respectively, subtracting and applying the continuity equation, Eqn.(4.2.1) to produce the following equation.

$$\begin{aligned} \frac{\partial}{\partial t} \left(-\frac{\partial u}{\partial y} - \frac{\partial v}{\partial x} \right) + u \frac{\partial^2 u}{\partial x \partial y} + v \frac{\partial^2 u}{\partial y^2} - u \frac{\partial^2 v}{\partial x^2} - v \frac{\partial^2 v}{\partial x \partial y} \\ = g\beta \frac{\partial T}{\partial y} + \nu \left(\frac{\partial (\nabla^2 u)}{\partial y} - \frac{\partial (\nabla^2 v)}{\partial x} \right) \end{aligned} \quad (4.2.4)$$

where ∇^2 is the Laplace operator in x and y coordinates.

Energy equation in melt:

$$\frac{\partial T}{\partial t} + u \frac{\partial T}{\partial x} + v \frac{\partial T}{\partial y} = \alpha_1 \left(\frac{\partial^2 T}{\partial x^2} + \frac{\partial^2 T}{\partial y^2} \right) \quad (4.2.5)$$

The problem can be further simplified by writing Eqn.(4.2.4) in terms of vorticity ω and stream function ψ ,

which eases the computational problems.

Thus Eqn.(4.2.4) becomes

$$\frac{\partial \omega}{\partial t} + u \frac{\partial \omega}{\partial x} + v \frac{\partial \omega}{\partial y} = -g\beta \frac{\partial T}{\partial y} + \nu (\nabla^2 \omega) \quad (4.2.6)$$

where,

$$\omega = -\left(\frac{\partial^2 \psi}{\partial x^2} + \frac{\partial^2 \psi}{\partial y^2}\right) \quad (4.2.7)$$

$$u = \frac{\partial \psi}{\partial y} \text{ and } v = -\frac{\partial \psi}{\partial x} \quad (4.2.8)$$

The energy equations in the solid and the mold are two dimensional conduction equations:

$$\frac{\partial T_s}{\partial t} = \alpha_s \left(\frac{\partial^2 T_s}{\partial x^2} + \frac{\partial^2 T_s}{\partial y^2} \right) \quad (4.2.9)$$

and

$$\frac{\partial T_m}{\partial t} = \alpha_m \left(\frac{\partial^2 T_m}{\partial x^2} + \frac{\partial^2 T_m}{\partial y^2} \right) \quad (4.2.10)$$

These equations, along with the energy balance at the interface and the other boundary conditions, are to be solved in a domain whose boundaries do not fall along the coordinate lines in any well defined coordinate system. In particular, the thickness of the solid formed varies with x as well as time as the solidification proceeds. This state of affairs precludes an analytical solution and requires that, even in a numerical solution, approximations must be made in order to obtain results with a realistic computational effort.

The initial and boundary conditions for the equations discussed above are:

In the melt:

$$\text{at } t = 0: \quad T_1 = T_i \quad (4.2.11a)$$

$$\text{at } y = 0: \quad \frac{\partial T_1}{\partial y} = 0; \quad \frac{\partial u}{\partial y} = 0; \quad v = 0 \quad (4.2.11b)$$

$$\text{at } y = Y': \quad T_1 = T_{\text{sat}}; \quad u = 0; \quad v = 0 \quad (4.2.11c)$$

The boundary conditions describing the movement of the interface can be obtained by writing the heat balance equation at $y=Y'$.

Thus,

$$\left(k_s \frac{\partial T_s}{\partial y} - k_l \frac{\partial T_l}{\partial y} \right) \left(1 + \left(\frac{\partial Y'}{\partial x} \right)^2 \right) = \rho L_q \frac{\partial Y'}{\partial t} \quad (4.2.11d)$$

where L_q = Latent heat of solidification.

The steps involved in obtaining Eqn.(4.2.11d) are discussed in Appendix IV.

$$\text{at } x = 0: \quad \frac{\partial T_l}{\partial x} = 0; \quad u = 0; \quad v = 0 \quad (4.2.11e)$$

$$\text{at } x = L: \quad u = 0; \quad v = 0 \quad (4.2.11f)$$

For cases I and II,

$$\frac{\partial T_l}{\partial x} = 0; \quad (4.2.11g)$$

For case III,

$$-k_l \frac{\partial T_l}{\partial x} = h_2(T_l - T_c) + \epsilon_2 \sigma (T_l^4 - T_c^4); \quad (4.2.11h)$$

In the solid:

$$\text{at } y = Y': \quad T_s = T_{\text{sat}}; \quad (4.2.12a)$$

$$\text{at } y = Y_0: \quad T_s = T_m; \quad (4.2.12b)$$

$$\text{at } x = 0: \quad \frac{\partial T_s}{\partial x} = 0; \quad (4.2.12c)$$

$$\text{at } x = L:$$

For cases I and II,

$$\frac{\partial T_s}{\partial x} = 0; \quad (4.2.12d)$$

For case III,

$$-k_s \frac{\partial T_s}{\partial x} = h_2(T_s - T_c) + \epsilon_2 \sigma(T_s^4 - T_c^4) \quad (4.2.12e)$$

In the mold:

$$\text{at } t = 0: \quad T_m = T_c; \quad (4.2.13a)$$

$$\text{at } y = Y_0: \quad k_s \frac{\partial T_s}{\partial y} = k_m \frac{\partial T_m}{\partial y}; \quad (4.2.13b)$$

$$\text{at } y = D:$$

For case I,

$$T_m = T_c = \text{Constant} \quad (4.2.13c)$$

For cases II and III,

$$-k_m \frac{\partial T_m}{\partial y} = h_1(T_m - T_c) + \epsilon_1 \sigma(T_m^4 - T_c^4) \quad (4.2.13d)$$

$$\text{at } x = 0: \quad \frac{\partial T_m}{\partial x} = 0 \quad (4.2.13e)$$

$$\text{at } x = L:$$

For cases I and II,

$$-\frac{\partial T_m}{\partial x} = 0; \quad (4.2.13f)$$

For case III,

$$-k_m \frac{\partial T_m}{\partial x} = h_2(T_m - T_c) + \varepsilon_2 \sigma (T_m^4 - T_c^4) \quad (4.2.13g)$$

4.2.4 Non-dimensionalization: To make the results more general and to transform the solution domain into a more tractable shape the equations are non-dimensionalized with the help of new coordinates x^* and y^* . The following non-dimensional parameters are defined.

$$\begin{aligned} x^* &= x/L; \quad y_1^* = y/Y_1(x, t); \quad t^* = \alpha_1 t/D^2; \\ u^* &= uD^2/\alpha_1 L; \quad v^* = vD/\alpha_1; \quad \psi^* = \psi D/\alpha_1 L; \\ \omega^* &= \omega D^3/\alpha_1 L; \quad T_1^* = (T_1 - T_c)/(T_i - T_c); \\ T_s^* &= (T_s - T_c)/(T_i - T_c); \quad y_s^* = \frac{y - Y_1(x, t)}{Y_0 - Y_1(x, t)}; \\ T_m^* &= (T_m - T_c)/(T_i - T_c); \quad y_m^* = (y - Y_0)/(D - Y_0); \end{aligned} \quad (4.2.14)$$

The key result of the non-dimensionalization is that the range of y_1^* (or y_s^* or y_m^*) extends from zero to one at all x^* during any time interval. The coordinates x^* and y^* become non-orthogonal as are the transformed coordinates in a conventional boundary layer analysis. Further the maximum range of temperature between the center line of the enclosure

and the mold outer surface becomes zero to one, during solidification.

Applying these non-dimensional parameters, Eqs.(4.2.5) to (4.2.13) get transformed to Eqs (4.2.15) to (4.2.23) (See Appendix V):

Energy equation in melt:

$$\frac{\partial T_1^*}{\partial t^*} + u^* \frac{\partial T_1^*}{\partial x^*} + v^* \left(\frac{D}{Y_1}\right) \frac{\partial T_1^*}{\partial y_1^*} = \left(\frac{D}{L}\right)^2 \frac{\partial^2 T_1^*}{\partial x^{*2}} + \left(-\frac{D}{Y_1}\right)^2 \frac{\partial^2 T_1^*}{\partial y_1^{*2}} \quad (4.2.15)$$

Vorticity equation:

$$\begin{aligned} \frac{\partial \omega^*}{\partial t^*} + u^* \frac{\partial \omega^*}{\partial x^*} + v^* \left(\frac{D}{Y_1}\right) \frac{\partial \omega^*}{\partial y_1^*} = & -\left(\frac{D}{L}\right) \left(\frac{D}{Y_1}\right) \left(\frac{D}{Y_0}\right)^3 RaPr \frac{\partial T_1^*}{\partial y_1^*} \\ & + \left(\frac{D}{L}\right)^2 Pr \frac{\partial^2 \omega^*}{\partial x^{*2}} + \left(\frac{D}{Y_1}\right)^2 Pr \frac{\partial^2 \omega^*}{\partial y_1^{*2}} \end{aligned} \quad (4.2.16)$$

where $Ra = \text{Rayleigh number}$

$$= \left(\frac{g\beta(T_1 - T_c)Y_0^3}{2\nu} \right) \left(\frac{\nu}{\alpha_1} \right)$$

and $Pr = \text{Prandtl number}$

$$= \nu / \alpha_1$$

Stream function equation:

$$\omega^* = -\left(\frac{D}{L}\right)^2 \frac{\partial^2 \psi^*}{\partial x^{*2}} - \left(\frac{D}{Y_1}\right)^2 \frac{\partial^2 \psi^*}{\partial y_1^{*2}} \quad (4.2.17)$$

Velocity equations:

$$u^* = \left(\frac{D}{Y_1}\right) \frac{\partial \psi^*}{\partial y_1^*} ; \quad v^* = - \frac{\partial \psi^*}{\partial x^*} \quad (4.2.18)$$

Energy equation in solid:

$$\frac{\partial T_s^*}{\partial t^*} = \frac{\alpha_s}{\alpha_l} \left[\left(\frac{D}{L} \right)^2 \frac{\partial^2 T_s^*}{\partial x^{*2}} + \left(\frac{D}{Y_o - Y_i} \right)^2 \frac{\partial^2 T_s^*}{\partial y_s^{*2}} \right] \quad (4.2.19)$$

Energy equation in mold:

$$\frac{\partial T_m^*}{\partial t^*} = \frac{\alpha_m}{\alpha_l} \left[\left(\frac{D}{L} \right)^2 \frac{\partial^2 T_m^*}{\partial x^{*2}} + \left(\frac{D}{D - Y_o} \right)^2 \frac{\partial^2 T_m^*}{\partial y_m^{*2}} \right] \quad (4.2.20)$$

The initial and boundary conditions become:

In the melt:

$$\text{at } t^* = 0: \quad T_l^* = 1 \quad (4.2.21a)$$

$$\text{at } y_l^* = 0: \quad \frac{\partial T_l^*}{\partial y_l^*} = 0; \quad -\frac{\partial u^*}{\partial y_l^*} = 0 \text{ and } v^* = 0 \quad (4.2.21b)$$

$$\text{at } y_l^* = 1: \quad T_l^* = 1/(1+\phi); \quad u^* = 0; \quad v^* = 0 \quad (4.2.21c)$$

$$\text{where } \phi = (T_i - T_{\text{sat}})/(T_{\text{sat}} - T_c)$$

and,

$$\begin{aligned} & \left[-\frac{k_s}{k_l} \frac{1}{(1-\delta(x^*, t^*))} \frac{\partial T_s^*}{\partial y_s^*} - \frac{1}{\delta(x^*, t^*)} \frac{\partial T_l^*}{\partial y_l^*} \right] \left[1 + \left(\frac{Y_o}{L} \right)^2 \left(\frac{\partial \delta}{\partial x^*} \right)^2 \right] \\ & = \text{Ste} \left(\frac{Y_o}{D} \right)^2 \frac{\partial \delta}{\partial t^*} \end{aligned} \quad (4.2.21d)$$

$$\text{where, } \delta(x^*, t^*) = Y'(x, t)/Y_o$$

and Ste = Stefan number

$$= L_q / C_p (T_i - T_c)$$

$$\text{at } x^* = 0: \quad \frac{\partial T_l^*}{\partial x^*} = 0; \quad (4.2.21e)$$

$$\text{at } x^* = 1: \quad u^* = 0; \quad v^* = 0 \quad (4.2.21f)$$

For cases I and II,

$$\frac{\partial T_1^*}{\partial x^*} = 0 \quad (4.2.21g)$$

For case III,

$$\frac{\partial T_1^*}{\partial x^*} = -[Bi_2 T_1^* + Rc_2 \{ (T_1^* + T_c^*)^4 - T_c^{*4} \}] \quad (4.2.21h)$$

where Bi_2 = Biot number at the top surface of the enclosure

$$= h_2 L / k_1$$

Rc_2 = Radiation constant at the top surface of the enclosure.

$$= \epsilon_2 \sigma L (T_i - T_c)^3 / k_1$$

$$T_c^* = T_c / (T_i - T_c)$$

In the solid:

$$\text{at } y_s^* = 0: \quad T_s^* = 1 / (1 + \phi) \quad (4.2.22a)$$

$$\text{at } y_s^* = 1: \quad T_s^* = T_n^* \quad (4.2.22b)$$

$$\text{at } x^* = 0: \quad \frac{\partial T_s^*}{\partial x^*} = 0 \quad (4.2.22c)$$

$$\text{at } x^* = 1:$$

For cases I and II,

$$\frac{\partial T_s^*}{\partial x^*} = 0 \quad (4.2.22d)$$

For case III,

$$\frac{\partial T_s^*}{\partial x^*} = -\left(\frac{k_l}{k_s}\right) [Bi_2 T_s^* + Rc_2 \{ (T_s^* + T_c^*)^4 - T_c^{*4} \}] \quad (4.2.22e)$$

In the mold:

$$\text{at } t^* = 0: \quad T_m^* = 0 \quad (4.2.23a)$$

$$\text{at } y_m^* = 0: \quad \frac{k_s}{k_m} \frac{\partial T_s^*}{\partial y_s^*} = \left(\frac{Y_o - Y'(x, t)}{Y_o - Y_o} \right) \frac{\partial T_m^*}{\partial y_m^*} \quad (4.2.23b)$$

$$\text{at } y_m^* = 1:$$

For case I,

$$T_m^* = 0 \quad (4.2.23c)$$

For cases II and III,

$$\frac{\partial T_m^*}{\partial y_m^*} = - [Bi_1 T_m^* + Rc_1 \{ (T_m^* + T_c^*)^4 - T_c^{*4} \}] \quad (4.2.23d)$$

where Bi_1 = Biot number at the mold outer surface

$$= h_1 d / k_m$$

Rc_1 = Radiation constant at the mold outer surface.

$$= \epsilon_1 \sigma d (T_i - T_c)^3 / k_m$$

$$\text{at } x^* = 0:$$

$$\frac{\partial T_m^*}{\partial x^*} = 0 \quad (4.2.23e)$$

$$\text{at } x^* = 1$$

For cases I and II,

$$\frac{\partial T_m^*}{\partial x} = 0 \quad (4.2.23f)$$

For case III,

$$-\frac{\partial T_m^*}{\partial x} = -\left(\frac{k_l}{k_m}\right) [Bi_2 T_m^* + Re_2 \{ (T_m^* + T_c^*)^4 - T_c^{*4} \}] \quad (4.2.23g)$$

4.3 SOLUTION METHODOLOGY:

The crux of the problem lies in solving the simultaneous, partial differential Eqs (4.2.15) - (4.2.20) for the boundary conditions given in Eqs (4.2.21) - (4.2.23). It is evident that the problem cannot be solved analytically because of the complexity and the non-linear nature of the equations. This leads to the obvious choice of numerical methods.

In the computational model it has been assumed that there is a small time lag between the heat withdrawn at the interface and the resulting interface motion. Specifically, during a small interval of time, the fluid flow in the melt and the heat transfer in the melt, solid and the mold were solved assuming interface to be stationary. The heat transferred to the interface during this interval was then used to compute the small finite displacement associated with the solidification. With the new domains for the melt and the solid, which correspond to the displaced interface, the

solution for the next time interval was performed as just described. The nature of Eqs (4.2.15) - (4.2.23) implies that the methodology of solving them can be divided into four sections, viz,

- (i) Solution of vorticity and energy equations
which are parabolic in nature *with respect to time*.
- (ii) Solution of elliptic stream function
equation.
- (iii) Boundary conditions for the vorticity
equations.
- (iv) Solution of moving interface equation.

4.3.1 Vorticity and Energy Equations: The parabolic, vorticity and energy equations were solved using the Alternating Direction Implicit (ADI) technique introduced by Peaceman and Rachford (1955). This method was particularly chosen as it has been found suitable for solving similar kinds of problems by Wilkes and Churchill (1966) and, Szekely and Todd (1971). Also known as the method of variable direction, the method makes use of splitting the time step to obtain an implicit method which requires only the inversion of a tridiagonal matrix. The non-linear convective terms were written in their central difference forms as both the forward and backward forms led to numerical instability. For high Rayleigh numbers ($Ra \geq 10^5$) the convective terms were modified using 'Second upwind differencing method' (see Appendix VI)

as the program became numerically unstable. The tridiagonal matrix formed was solved using 'General Tridiagonal Algorithm' discussed by Roache (1976). The accuracy of the grid size and the time steps was checked by doing the calculations for different grid sizes and time step. For example, computations were done for $Ra = 10^3$, by choosing grid sizes of 10×10 , 12×12 , 15×15 and 20×20 . The variation in the results for the first three cases was less than 1 per cent. In the last case, the variation is about 3 percent which is due to round-off errors. The computational time depends upon the grid size chosen. For $Ra = 10^3$, when the grid size was 10×10 , the CPU time was 180 sec. for $t^* = 0.27$; for $Ra = 10^6$, the grid size was 50×50 and the CPU time was 900 sec. upto $t^* = 0.18$. An example of the ADI algorithm written for the velocity Eqn. (4.2.16) is shown in Appendix VII.

4.3.2 Stream Function Equation: The elliptic stream function Eqn. (4.2.17) was solved using Successive Over-Relaxation (SOR) method discussed by Forsyth and Wasow (1969). This method was particularly chosen as the convergence rate was faster than the other methods such as Southwell's residual relaxation method, Gauss-Seidel iteration method etc. Eqn. (4.2.17), when written in finite - difference form gives,

$$\omega_{i,j} = \left[\left(\frac{D}{L} \right)^2 \left(\frac{\psi_{i-1,j} - 2\psi_{i,j} + \psi_{i+1,j}}{(\Delta x)^2} \right) + \left(\frac{D}{Y_1} \right)^2 \right. \\ \left. \left(\frac{\psi_{i,j-1} - 2\psi_{i,j} + \psi_{i,j+1}}{(\Delta y)^2} \right) \right] \quad (4.3.1)$$

This can be simplified to give,

$$\psi_{i,j}^{k+1} = \psi_{i,j}^k + \frac{\Omega_{opt}}{2(\gamma_1 + \gamma_2)} \left[\gamma_1 \psi_{i-1,j}^{k+1} + \gamma_2 \psi_{i,j-1}^{k+1} \right. \\ \left. + \gamma_1 \psi_{i+1,j}^k + \gamma_2 \psi_{i,j+1}^k + \omega_{i,j} (\Delta y)^2 - 2(\gamma_1 + \gamma_2) \psi_{i,j}^k \right] \quad (4.3.2)$$

where

$$\gamma_1 = \left(\frac{\Delta y}{\Delta x} \right)^2 \left(\frac{D}{L} \right)^2$$

$$\gamma_2 = \left(\frac{D}{Y_1} \right)^2$$

i, j denote space while k denotes iteration step. In Eqs. (4.3.1) and (4.3.2) the superscript $*$ is omitted in ψ , ω , Δx and Δy for convenience. Convergence is assumed when $|\psi_{i,j}^{k+1} - \psi_{i,j}^k| = 0.001$.

Ω_{opt} is the optimum relaxation factor, the value of which is to be found by trial and error. For this particular problem $\Omega_{opt} = 1.5$.

4.3.3 Vorticities at Boundaries:

Special attention has to be given to the vorticities at the boundaries as these values are not known explicitly.

If $\psi_{w,j}$ is the stream function at the wall, expansion of $\psi_{w,j}$ by the Taylor series gives,

$$\psi_{w-1,j} = \psi_{w,j} + \left. \frac{\partial \psi}{\partial x} \right|_{w,j} \Delta x + \frac{1}{2} \left. \frac{\partial^2 \psi}{\partial x^2} \right|_{w,j} (\Delta x)^2 + O(\Delta x)^3 \quad (4.3.3)$$

and,

$$\left. \frac{\partial \psi}{\partial x} \right|_{w,j} = v \Big|_{w,j} = 0 \quad (\text{no slip condition}) \quad (4.3.4)$$

$$\psi_{w,j} = 0 \quad (4.3.5)$$

Thus Eqn.(4.3.3) becomes,

$$\psi_{w-1,j} = \frac{1}{2} \left. \frac{\partial^2 \psi}{\partial x^2} \right|_{w,j} (\Delta x)^2 \quad (4.3.6)$$

From the stream function Eqn.(4.2.17)

$$\omega_{w,j} = - \left(\frac{D}{L} \right)^2 \left. \frac{\partial^2 \psi}{\partial x^2} \right|_{w,j} \quad \left(\because \left. \frac{\partial^2 \psi}{\partial y^2} \right|_{w,j} = 0 \right) \quad (4.3.7)$$

Substituting Eqn.(4.3.6) in Eqn. (4.3.7),

$$\omega_{w,j} = - \left(\frac{D}{L} \right)^2 \frac{2 \psi_{w-1,j}}{(\Delta x)^2} \quad (4.3.8)$$

$\psi_{w-1,j}$ is the interior stream function discussed in Section 4.3.2. The vorticity values calculated using higher order terms of the Taylor series were found to create stability problems. This is in confirmation with Samuels and Churchill (1967) who have reported similar problems.

4.3.4 Moving Boundary Equation: The moving boundary Eqn. (4.2.21d) is a cubic polynomial similar to the one described in Chapter III. This has been solved using Chebyshev approximation discussed by Carnahan, Luther and Wilkes (1969).

4.3.5 Choice of Grid System: The choice of grid system is very important in two dimensional solidification problems as the interface is moving with respect to time, the shape of which is not known. In most of the conduction based problems Cartesian grid system has been chosen for computation. Figure 4.2a illustrates Cartesian grid of points formed between the interface and the other boundaries in the melt and the solid. This may be regarded as the most obvious choice of the grids; yet it has the following disadvantages:

- (i) It puts only a few points in the melt wherever that is thin (i.e. at the bottom of the enclosure) and so cannot provide high accuracy there. If more points are provided in those regions, it increases storage space and computation time enormously.
- (ii) Calculation of the grid length near the interface is complex.

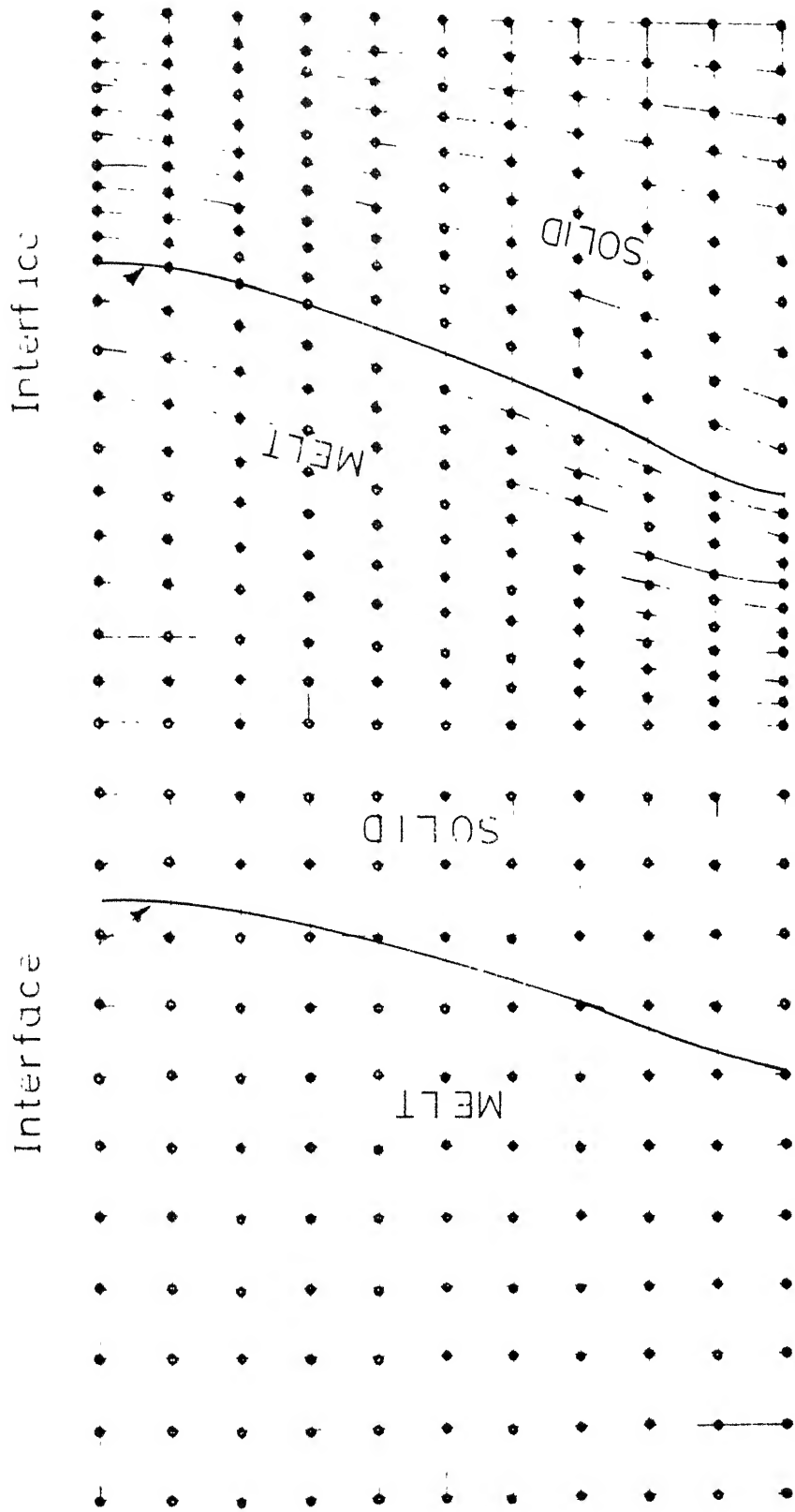


Fig.4.2a Cartesian grid system

(iii) Very few grid points can be provided in the solid region during initial stages of solidification.

This led to the choice of a new grid system described by Patankar and Spalding (1967). Figure 4.2b illustrates the grid system adopted for the present problem. In the x^* coordinate, the length of the enclosure has been divided into grids of equal size. At any instant of time and for any x^* , the width of the melt or solid region has been divided into equal number of grids. This method of division of grids is devoid of all the disadvantages mentioned for the Cartesian grids and has been successfully used by Spalding (1977) in solving boundary layer problems. Spatial grids of 10×10 were established, each for the melt, solid and mold. For $Ra \geq 10^5$ closer grid was provided to take care of the stability problems.

4.3.6 Computational Steps: The following steps were adopted in solving Eqs.(4.2.15) - (4.2.23).

(i) At time $t^*=0$, the initial values of T_l^* , T_s^* , T_m^* , ω^* , ψ^* , u^* and v^* were established.

(ii) At any intermediate time, thickness of the solid formed was calculated through Eqn.(4.2.21d). The temperature gradients involved in Eqn. (4.2.21d) were calculated using the temperature fields known from previous time steps. The field variables T^* , ψ^* , ω^* , u^* and v^* were redefined for every time step to take cognizance of the change in the relationship between the physical and transformed plane. At any time step, the re-evaluation of

these variables in the grid points was done by interpolating through the known values of the previous time step grid points using Lagrange formula of interpolation. To conserve the momentum the interpolation of the variables was performed by first evaluating the stream function at the locations of the interest and then differentiating it. Similarly the temperature was interpolated through the evaluation of the enthalpy.

(iii) For the known values of velocities, the temperature was advanced by one time step by solving Eqn.(4.2.15) using ADI technique.

(iv) From the temperature, estimated through step (iii), interior vorticity field was calculated through Eqn.(4.2.16) using the ADI technique. The boundary vorticity values computed for the previous time step were used for the calculation.

(v) The stream function Eqn.(4.2.17) was then solved using SOR method.

(vi) The boundary vorticities were then calculated using the stream function computed via step (v).

(vii) From the stream function, the velocity components were calculated.

(viii) The last step in the computation involved the calculation of temperature fields in the solid and the mold through Eqs. (4.2.19) and (4.2.20), respectively.

The computational cycle was repeated until desired time or desired amount of solidification was reached.

Schematically, the computational procedure is illustrated in Figure 4.3. A listing of the computer program used on DEC 1090 computer is available with author.

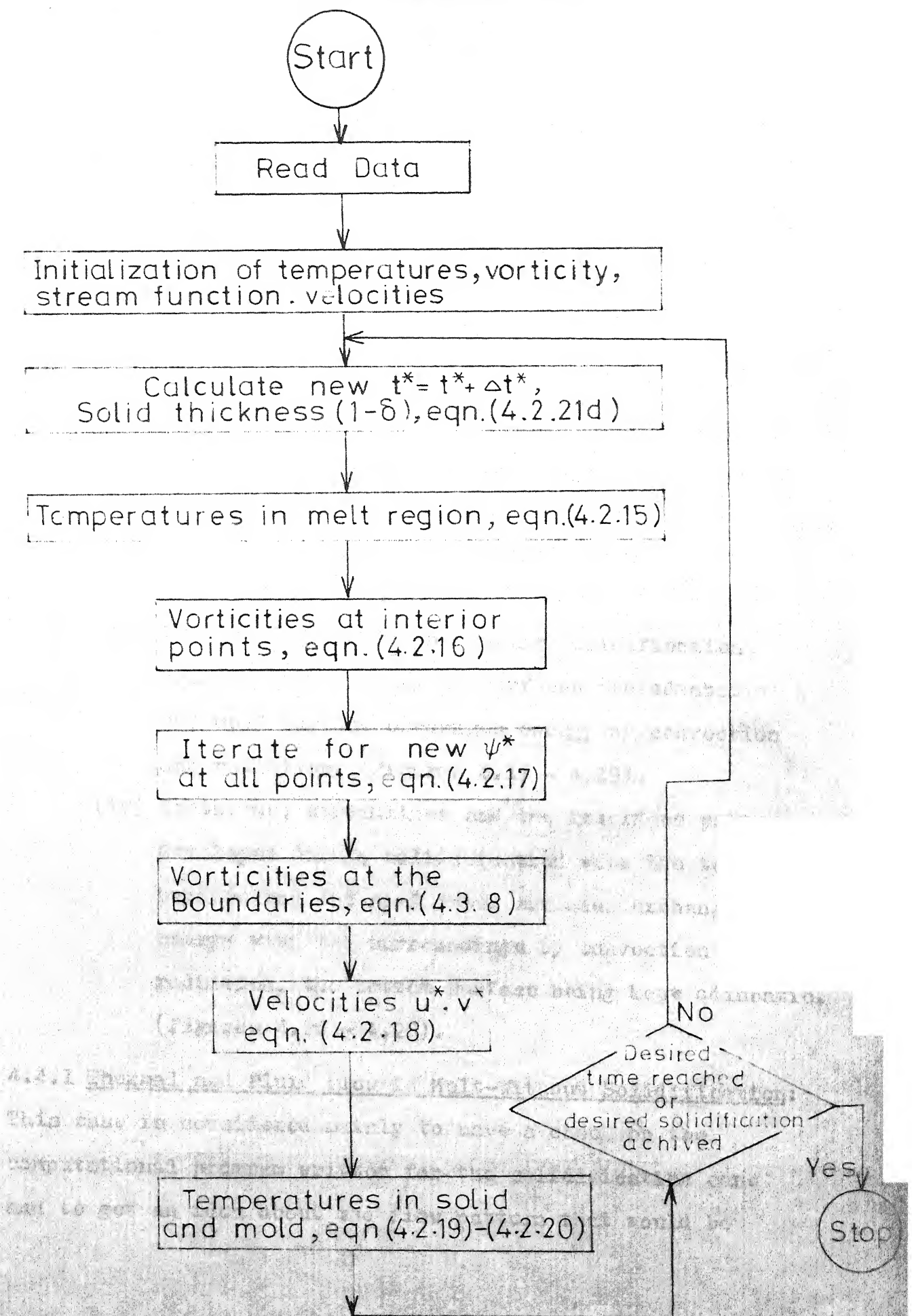


Fig. 4.3 Flow chart for the computation cycle

4.4 RESULTS AND DISCUSSION:

The following results are presented:

- (i) Isotherm and streamline patterns developed in a rectangular enclosure, in which the melt does not solidify at any time. (Figures 4.4 - 4.6).
- (ii) Temperature and velocity patterns and interface movement developed in a rectangular enclosure in which solidification occurs. The top and bottom of the enclosures are kept adiabatic and mold outer surface is kept at a constant temperature. (Figures 4.7 - 4.16).
- (iii) The interface movement during solidification when the top and bottom surfaces are adiabatic and mold surface exchanges energy by convection and radiation. (Figures 4.17 - 4.19).
- (iv) Isotherms, streamlines and the interface patterns developed during solidification when the top surface and the mold outer surfaces exchange energy with the surroundings by convection and radiation, the bottom surface being kept adiabatic. (Figures 4.20 - 4.28).

4.4.1 Thermal and Fluid Flow in Melt-Without Solidification:

This case is considered mainly to have a check on the computational program written for the solidification case and to get an idea about the flow pattern that would be

developed due to temperature gradients.

Figure 4.4 represents the transient streamlines and isotherms when the top and bottom surfaces of the enclosure are kept adiabatic while the sides are kept at a constant temperature. Figure 4.5 shows the streamlines and isotherms when the top surface is cooled by convection and radiation, sides at a constant temperature, the bottom being adiabatic. The hot fluid rises up near the center of the enclosure and the cold fluid comes down near the side walls where the temperature is minimum. The flow pattern for $Ra = 10^3$ reveals a rolling vortex centered at approximately $x^* = 0.5$, $y^* = 0.5$. The maximum value of the stream function ψ_{\max} occurs at the center of this vortex. As the Rayleigh number increases the vortex center moves to the right-hand side. At very high Rayleigh number ($Ra = 10^8$), the entire enclosure is more or less occupied by the rising hot fluid. The streamlines near the wall move closer together as a result of high flow in this region.

At low Rayleigh numbers, the isotherms are almost vertical indicating the predominance of conduction. The isotherms take an inward turn at the top when the enclosure is cooled from the top, as shown in Figure 4.5. As the Rayleigh number increases, isotherms deviate from the vertical position as convection starts to play a major role.

Figure 4.6 represents the streamlines pattern when a fluid of $Pr=1$, is heated in a rectangular enclosure. A

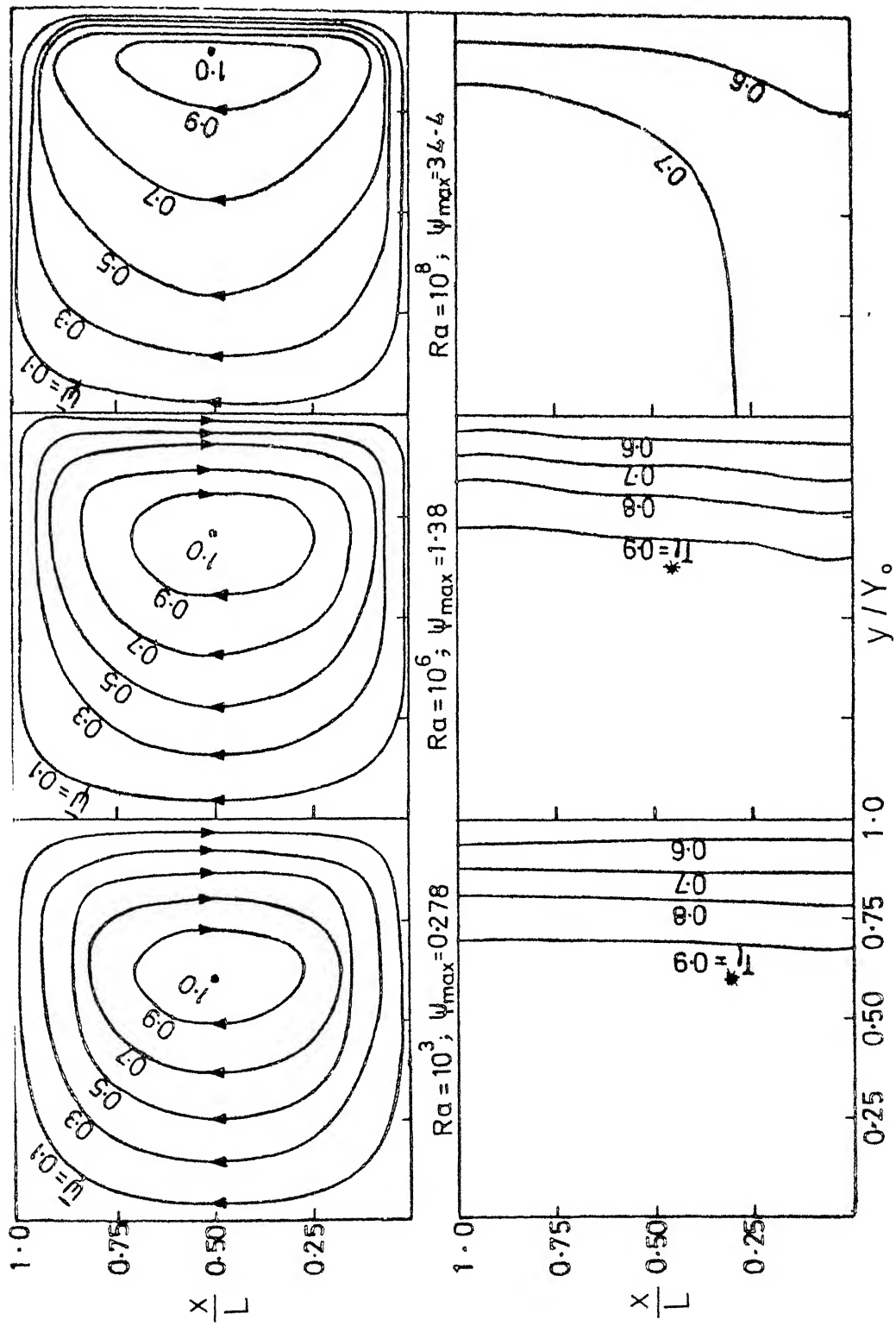


Fig.4.4 Streamlines and isotherms for different Rayleigh numbers at $t^* = 0.027$ — without solidification, top and bottom surfaces adiabatic, sides at a constant temperature

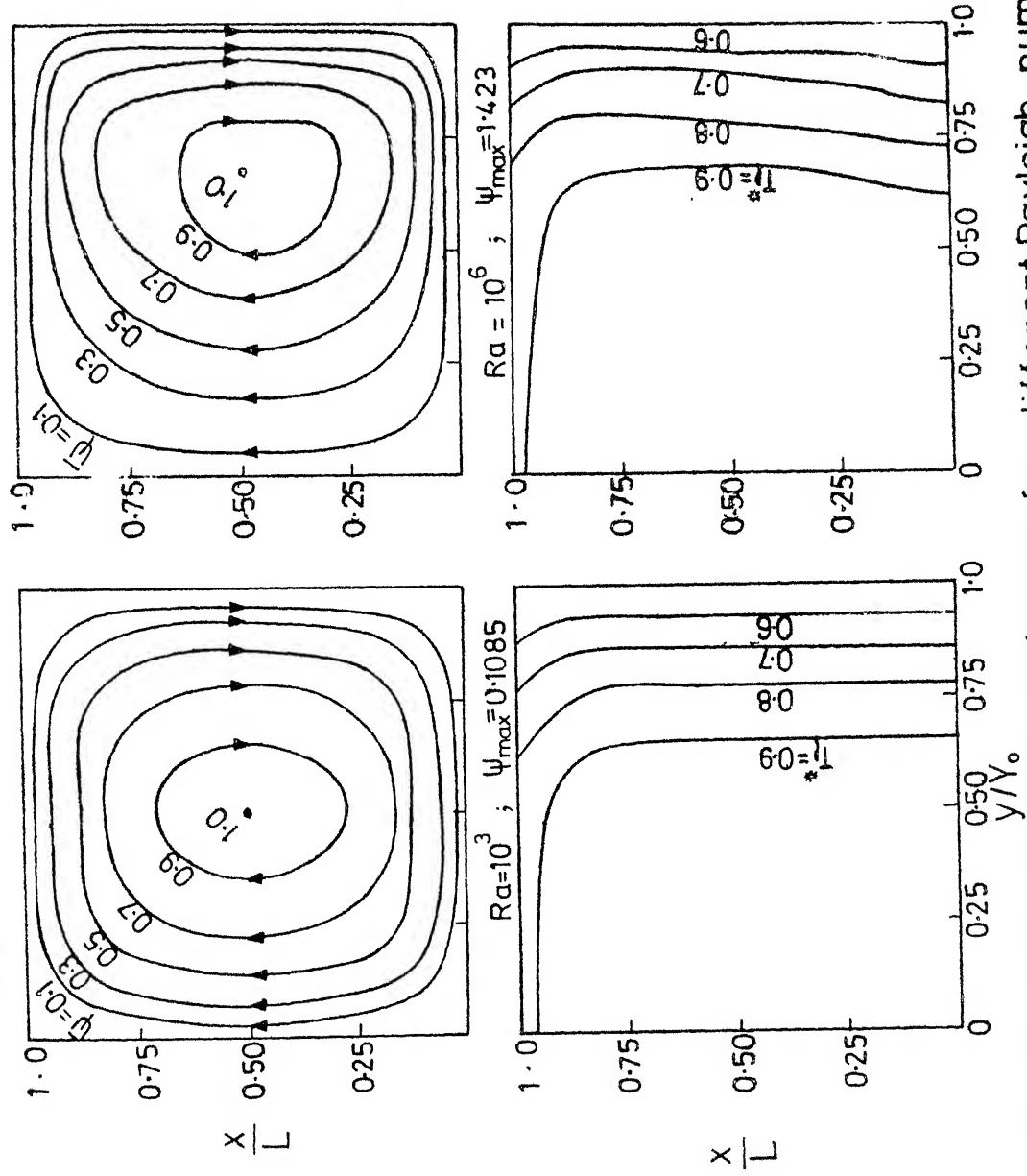


Fig.4.5 Streamlines and isotherms for different Rayleigh numbers at $t^* = 0.027$ - without solidification, bottom surface adiabatic, top surface convecting and radiating, sides at a constant temperature

$$Ra = 5000$$

$$Pr = 1.0$$

$$t^* = 0.05$$

$$\text{At } t^* = 0, T_1^* = 0$$

$$\text{At } t^* > 0, T_1^* = 0.5 \text{ at } y = Y_0 \text{ (heating)}$$

— Present work

• Szekely and Todd (1971)

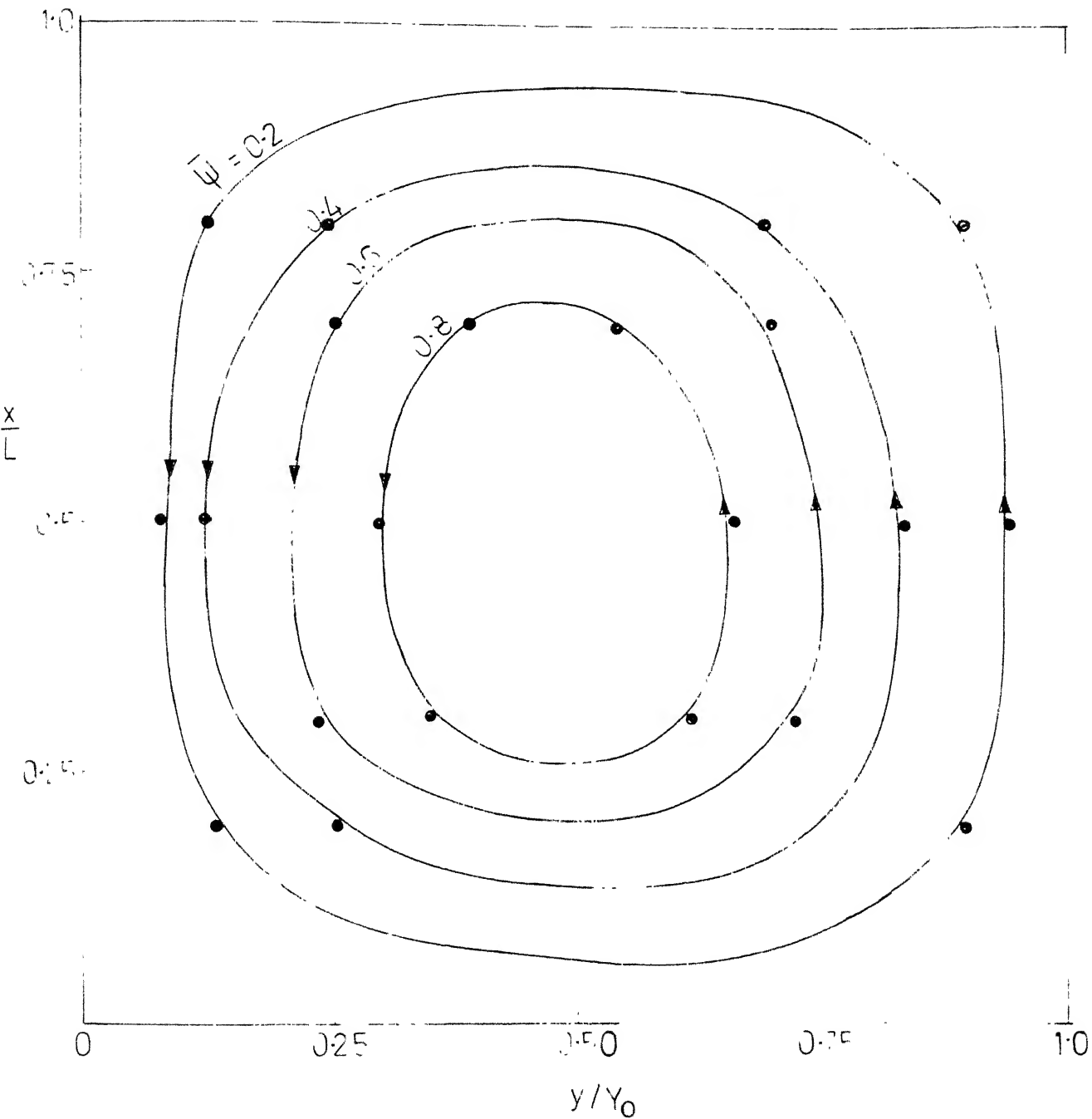


Fig. 4.6 Comparison of the streamlines of present work with literature—without solidification

comparison of the results, obtained from the present numerical scheme with the results reported by Szekely and Todd (1971) shows a reasonably good agreement.

4.4.2 Thermal and Fluid Flow in Melt-with Solidification, Top and Bottom of the Enclosure Adiabatic, Mold Wall at a Constant Temperature:

The temperature profiles in the melt, the solid and the mold at various heights, with non-dimensional time t^* as the parameter are shown in Figure 4.7. As the time progresses the temperature decays in the melt. The temperature of the melt is found to increase with the height because of the natural convection developed in the melt. Initially, the temperature variation with the height of the enclosure is very little since conduction is dominating. Subsequently, natural convection currents are developed due to thermal gradients, which in turn take the hotter melt to the top of the enclosure driving the cooler melt to the bottom.

The time dependent velocity profiles in the melt are shown in Figure 4.8. The velocity profiles are symmetric about $y^* = 0$ and the net upward flow equals the net downward flow. With the progress in solidification, the vertical velocity of the melt increases, reaches a maximum value at some intermediate time and then decays. At time $t^* = 0.03$, the convection currents have just set in. The velocity near the top ($x/L = 0.9$) and near the bottom ($x/L = 0.1$) of the enclosure is found to be the same, and the melt-solid

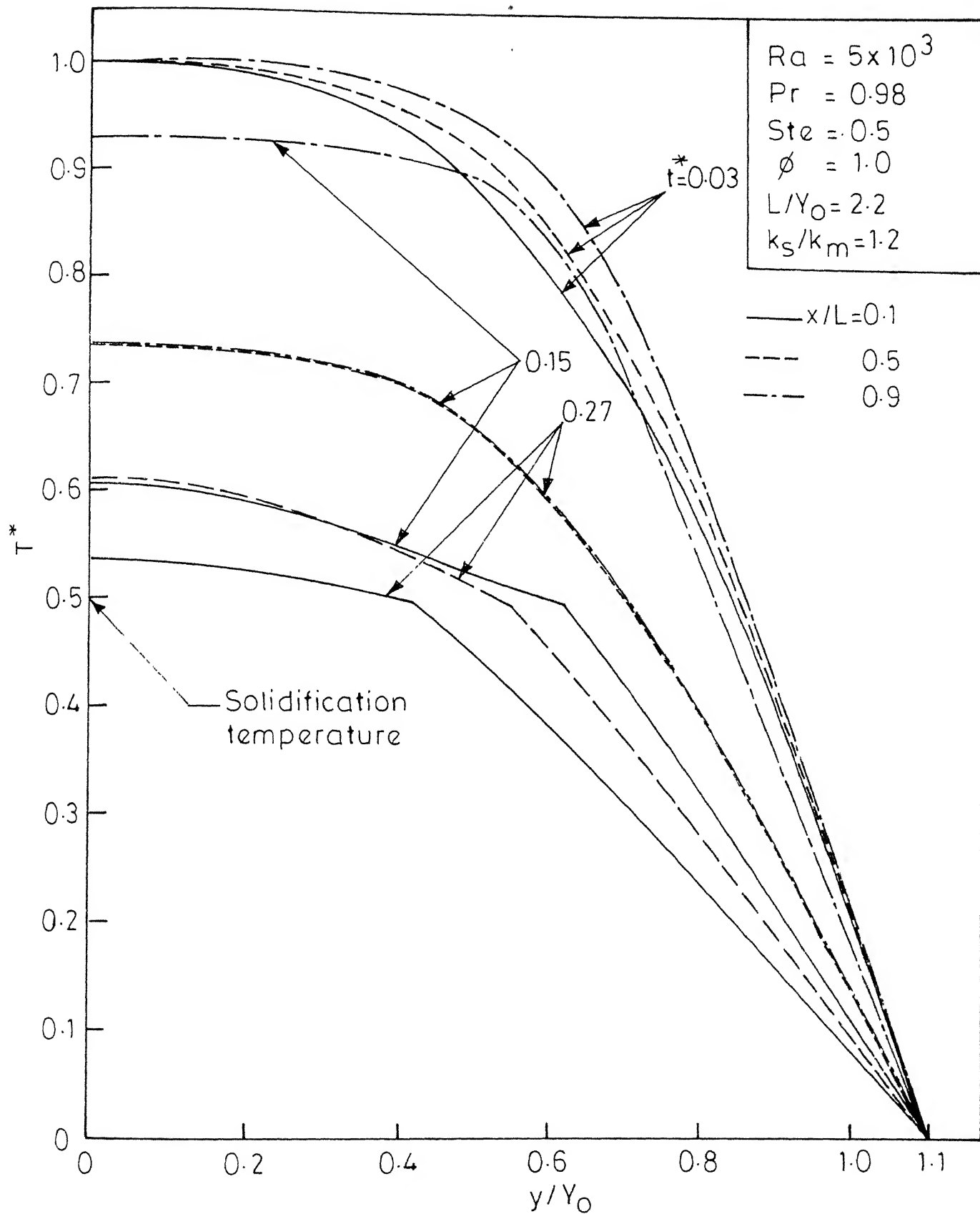


Fig.4.7 Temperature distributions in the three regions, at different X^* , for constant temperature at the outer surface of the mold and adiabatic at top and bottom of the enclosure.

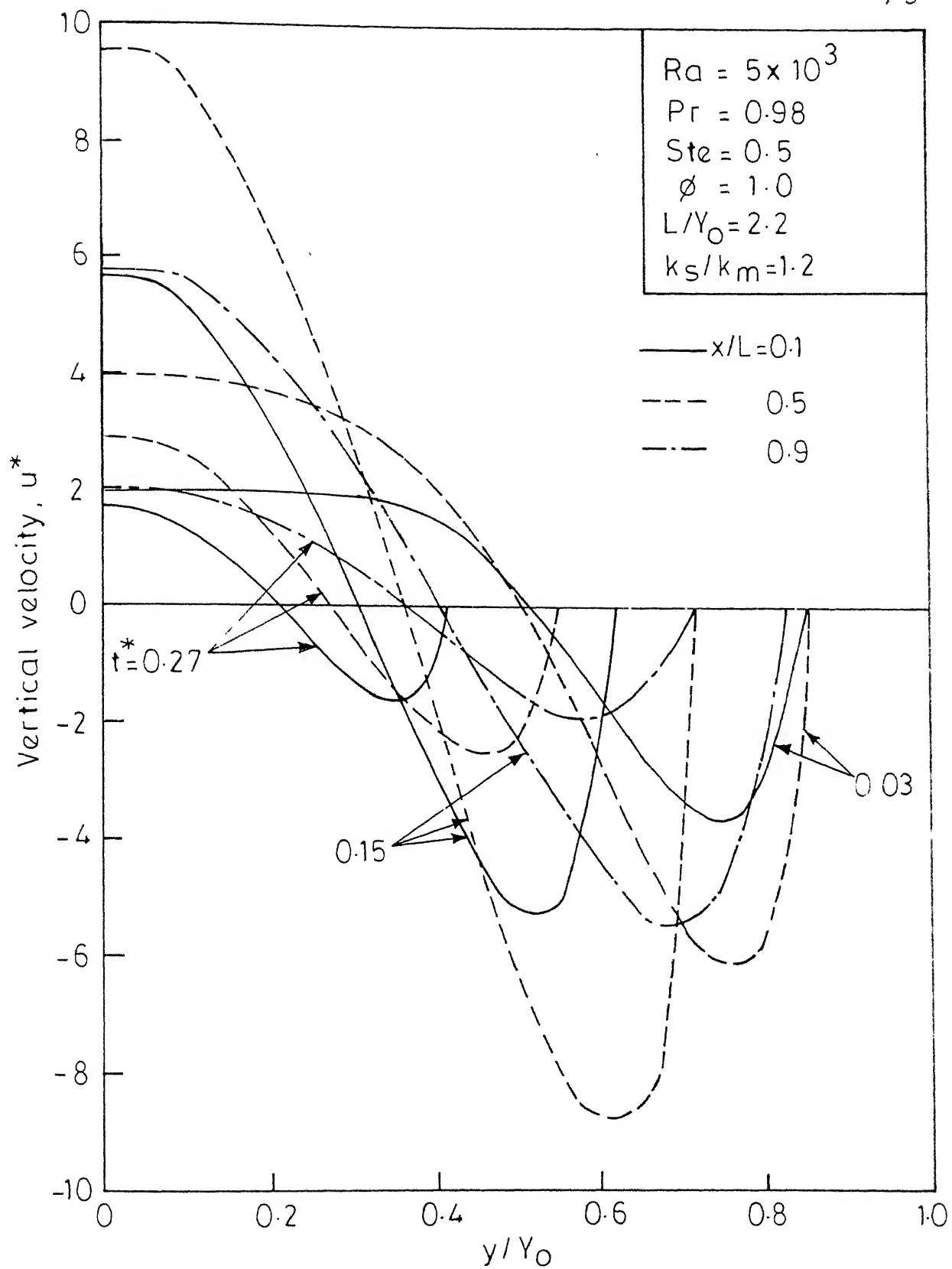


Fig. 4. 8 Vertical velocity distribution in the melt at different X^* .

interface is almost parallel to the wall. As solidification progresses, the slope of the interface changes, and the velocity near the top becomes more than that near the bottom surface of the enclosure. A comparison of Figures 4.7 and 4.8 at equal heights but different times indicates that the thermal field and the fluid motion decay almost at equal rates. This is true since $Pr=0.98$, which implies that the thermal and momentum diffusivities are nearly equal.

The streamlines and isotherms for the Rayleigh number 5×10^3 and at time $t^*=0.27$ are shown in Figures 4.9 and 4.10 respectively. The flow pattern during early stages of solidification is very nearly similar to the one reported in Section 4.4.1 and is not reported here for brevity. From Figure 4.9 it can be easily observed that the general characteristic of the flow pattern is upflow near the center of the enclosure, where the melt is hotter and downflow near the melt-solid interface where the melt is cooler. Both the streamlines and isotherms indicate that at larger time, the thickness of the melt layer is greatest at the top and least at the bottom of the enclosure. It is interesting to note that the streamlines of higher values are restricted to the top portion of the enclosure where the temperature and hence the flow is maximum. At high Rayleigh number ($Ra = 5 \times 10^5$) secondary cells are observed near the center of

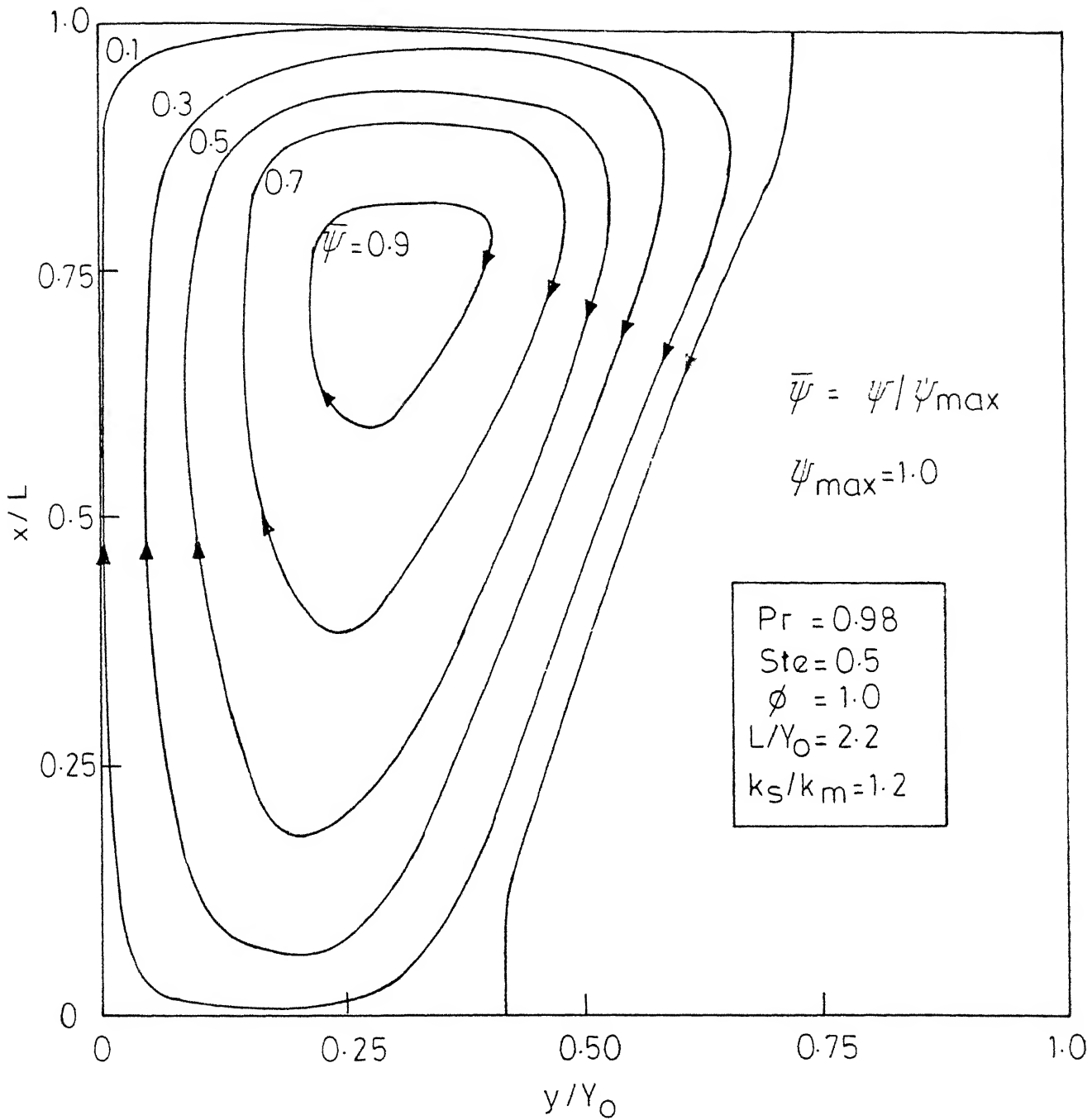


Fig.4.9 Streamline pattern in the melt for $Ra = 5 \times 10^3$ and $t^* = 0.27$, for constant temperature at the mold surface, adiabatic at top and bottom of the enclosure.

the enclosure during initial period of solidification as shown in Figure 4.11.

An examination of Figure 4.10 would indicate the predominance of the natural convection where the isotherms are non-linear, contrary to the linear vertical isotherms one would expect in the case of pure conduction. Isotherms of higher values are concentrated near the top surface of the enclosure where the temperature is maximum.

The dependence of the interface movement on the Rayleigh number is shown in Figure 4.12. At low Rayleigh number ($Ra = 5 \times 10^2$) where the natural convection is minimum, the shape of the interface is found to be almost vertical and parallel to the mold. As Ra approaches zero, the interface will be exactly vertical since conduction is the only mode of heat transfer then. As Ra increases heat transfer due to convection increases and the slope of the interface changes (Figure 4.12). At low and moderate Rayleigh numbers the computation is carried upto non-dimensional time $t^* = 0.30$, whereas for high Rayleigh numbers, the computation is restricted to a time $t^* = 0.18$, due to enormous computation time required in the latter case.

The movement of the interface with time t^* , for different aspect ratios ($L/2Y_0 = 1.1$ and 5.5) is shown in Figure 4.13. At low aspect ratio, where the convection is maximum, the slope of the interface is high and it increases

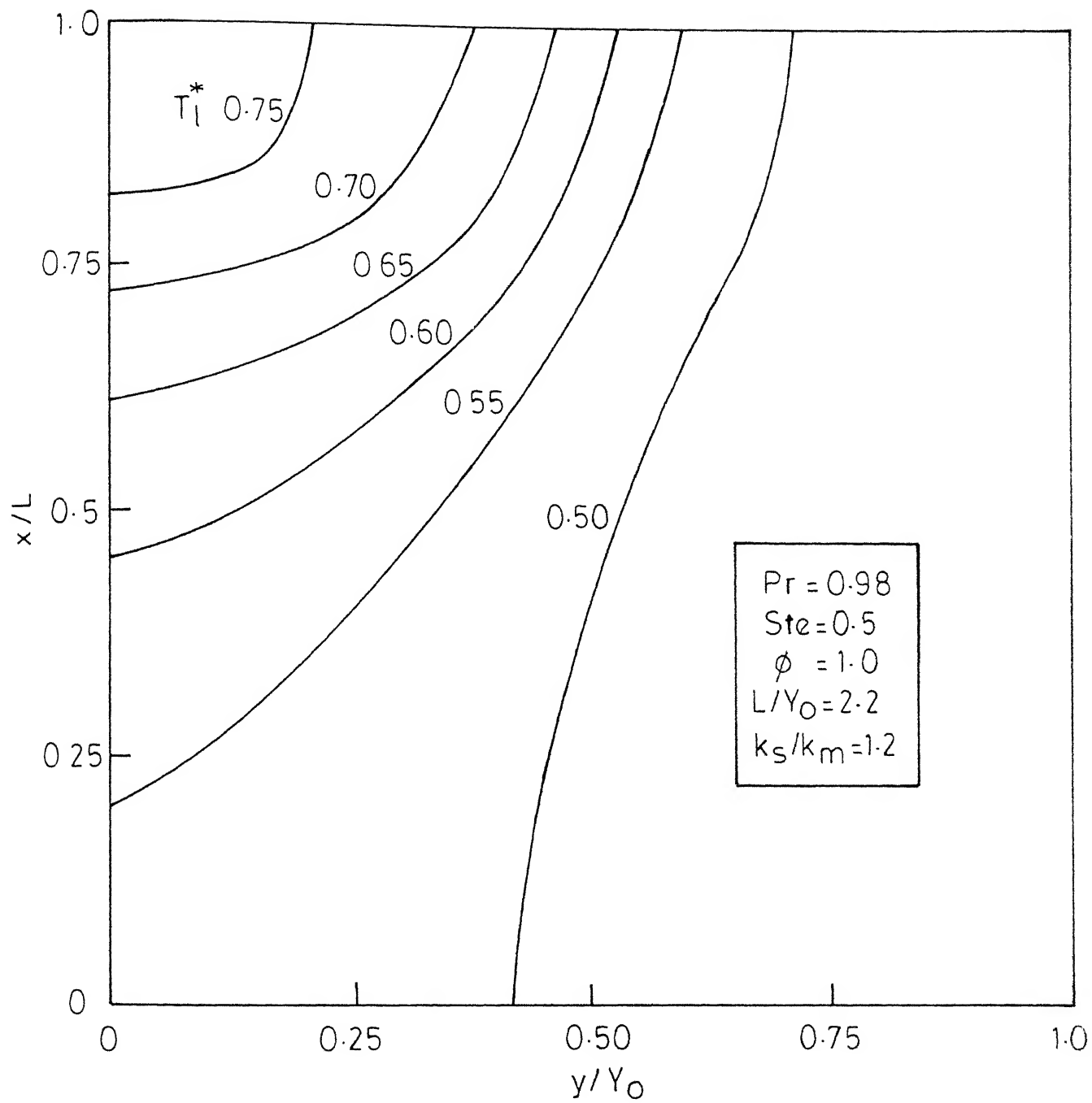


Fig. 4.10 Isotherm pattern in the melt for $Ra = 5 \times 10^3$ and $t^* = 0.27$, for constant temperature at mold outer surface, adiabatic at top and bottom of the enclosure

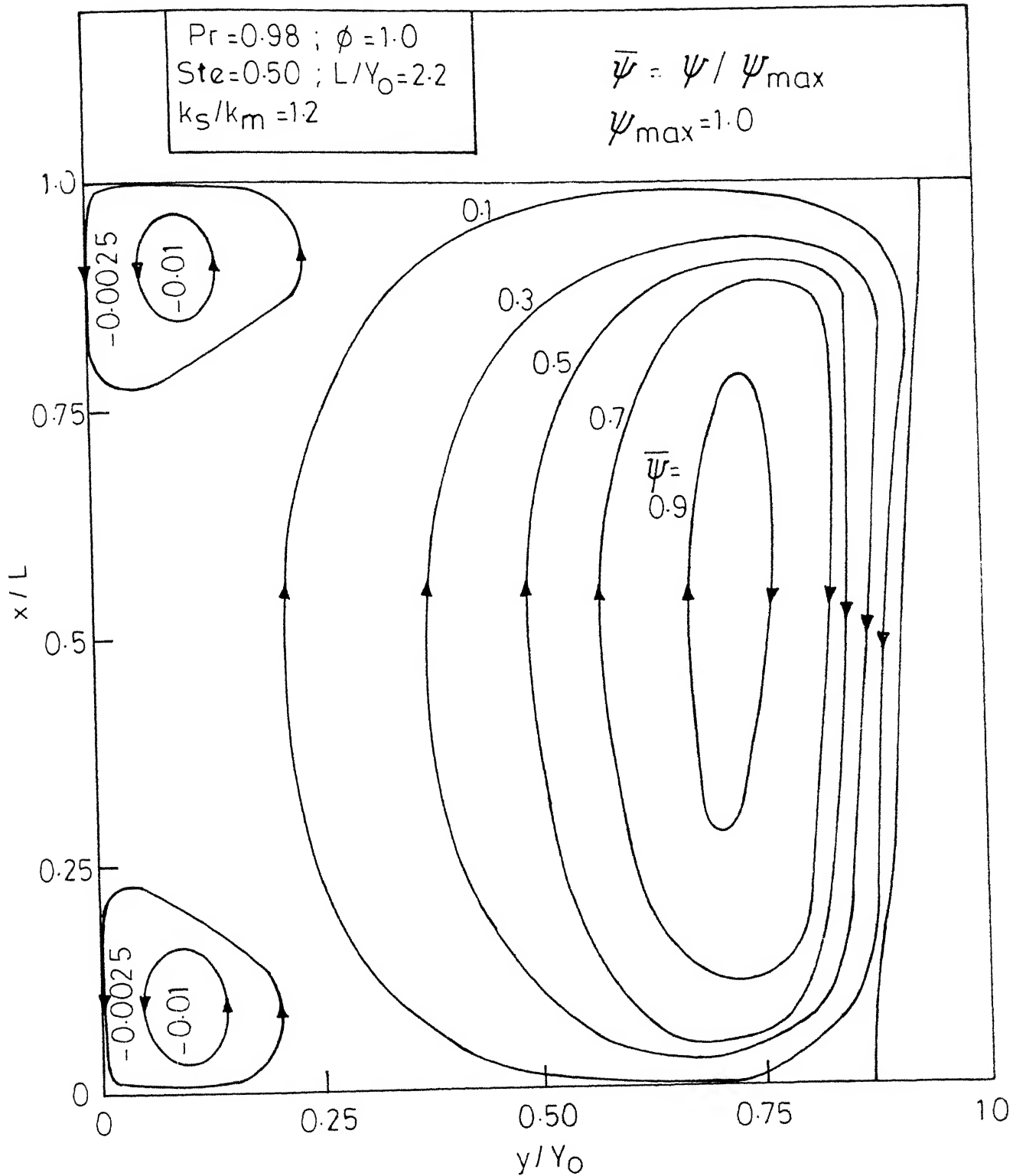


Fig. 4.11 Streamline pattern in the melt for $Ra = 5 \times 10^5$ and $t^* = 0.03$, for constant temperature at mold surface, adiabatic at the top and bottom of the enclosure

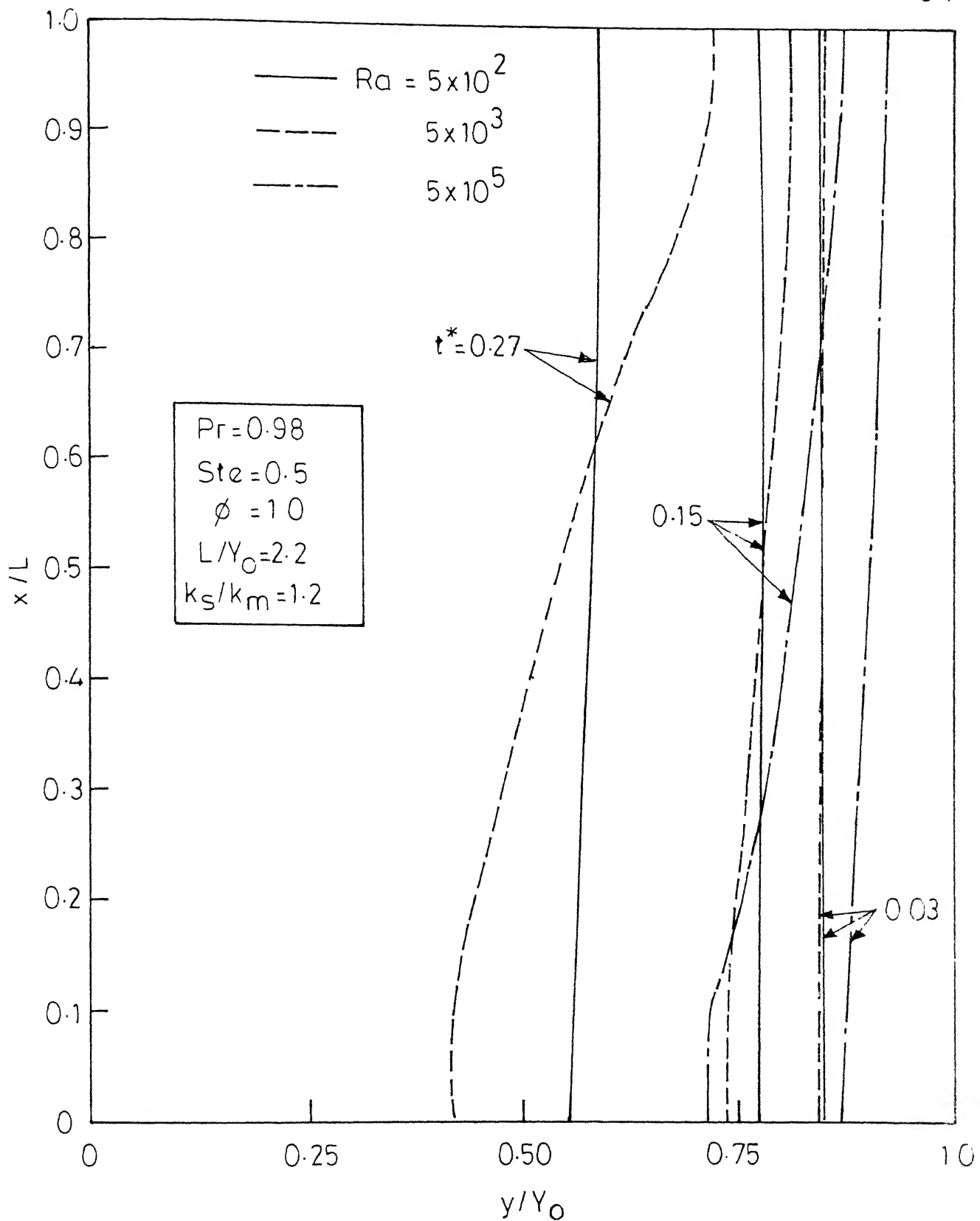


Fig.4.12 Dependence of the interface movement on Rayleigh number at different time, for constant temperature at mold surface, adiabatic at top and bottom of the enclosure

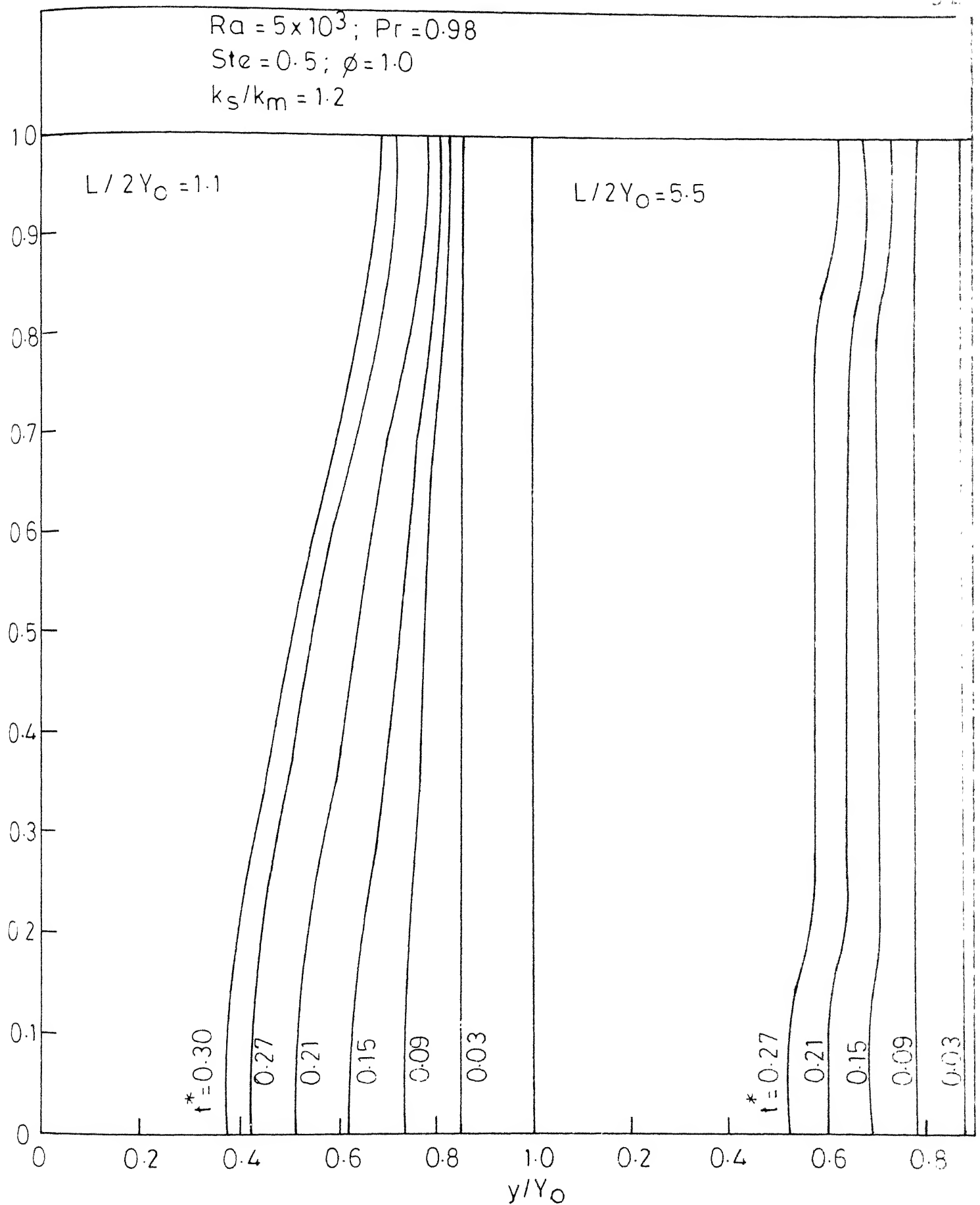


fig.4.13 Interface movement at various time intervals, for L/D ratios of 2.0 and 10.0, for constant temperature at the mold surface, adiabatic at the top and bottom of the enclosure

with time. At high aspect ratio, the interface is almost vertical except near the top and bottom of the enclosure, where the boundary effects start influencing the shape of the interface. Ramachandran, Gupta and Jaluria (1981b) suggest that one can assume the heat transfer to be unidirectional when the aspect ratio is high.

The influence of Prandtl number (Pr) on the interface movement is shown in Figure 4.14. As Pr increases the interface slope increases upto Pr=10. Interestingly, Prandtl number greater than 10 does not have any influence on the interface movement and an asymptotic solution is reached. This supports the results obtained by Sparrow, Patankar and Ramadhyani (1977). This behaviour can be better understood from the vorticity Eqn.(4.2.16), which can be simplified for high Prandtl number as:

$$\left(\frac{D}{L}\right)^2 \frac{\partial^2 \omega^*}{\partial x^{*2}} + \left(\frac{D}{Y_1}\right)^2 \frac{\partial^2 \omega^*}{\partial y_1^{*2}} = \left(\frac{D}{L}\right) \left(\frac{D}{Y_1}\right) \left(\frac{D}{Y_0}\right)^3 Ra \frac{\partial T_1^*}{\partial y_1^*} \quad (4.4.1)$$

It is important to note that the solution of Eqn.(4.4.1) is much simpler than the parabolic vorticity Eqn.(4.2.16).

The effect of Stefan number (Ste) on the rate of interface movement is shown in Figure 4.15. The melt-solid interface is found to proceed faster when Ste is small, as expected.

The dependence of the solidification on superheat(ϕ) is given in Figure 4.16, where the thickness of the solid

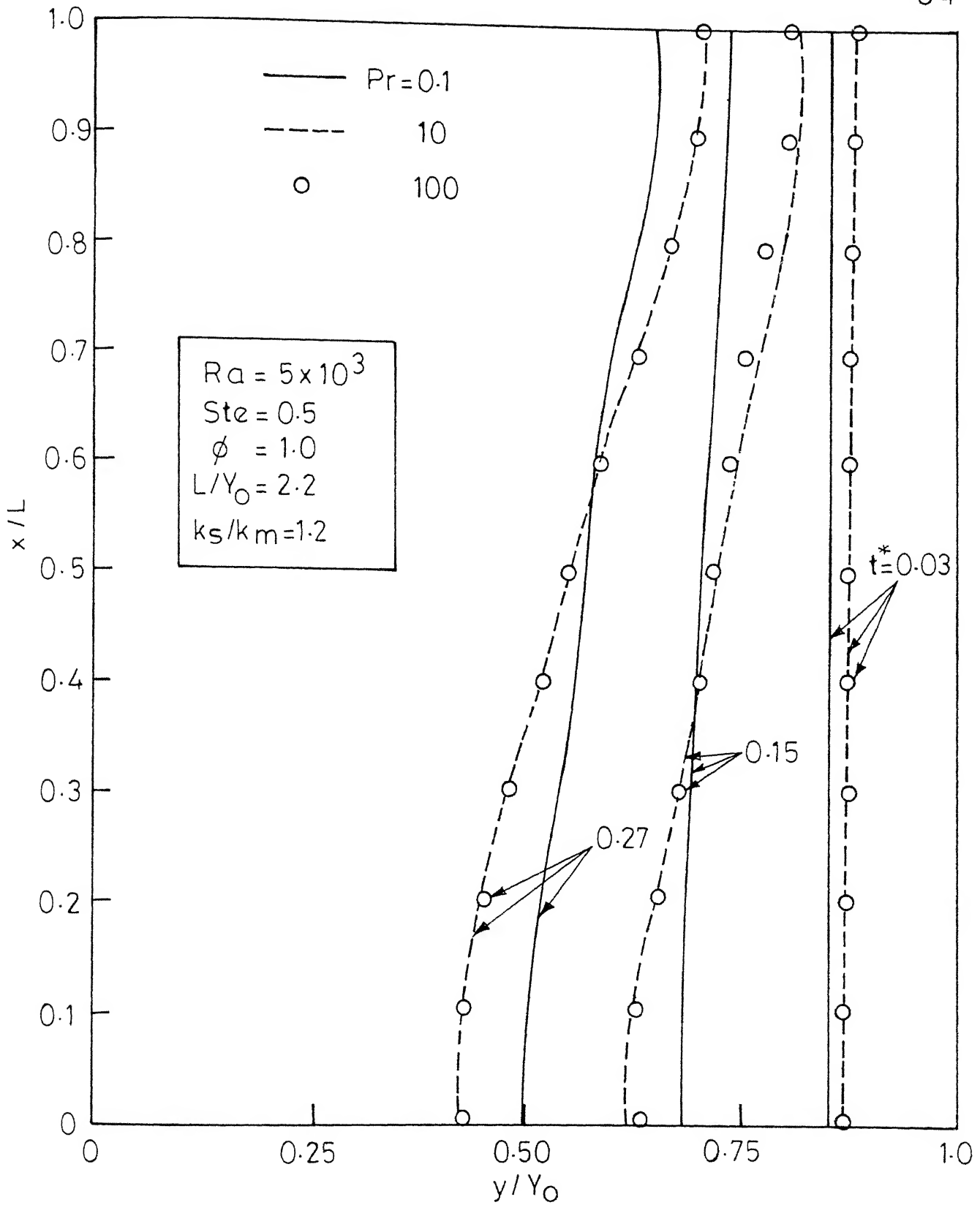


Fig.4.14 Dependence of interface movement on Prandtl number at different times, for constant temperature at the mold surface, adiabatic at top and bottom of the enclosure

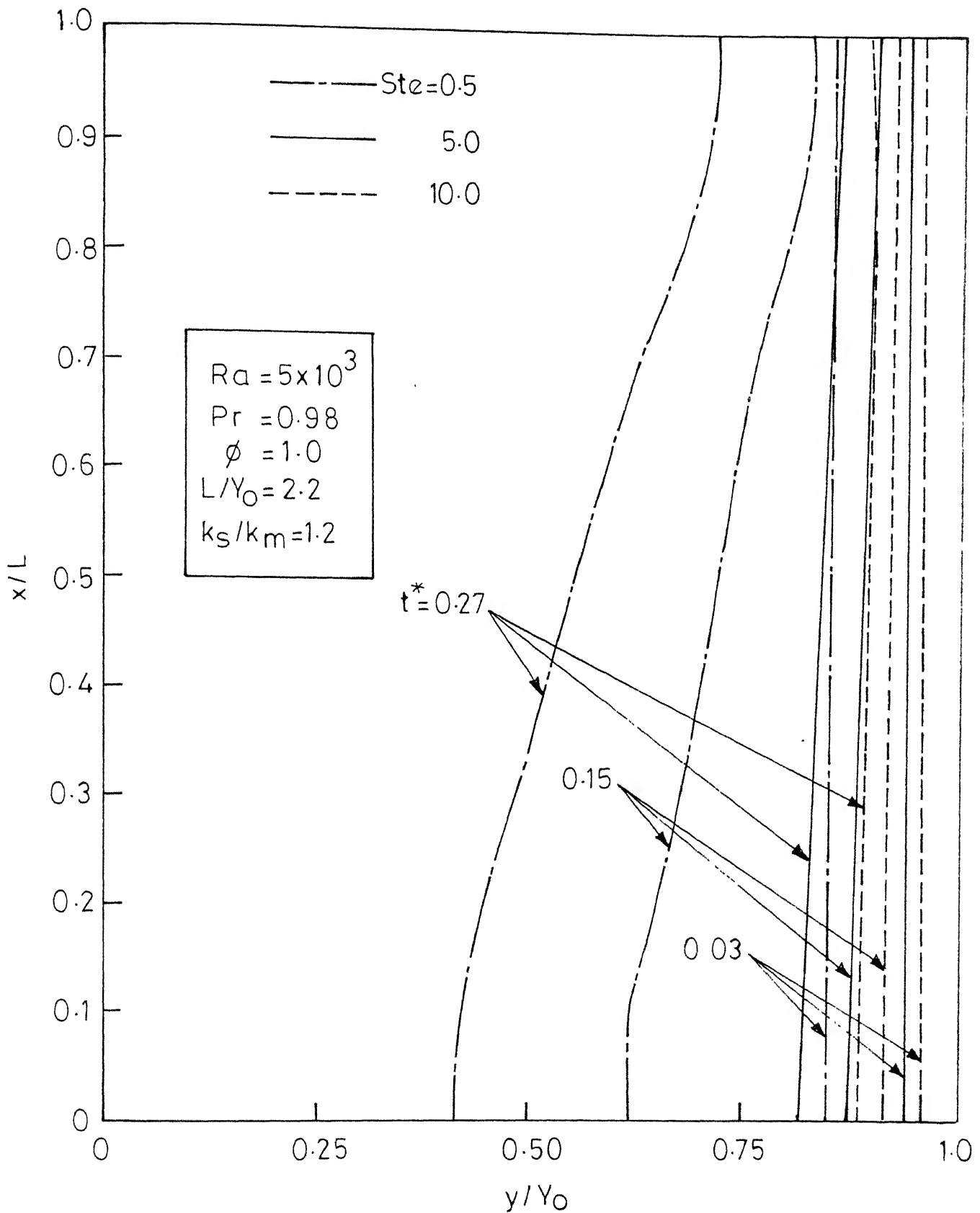


Fig.4.15 Dependence of interface movement on Stefan number at various time intervals, for constant temperature at the mold surface, adiabatic at top and bottom of the enclosure

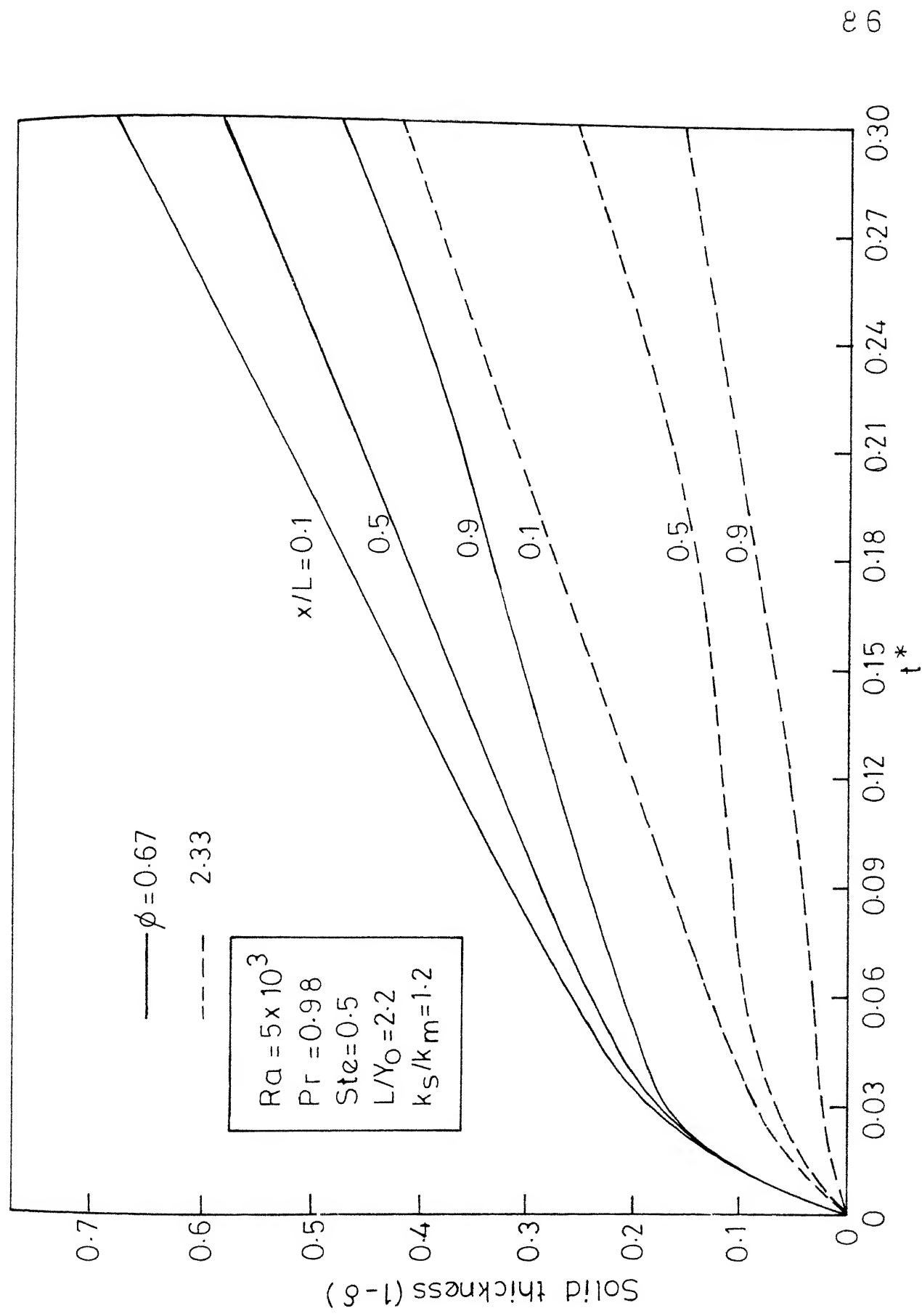


Fig.4.16 The effect of superheat on solid formed, for constant temperature at the mold surface, adiabatic at top and bottom of the enclosure

formed is plotted against time with ϕ as the parameter.

The rate of movement of solidification front decreases with increase in ϕ . This is expected from the results of one dimensional analysis, as large ϕ implies higher value of superheat and hence a decrease in the solidification rate.

4.4.3 Thermal and Fluid Flow in Melt-with Solidification, Top and Bottom Surface Adiabatic, and Convection and Radiation at the Mold Outer Surface:

The variation of temperature and the vertical velocity with height at the center of the enclosure and the dependence of interface movement on Biot number (Bi_1) and Radiation constant (Rc_1) are discussed in this section. The streamlines and isotherm patterns and the dependence of interface movement on non-dimensional parameters such as Ra , Pr , Ste and aspect ratio differ only quantitatively from the previous case (Section 4.4.2), and are not reported here.

The variation of temperature with height, at the center of the enclosure and at the mold outer surface are shown in Figure 4.17. Initially ($t^* = 0.06$) there is very little variation in the center line temperature in the x-direction, as conduction is dominating. At larger times the buoyancy forces play a predominant role and the temperature increases with height. It is also found from Figure 4.17 that the mold outer surface temperature does not vary with the height at any time. This is true since the mold thickness is very small compared to the height ($L/d=20$). This suggests

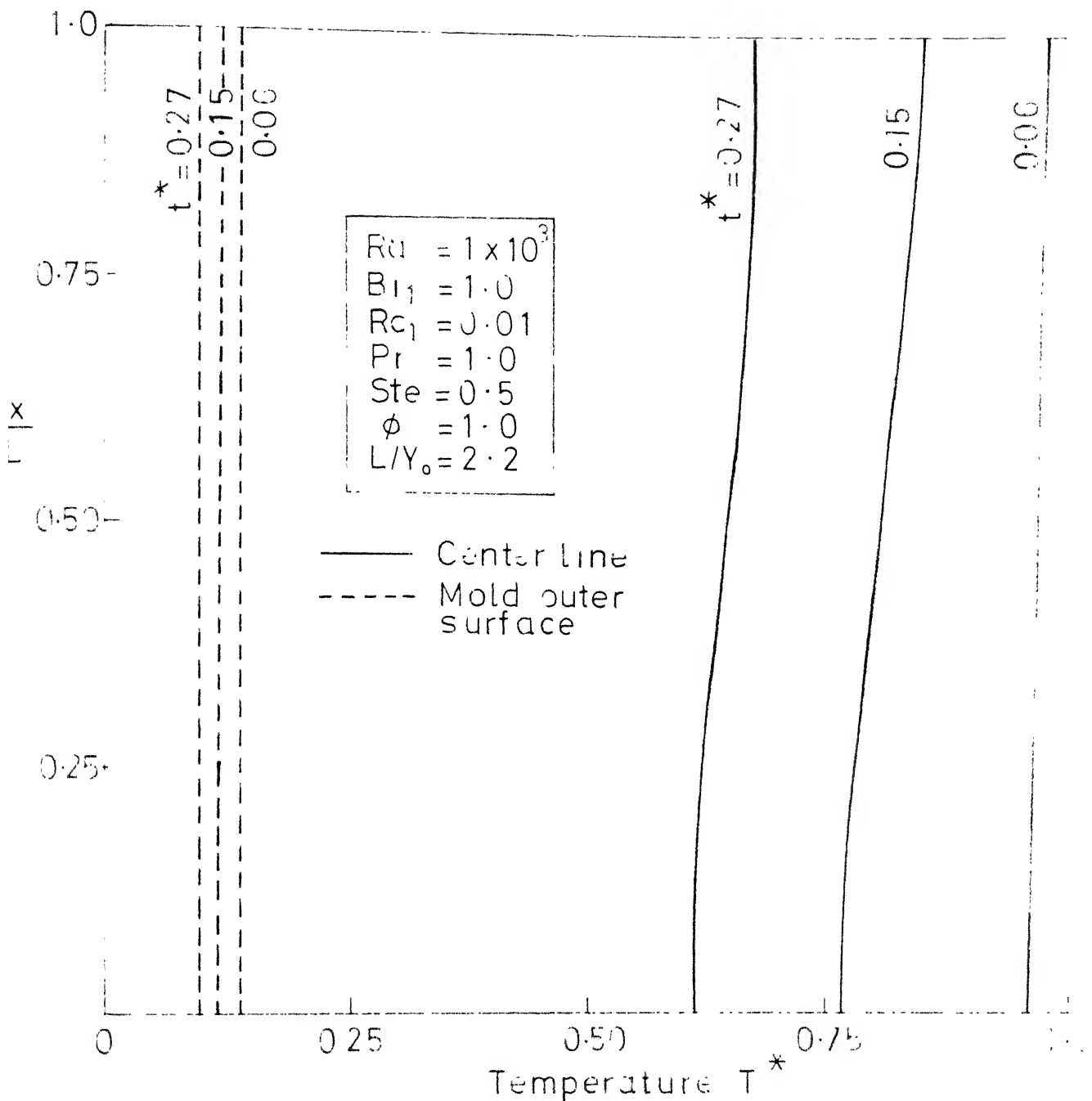


fig.4.17 Temperature profiles at the center line of the enclosure and mold outer surfaces at different times-Top and bottom of the enclosure a diabatic, mold surface convecting and radiating

that one can safely assume the heat transfer in the mold to be unidirectional if the L/d ratio is very high.

The variation of the center line vertical velocity u^* with the height is shown in Figure 4.18. The curves are symmetrical about $x/L=0.5$ and the maximum velocity occurs at $x/L=0.5$.

Figure 4.19 shows the dependence of interface movement on Biot number and Radiation constant. An increase in Biot number or Radiation constant increases the rate of solidification. It is seen from Figure 4.19 that very high Biot number ($Bi_1 > 15$) or Radiation constant ($Rc_1 > 500$) does not have any influence on the rate of solidification and an asymptotic solution is reached. This is true as high Biot number or Radiation constant indicates a high convective or radiative cooling and the mold approaches the ambient temperature.

4.4.4 Thermal and Fluid Flow in Melt-with Solidification, Bottom Surface Adiabatic, and, Convection and Radiation at the Top Surface and the Mold Outer Surface: The

computed results are presented mainly to study the effects of non-dimensional parameters on the rate of solidification, streamlines and on the isotherms. Of the non-dimensional parameters, attention is mainly focussed on the Rayleigh number, the Biot number and the Radiation constant. Rayleigh number is particularly chosen as it characterizes the role of natural convection. Ramachandran, Gupta and Jaluria(1981c)

$$\begin{array}{ll}
 Ra = 1 \times 10^3 & Ste = 0.5 \\
 Bi_r = 1.0 & \sigma = 1.0 \\
 Rc_1 = 0.01 & L/Y_o = 2.2 \\
 Pr = 1.0 &
 \end{array}$$

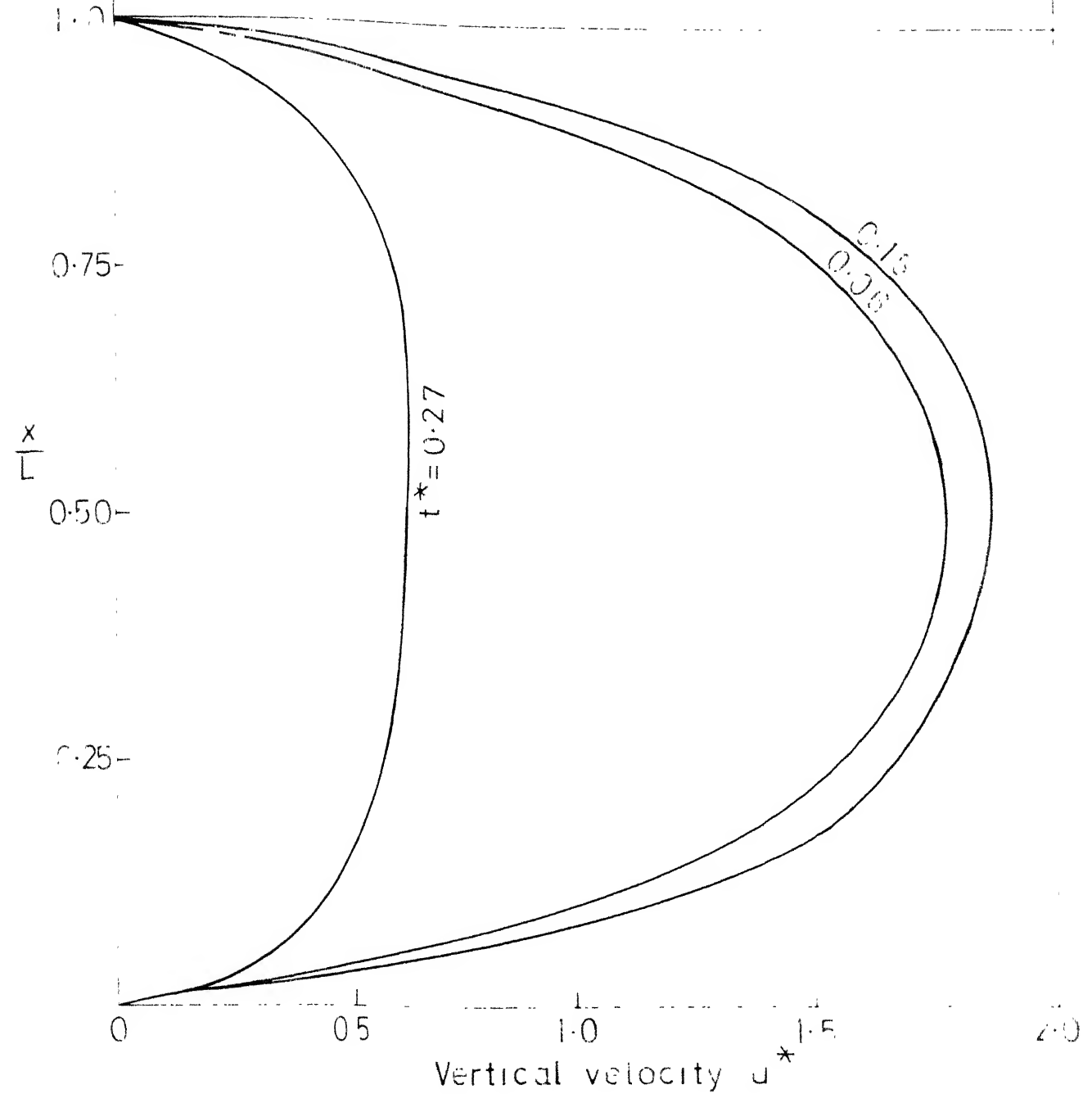


Fig.4.18 Velocity profiles at the center line of the enclosure for different times—Top and bottom surfaces adiabatic, mold surface convecting and radiating

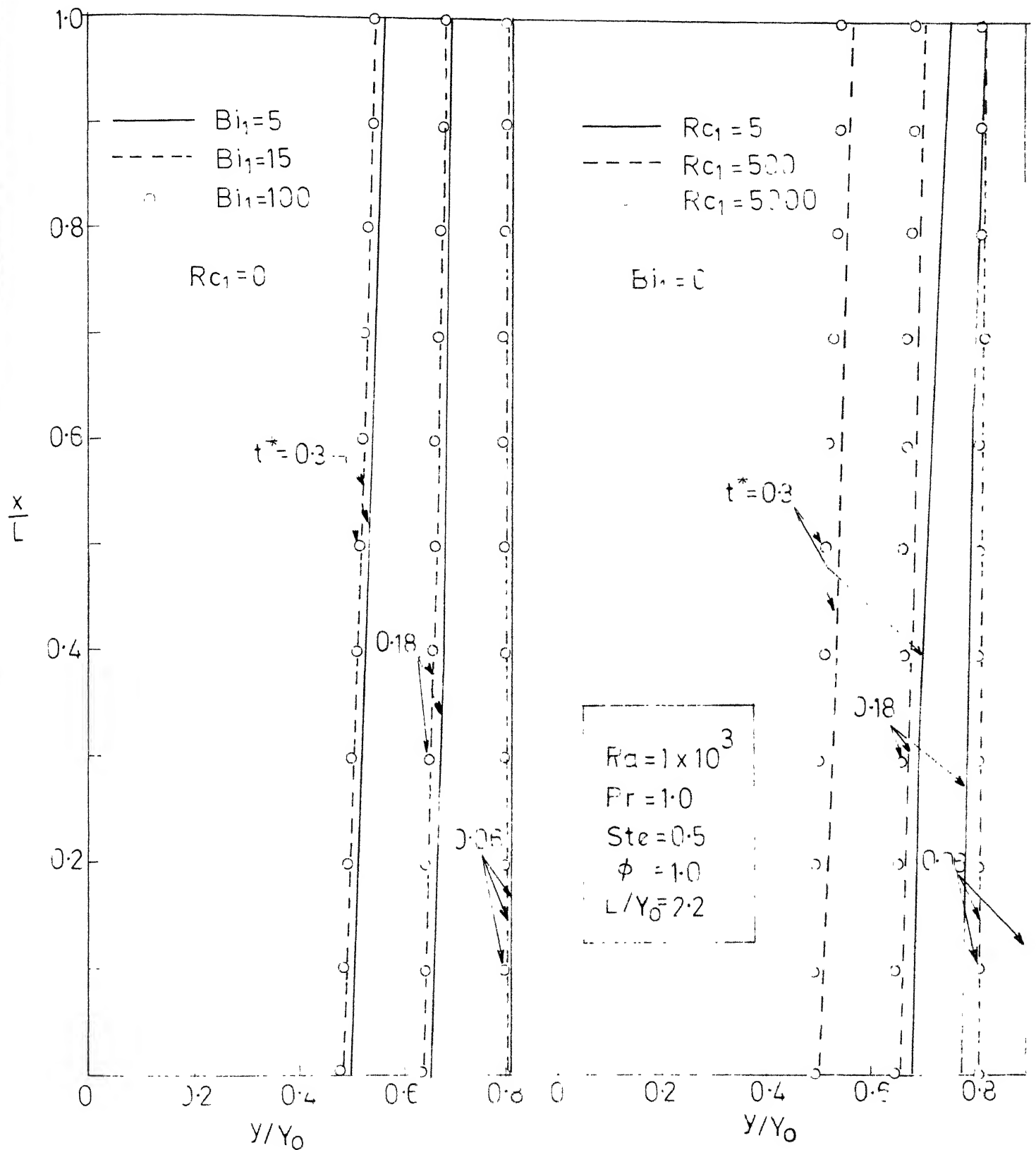


Fig. 4-19 Dependence of interface movement on Biot number and Radiation constant—Top and bottom surface adiabatic, mold surface convecting and radiating

have discussed the importance of Rayleigh number in characterizing the role of natural convection during two dimensional solidification.

The influence of the Rayleigh number on the interface movement is shown in Figure 4.20. Initially, for low Rayleigh number the shape of the interface is vertical and parallel to the mold except near the top of the enclosure, where it flares in due to cooling at the top surface. As Ra increases the interface deviates from the vertical position, slopes outward and then flares inside due to local cooling from the top. This effect is quite marked at time $t^*=0.18$, when the natural convection has started playing a significant role. This is contrary to the pure conduction where the interface slopes inside at any point inside the enclosure. At time $t^*=0.36$, the effect of cooling at the top surface is quite significant which changes the slope of the interface gradually inside even at the middle of the enclosure. For high Rayleigh number ($Ra = 1 \times 10^6$) computation is restricted to $t^* = 0.18$ due to enormous computational time required because of small time step.

The role of the Rayleigh number can be better understood by computing the heat transferred across the interface for different Rayleigh numbers and comparing with the results of pure conduction case. The quantity of heat transferred across the interface of length Δx and unit width in the z -direction can be written as

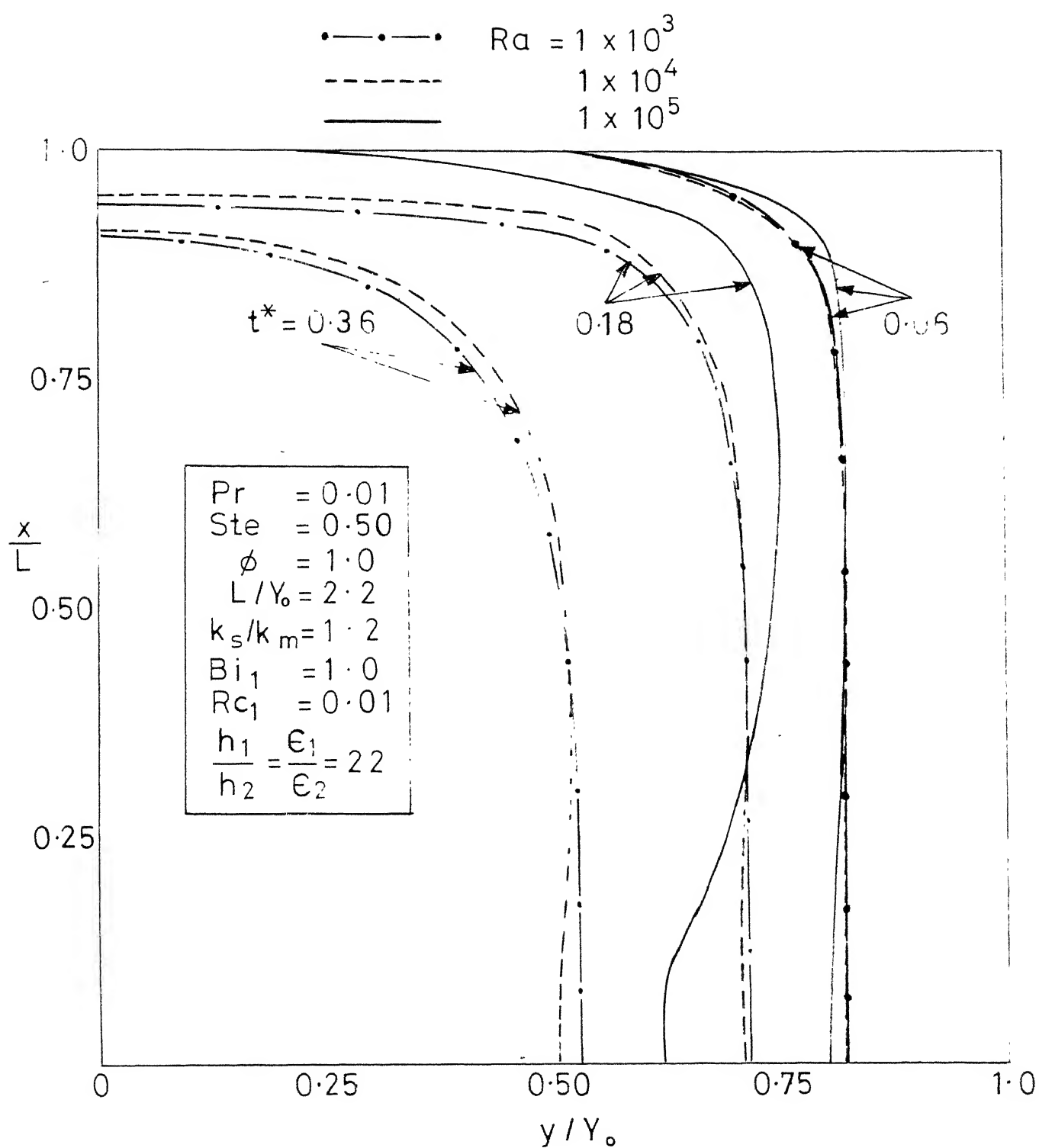


Fig. 4.20 Dependence of interface movement on Rayleigh number at different times – Bottom surface adiabatic, top surface and mold outer surfaces convecting and radiating

$$dQ = -k_1 \frac{\partial T_1}{\partial y} \left[1 + \left(-\frac{\partial Y_1}{\partial x} \right)^2 \right] dx \cdot \Delta t \quad (4.4.2)$$

On non-dimensionalization this becomes,

$$dQ = - \frac{\rho C_p L Y_o (T_i - T_c)}{\delta(x^*, t^*)} \frac{\partial T_1^*}{\partial y_1^*} \left[1 + \left(\frac{Y_o}{L} \right)^2 \left(-\frac{\partial \delta}{\partial x^*} \right)^2 \right] \left(\frac{D}{Y_o} \right)^2 \Delta t^* dx^* \quad (4.4.3)$$

Integrating both sides we get,

$$\frac{Q}{Q_o} = - \frac{1}{\delta(x^*, t^*)} \left(\frac{D}{Y_o} \right)^2 \Delta t^* \int_0^1 \left[1 + \left(\frac{Y_o}{L} \right)^2 \left(-\frac{\partial \delta}{\partial x^*} \right)^2 \right] \frac{\partial T_1^*}{\partial y_1^*} dx^* \quad (4.4.4)$$

where, $Q_o = \rho C_p L Y_o (T_i - T_c)$

Equation (4.4.4) is integrated for every time step and the value of Q/Q_o is found for different Rayleigh numbers and for the pure conduction case. The ratio $Q_{(cond+conv)}/Q_{cond}$ is plotted against time as shown in Figure 4.21, for different Rayleigh numbers.

$Q_{(cond+conv)}$ is the heat transferred at the interface with consideration given to the natural convection in the melt apart from the heat transferred by conduction.

Q_{cond} is the heat transferred by conduction at the interface without considering the natural convection in the melt. As solidification progresses the ratio $Q_{(cond+conv)}/Q_{cond}$ increases, attains a maximum and then decreases. In case of low Rayleigh numbers the occurrence of these events is shifted to larger times which is not shown in the figure. Initially

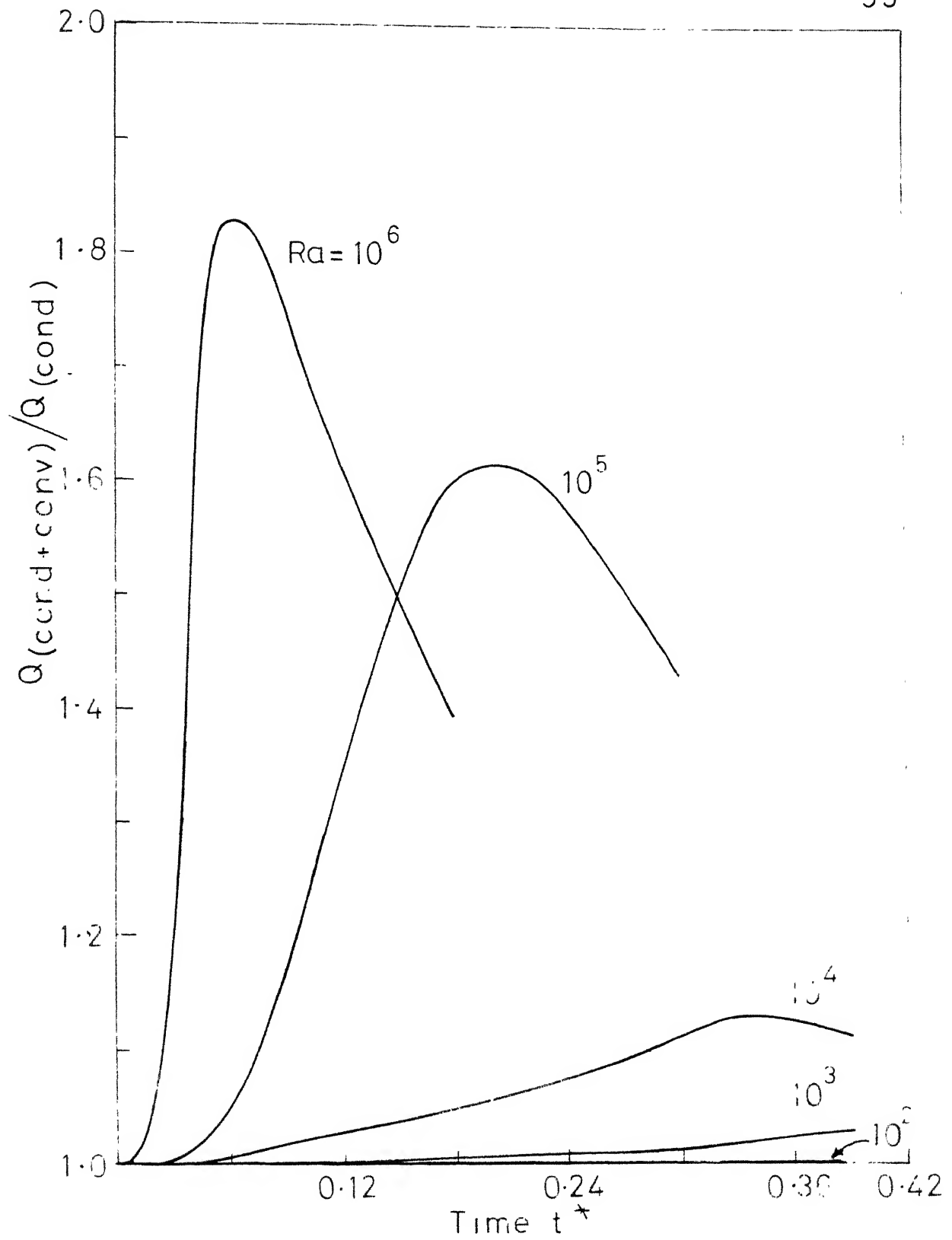


Fig.4.21 Variation of interface heat transfer rate with time for different Rayleigh numbers

the ratio increases as appreciable heat is transferred by natural convection, which is quite predominant in the case of high Rayleigh numbers. As solidification progresses the thickness of the melt region decreases and so does the heat transfer by natural convection. This explains the decrease in heat transfer after some time.

Figures 4.22 and 4.23 show the dependence of the interface movement on Radiation constant and Biot number respectively. It is found that an increase in Radiation constant (or Biot number) increases the rate of interface movement, which is evident as discussed in Section 4.4.3, for different set of boundary conditions.

The streamlines for the Rayleigh number 1×10^4 at $t^* = 0.06$ and $t^* = 0.30$ are shown in Figures 4.24 and 4.25 respectively. Figure 4.26 shows the streamlines for the Rayleigh number of 1×10^5 at time $t^* = 0.06$. The streamlines are normalized with respect to the maximum value of the stream function which is shown as a dot in all the figures. The interface, center and the top of the enclosure represent the streamline $\bar{\psi} = 0$. The direction of the motion of the melt along the streamlines is denoted with small arrowheads.

For $Ra = 10^4$ at $t^* = 0.06$, the streamlines are almost symmetrical about $x/L = 0.5$. This is because the interface is vertical and parallel to the mold wall except near the top of the enclosure. In this case the flow in the melt is similar to the flow that would develop in a rectangular

— $Rc_1 = 1.0 ; \epsilon_1 / \epsilon_2 = 44$
 - - - $Rc_1 = 50 ; \epsilon_1 / \epsilon_2 = 2200$

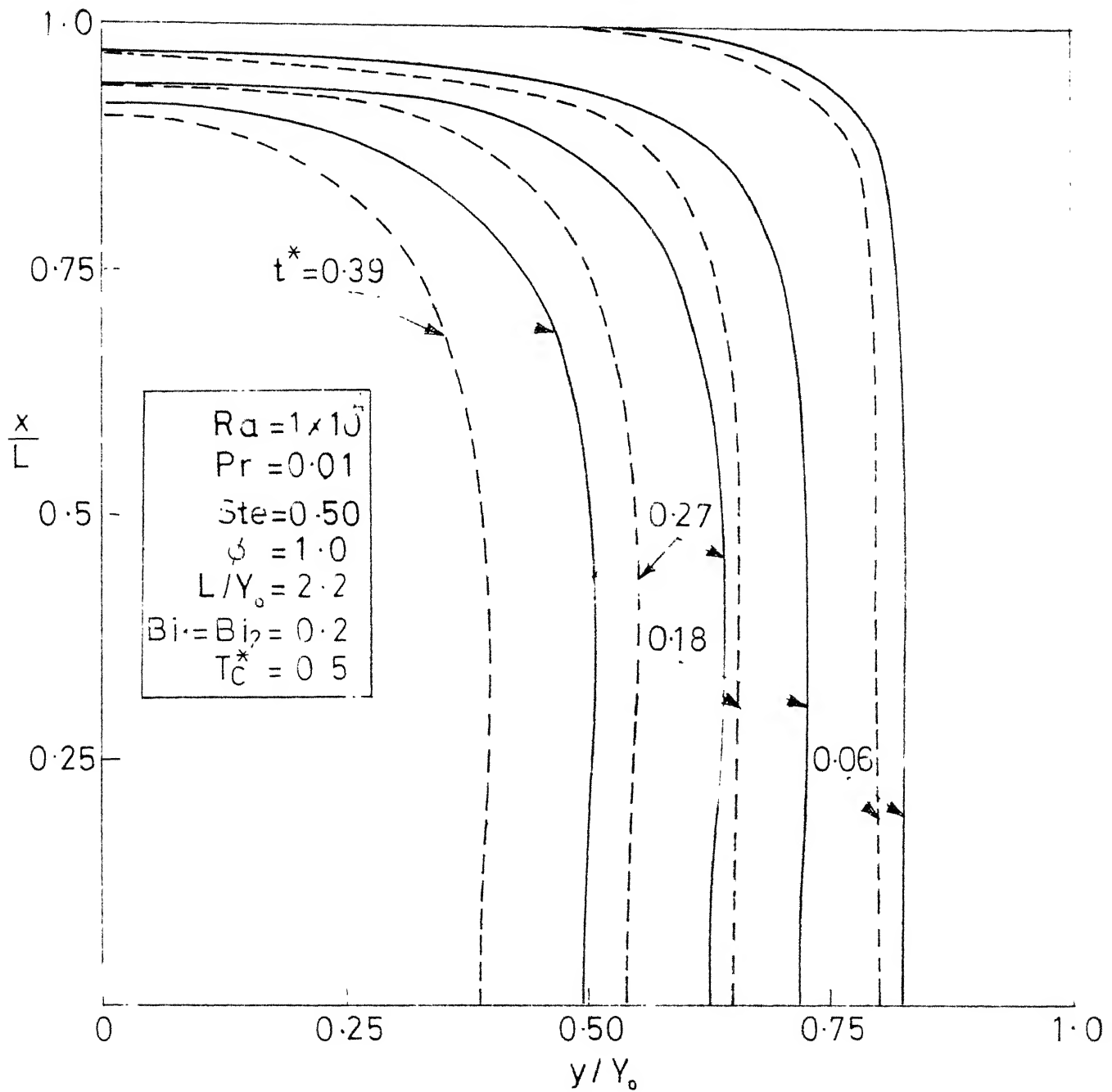


Fig. 4-22 Dependence of interface movement on Radiation constant at different times— Bottom surface adiabatic, top surface and mold surface convecting and radiating

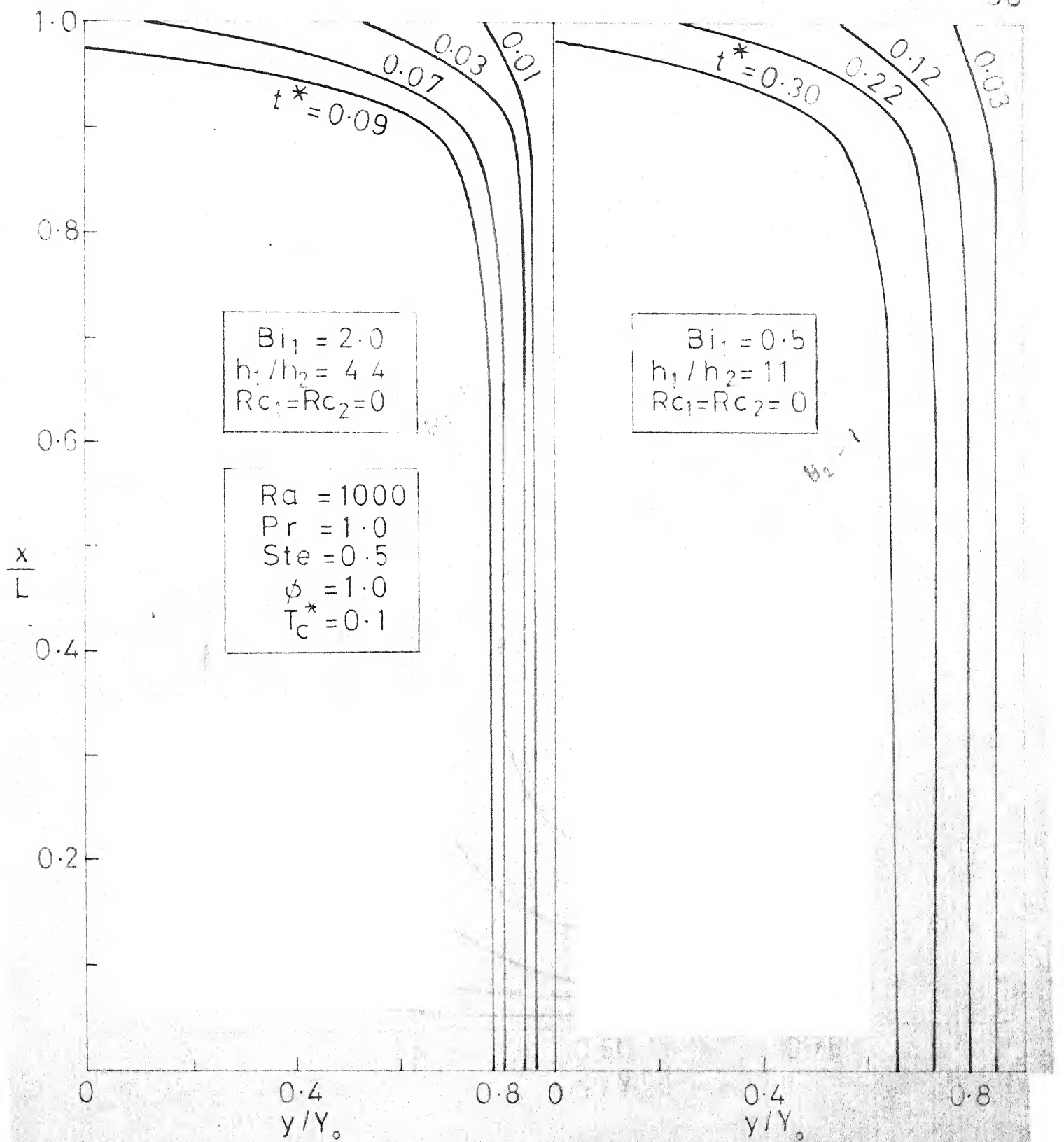


Fig. 4.23 Dependence of interface movement on Biot number at different times - Top surface and mold outer surfaces convecting & radiating, bottom surface adiabatic

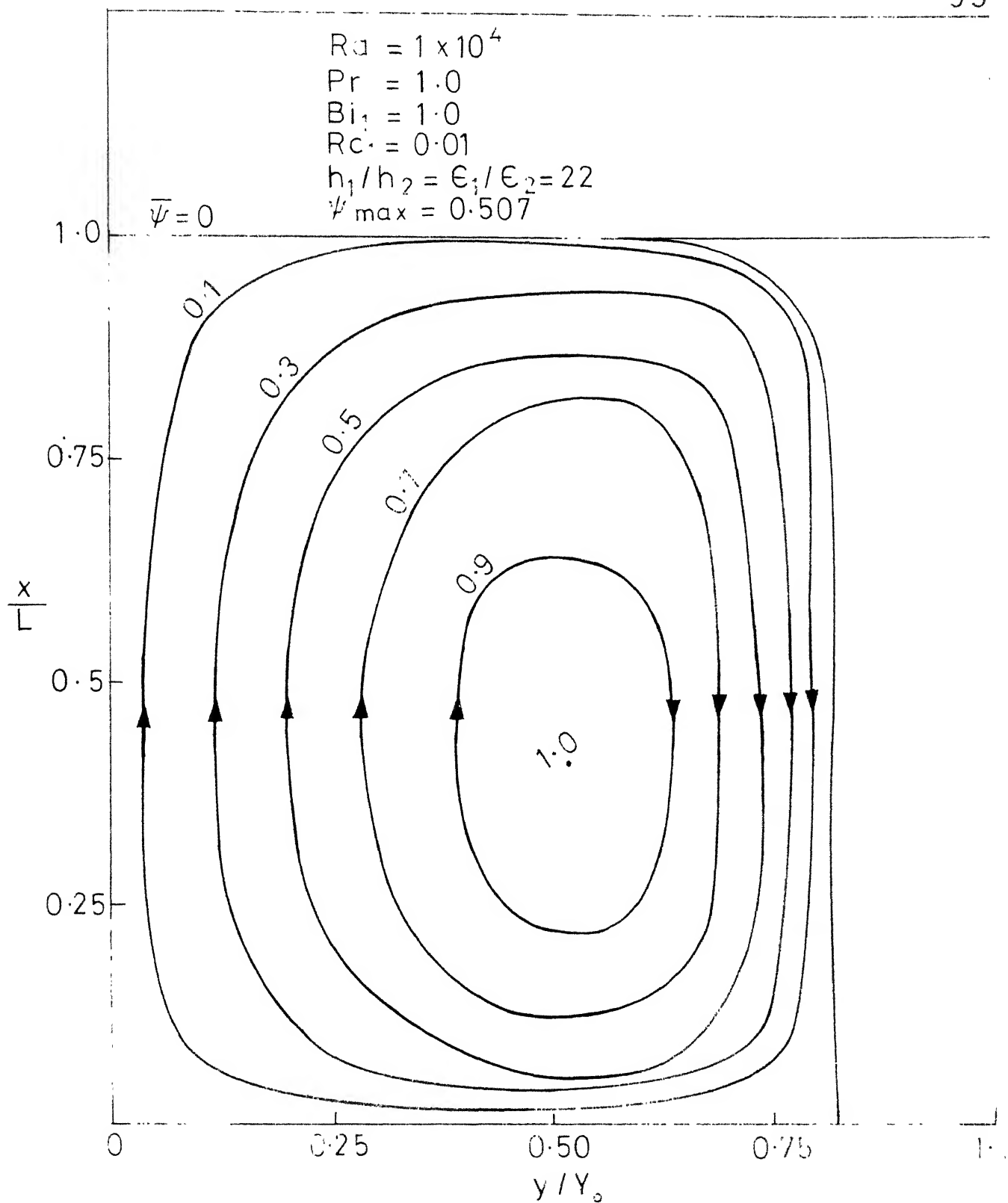


Fig. 4.24 Streamline pattern for $Ra = 1 \times 10^4$ and $t^* = 0.06$ —Bottom surface adiabatic, top surface and mold outer surfaces convecting and radiating

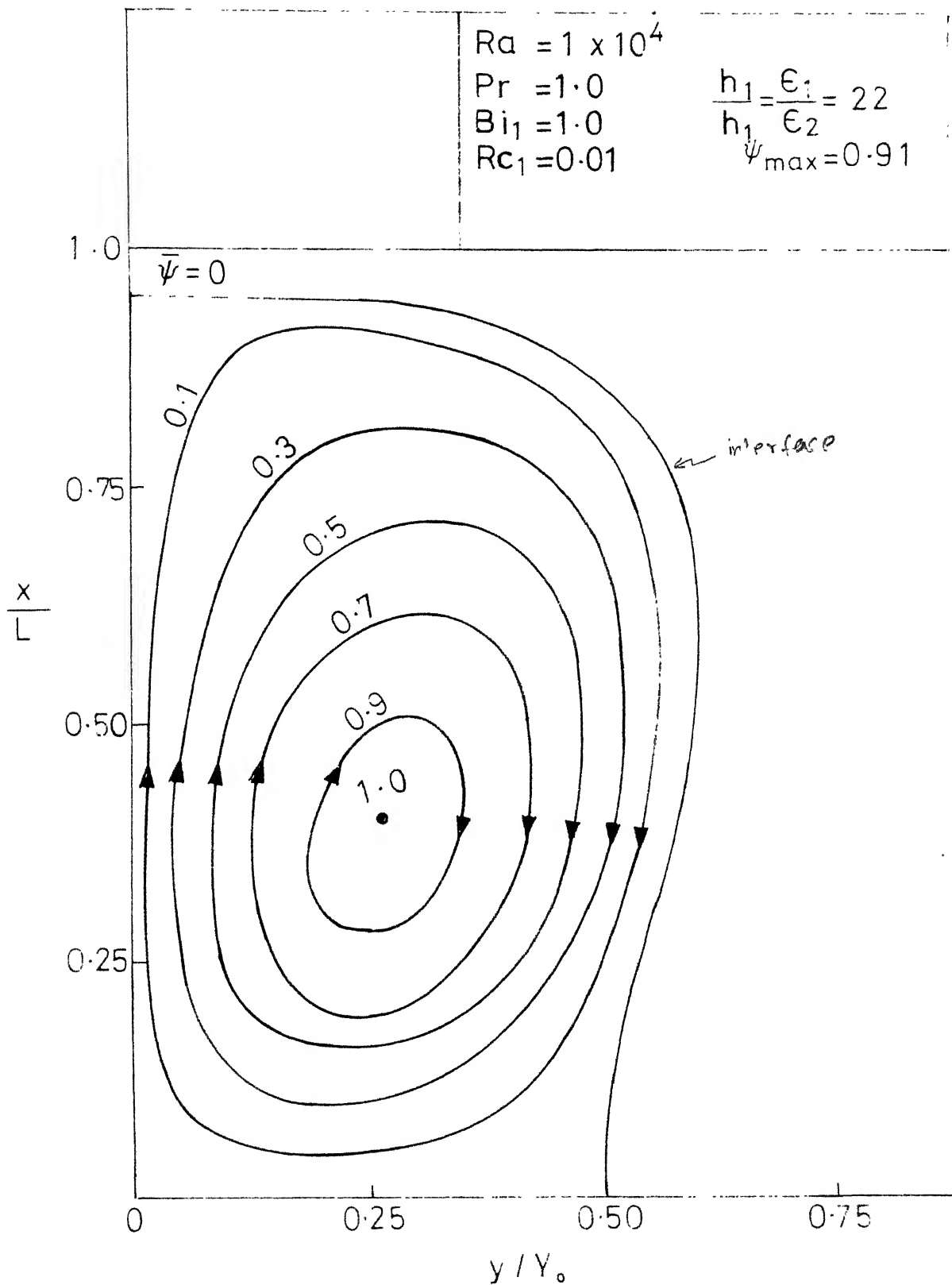


Fig. 4.25 Streamline pattern for $Ra = 1 \times 10^4$ and $t^* = 0.30$ - Bottom surface adiabatic, top surface and mold outer surfaces convecting and radiating

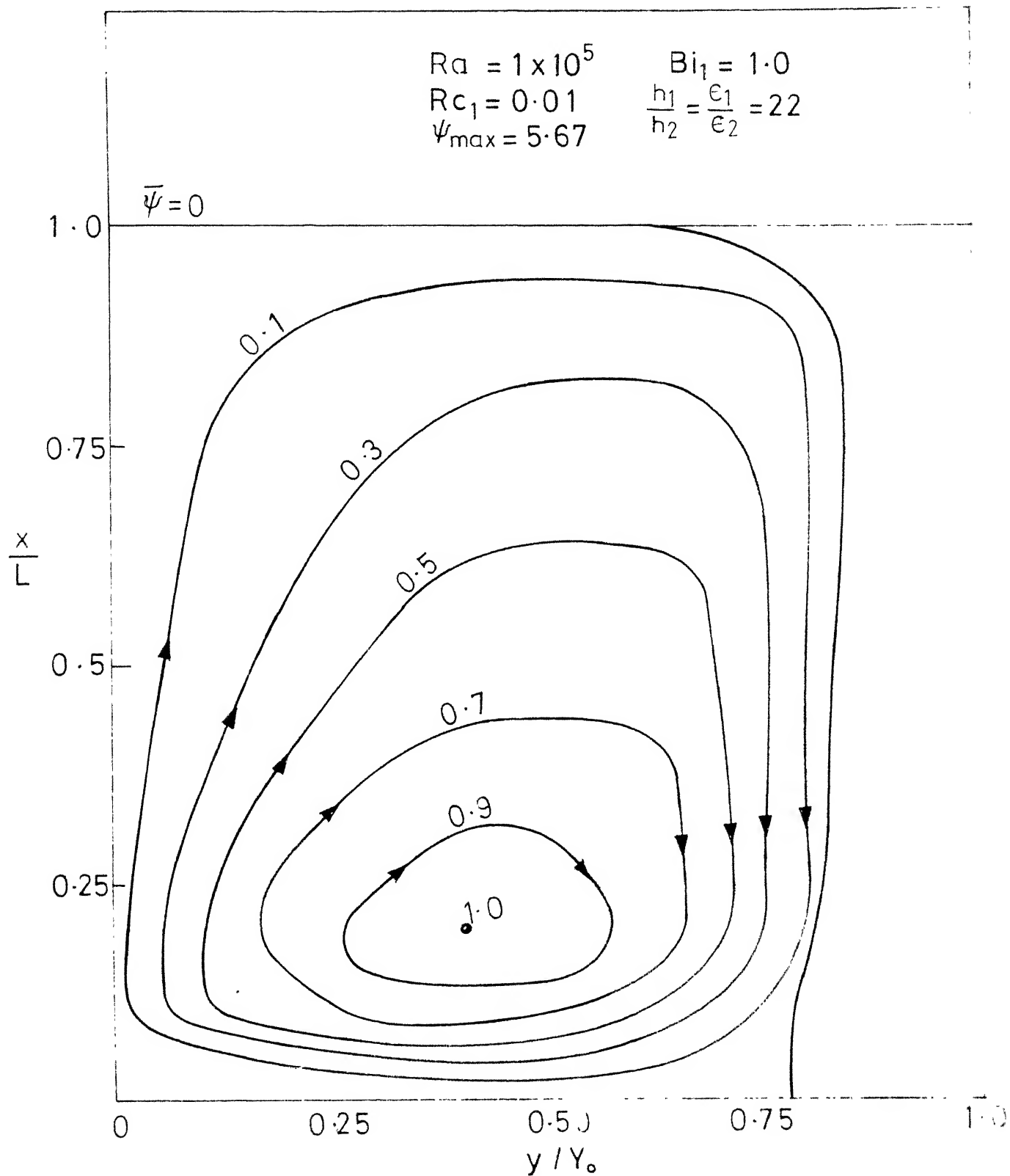


Fig. 4-26 Streamline pattern for $Ra = 1 \times 10^5$ and $t^* = 0.06$ —Bottom surface adiabatic, top surface and mold outer surfaces convecting and radiating

cavity in which no solidification occurs. The streamlines move closer together near the interface as a result of higher flow in this region. As solidification progresses the shape of the interface deviates from the vertical position and the streamlines are no more symmetrical about $x/L=0.5$. The melt moves upward near the center of the enclosure, flows gradually towards the interface as the temperature decreases with height near the top of the enclosure. The melt then flows down against the retarding effects of buoyancy. As the melt is slowed down it turns inward and rises to a height determined by its buoyancy. A comparison of Figures 4.24 and 4.26 indicates, for the same time as Rayleigh number increases, the melt moves towards the interface even near the center of the enclosure. The maximum value of the stream function is increased by more than ten times and this value occurs very near to the bottom of the enclosure.

Figures 4.27 and 4.28 show the isotherms for time $t^* = 0.06$ for Rayleigh numbers 1×10^4 and 1×10^5 respectively. In the case of $Ra=10^4$ where the flow is yet to develop the isotherms almost take the shape of the interface. For $Ra=10^5$ the magnitude of the flow is quite high and the shape of the isotherms of higher values deviates completely from the interface shape. As the top surface is cooled by radiation and convection there is a local cooling of the melt near the

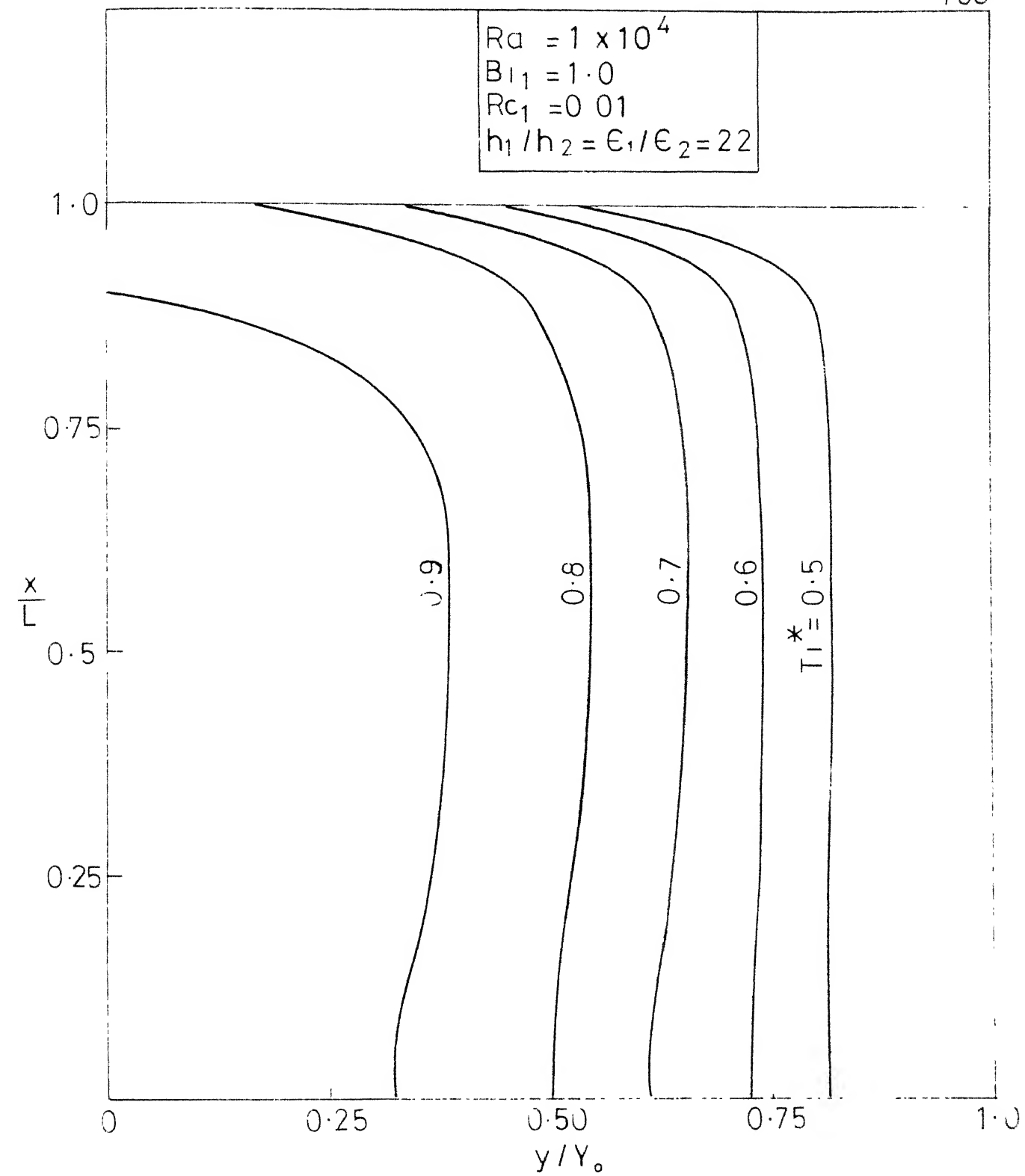


Fig. 4.27 Isotherm pattern in melt for $Ra = 1 \times 10^4$ and $t^* = 0.06$ - Bottom surface adiabatic, top surface and mold outer surfaces convecting and radiating

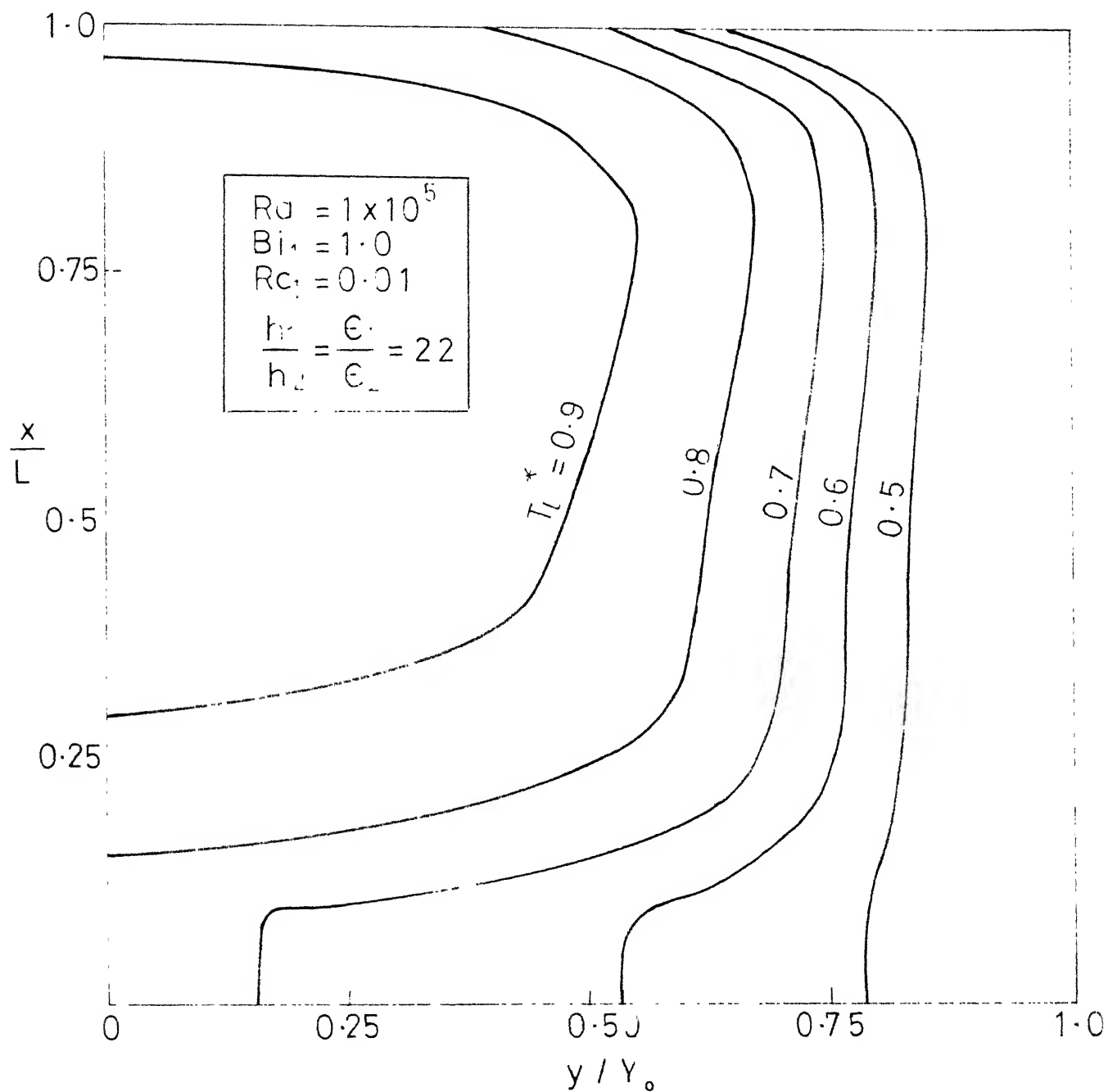


Fig. 4.28 Isotherm pattern in melt for $Ra = 1 \times 10^5$ and $t^* = 0.06$ - Bottom surface adiabatic, top surface and mold outer surfaces convecting and radiating

top of the enclosure and the warmer portion gets stratified in the center in between the cooler portion of the melt.

4.5 CONCLUSION:

An analysis has been carried out for the solidification in a rectangular enclosure. The equations are written for the temperature, vorticity, stream function and velocities in the melt. In the analysis, various combinations of boundary conditions are considered at the top and bottom surfaces of the enclosure and at the mold outer surface. Consideration has also been given to the heat conducted through and stored in the solid formed and the mold. The coupled, non-linear, simultaneous equations are non-dimensionalized and solved using ADI and SOR finite-difference techniques. The thickness of the solid formed at every time step has been found by solving the energy balance equation at the melt-solid interface.

The temperature and velocity profiles are plotted for various heights in the enclosure. The temperature is found to increase with height when the top surface of the enclosure is kept adiabatic. In the case of radiative and convective cooling from the top, the temperature first increases and then decreases with height. It has also been found that the natural convection has significant effect on the shape of the interface. The vertical velocity component and the temperature decay at almost equal rates when the Prandtl number is close

to unity. The effect of natural convection on solidification is clearly shown in the streamlines and isotherms plotted for different Rayleigh numbers and for different boundary conditions. Finally, the rate of solidification is also studied for various non-dimensional parameters such as Rayleigh number, Prandtl number, aspect ratio, Stefan number, Biot number, Radiation constant and the extent of superheat.

CHAPTER 5

EXPERIMENTS

5.1 INTRODUCTION

The experimental study of solidification of melt in an enclosure of finite dimensions has been made by many investigators. Most of the experiments have been conducted to study the shape of the interface and the temperature profile in the melt and the solid without considering the natural convection in the melt. The main reason for this is the sensitivity of the experiments to different parameters involved, as the results can vary to a large extent from one experiment to another depending upon the extent of superheat in the melt, the exact position of the mold, the cooling rate at the mold surface and the attitude of the enclosure with respect to gravity. In fact only recently attempts are being made to compare the experimental results of solidification with the analytical work. Sparrow, Ramsey and Kemink (1979) have conducted experiments in an annulus of concentric cylinders and compared the results with the theory developed by Sparrow, Patankar and Ramadhyani (1977).

In most of the experiments, a low melting paraffin or ammonium chloride solution has been used as the solidifying material. A low melting paraffin is mainly used because it freezes at a constant temperature. Ammonium

chloride solution is very useful to study the solidification of binary dendritic systems because due to its low entropy of fusion the material solidifies very much like metallic alloys. In most of the cases only temperature measurements using thermocouples have been made as it is very difficult to measure the fluid flow developed in the melt.

In this chapter, the experiments performed for the solidification in an enclosed region with paraffin wax (properties in Appendix VIII) as the solidifying material are described. Paraffin wax (melting point $\approx 60.5^{\circ}\text{C}(140.9^{\circ}\text{F})$) is particularly chosen because of its low melting, easy handling nature. Water is used as a coolant for solidification. The temperature of the solidifying wax is measured with thermocouples kept at different predetermined levels inside the enclosure. The recording of the temperatures has been done with the help of a programmable Data Acquisition System. The variation of temperature with time is plotted and compared with the theory. From the temperature vs time plots, the time taken for the melt-solid interface to touch a particular thermocouple is interpolated. The position of the interface is then plotted against time and compared with the analytical solutions given in the previous chapters (Chapters 3 and 4). The experiments are conducted for different aspect ratios and superheats of the melt, in the laminar range of natural convection.

5.2 EXPERIMENTAL APPARATUS:

The heart of the experimental set up is the test cell where the solidification takes place. In addition to the test cell, the apparatus includes auxiliary systems for controlling the temperature of cooling water, Data Acquisition System to record temperatures and a heating device for melting the wax.

Separate test cells were fabricated for conducting experiments of one dimensional and two dimensional solidification cases. Figure 5.1 shows a schematic diagram of the experimental set up used.

5.2.1 Test Cell for one Dimensional Case: The test cell for the one dimensional experiment consisted a plexiglas rectangular container of dimensions $14 \times 50 \times 50$ cm ($5.5 \times 19.7 \times 19.7$ in), into which two 0.64 cm ($1/4$ in) thick aluminium plates were inserted, thus dividing it into three compartments. The paraffin wax was solidified in the central compartment of dimensions $10 \times 50 \times 50$ cm ($3.9 \times 19.7 \times 19.7$ in) and the cooling water was circulated in the side compartments of dimensions $2 \times 50 \times 50$ cm ($0.79 \times 19.7 \times 19.7$ in). The aluminium plates formed the two vertical opposing walls of the mold. A Plexiglas sheet of 1.25 cm ($1/2$ in) thick, used to cover the molten wax in the central compartment, formed the top surface of the enclosure. The top surface was kept at a height of 47 cm (18.5 in) from the bottom of the enclosure ($L/2Y_0 = 4.7$).

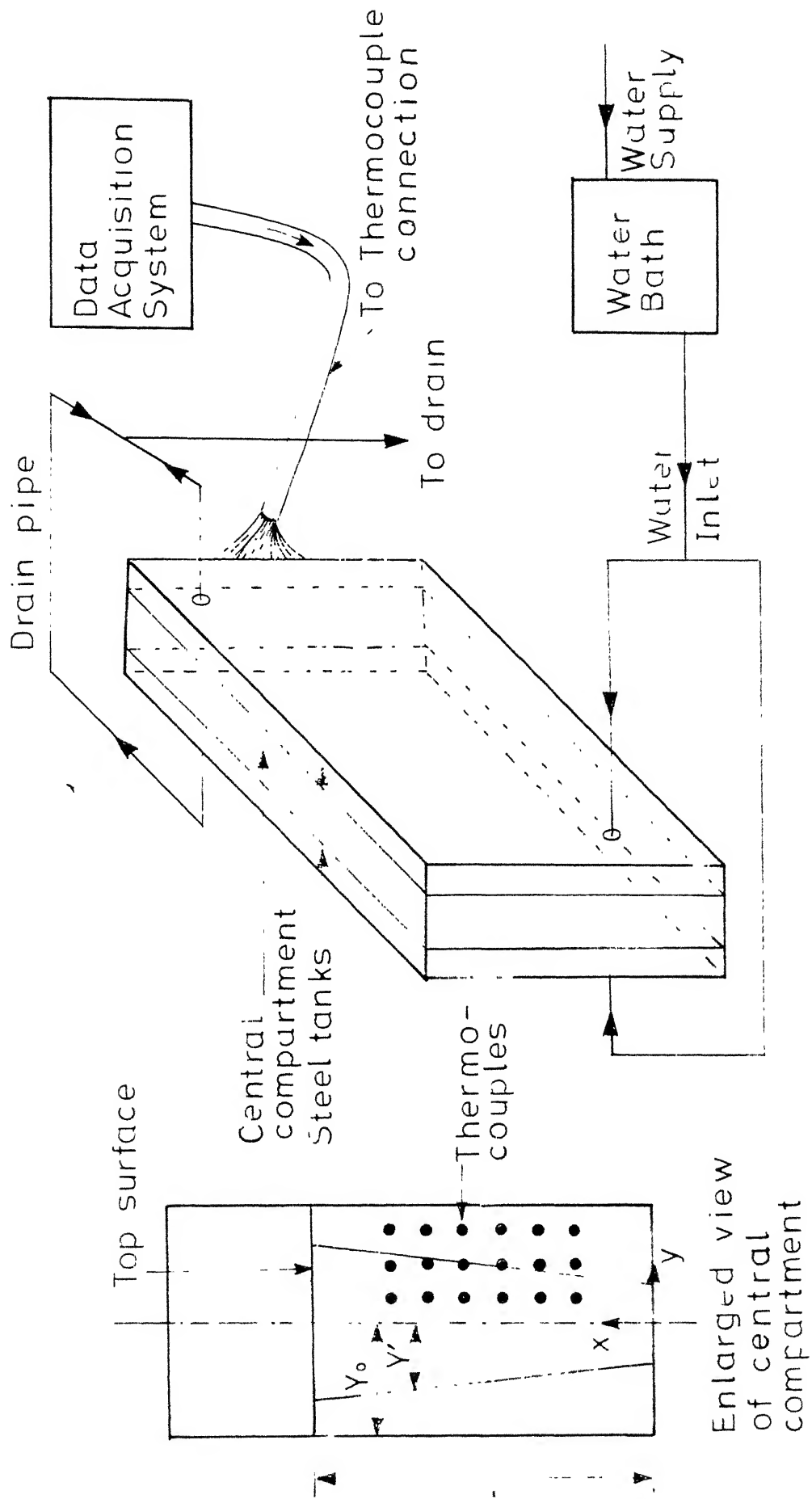


Fig. 5.1 Diagrammatic sketch of the apparatus

An opening was provided at the top surface for pouring the molten wax into the central compartment. The wax can be drained through an outlet kept at the bottom of the central compartment. All the sides, top and the bottom of the enclosure were insulated with 1.25 cm (1/2 in) thick asbestos and 2.5cm (1 in) thick styrofoam sheets.

5.2.2 Test Cell for two Dimensional Case: The test cell for the two dimensional experiments was similar to the one described above with slight modifications. The size of the cell was much smaller than the previous case so that the Rayleigh number was well within the laminar range ($Ra \approx 8 \times 10^4$). The test cell, with dimensions 2x20x20cm (0.79x7.9x7.9 in) had two walls of steel (20 x 20 cm; 7.9x7.9 in) and two side walls of Plexiglas (2 x 20 cm; 0.79x7.9 in). The steel walls were 0.2 cm (0.079 in) thick and acted as mold as considered in the theoretical analysis (Chapter 4). The steel walls had jackets (5x20x20 cm; 1.97x7.9x7.9 in) in the other sides for circulating cold water through them at controlled temperature.

The height L to which the molten wax was poured can be varied by placing 1.0 cm (0.4 in) thick Bakelite sheet in the test cell, at the levels of 3.5, 5, 6 cm (1.38, 2.0, 2.4 in) from the bottom of the container. Grooves were made at these levels for sliding the Bakelite sheet which served as the top surface of the enclosure. The molten

wax can be drained out through an outlet provided at the bottom of the test cell. The whole test cell was insulated with 2.5 cm (1.0 in) thick styrofoam sheets.

5.2.3 Temperature Measurements: Temperature of the solidifying wax was measured using a double insulated, 24 gauge, Iron-Constantan thermocouples. The thermocouples were sheathed inside copper capillaries, fixed inside the test cell. **Eighteen** thermocouples were used for measuring the temperature of the wax, kept at six different levels in the x-direction, each level containing three thermocouples. Separate thermocouples were provided for measuring the temperatures of the mold wall and cooling water. For one dimensional experiments, only eight thermocouples were used, all kept at a height of 25 cm (9.8 in) from the bottom of the test cell. Figure 5.2**5** shows the photograph of the thermocouple assembly used for the two dimensional experiments.

The output of the thermocouples was recorded by a 3052A Hewlett Packard, Data Acquisition System (DAS). The DAS is basically a high speed automated instrument that provides an on-line analysis for the real time experiments. The system is composed of 3455A high resolution, digital voltmeter (DVM), 3495A scanner, 59309A real time clock and 9825A programmable calculator, all interfaced through 98034A HP-IB interface.

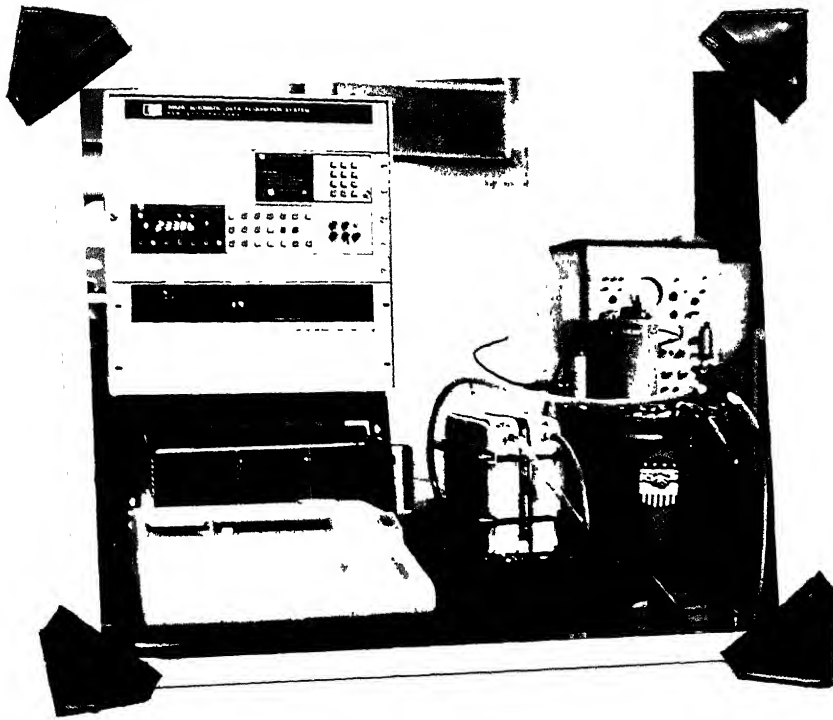


Fig. 5(a) Photograph of the Experimental Set-up



Fig. 5(b) Photograph of Thermocouple Assembly

The thermocouples were connected to different channels of the scanner which is basically a programmable relay box. Through the scanner relays, thermocouple output signals were routed to DVM at specific time as controlled by the calculator program. The speed of the scanner is 19 channels/sec. The input signals of the DVM were then digitalized and converted to temperatures through a polynomial written according to standard tables specified by NBS Monograph 125. The program for the calculator is written in HP basic language and can be stored in tape cartridges. The accuracy of temperature measured with DAS is $\pm 0.2^{\circ}\text{C}$.

The other equipment used in the experiments includes a water bath (COLONA-Germany, KLZ42.60-2-160D) which maintains the water temperature to an accuracy of $\pm 0.05^{\circ}\text{C}$. Figure 5.2a shows the photograph of the test cell for two dimensional case, water bath and DAS used for the experiments.

5.3 EXPERIMENTAL PROCEDURE:

At the start of each experimental run the HP basic program was transferred from the tape cartridge to the memory of DAS. The program was written in such a way that the temperature was recorded for every 15 sec in case of two dimensional experiments and for every 1 min in case of one dimensional experiments.

The horizontal and vertical locations of all the thermocouples were then measured with the help of a travelling

microscope (OSAW-India) to an accuracy of 0.01 mm. The top surface was then fixed at a known height inside the test cell. The circulation of cooling water was started 10 min before pouring the molten wax for solidification so that water temperature reached a constant value. The capillary tubes supporting the thermocouples were heated to initial temperature (T_i) of the molten wax by blowing hot air on them using a hot air blower (MOULINEX-France, SH2A). This was to ensure that the wax did not solidify on the capillaries and the thermocouple beads, immediately after pouring it inside the test cell.

The molten wax heated to predetermined temperature T_i was then poured into the test cell through the opening provided at the top surface. Immediately after pouring the wax, the top surface was covered with insulating materials and the program in DAS was run. The wax was allowed to solidify for 10 min in case of smaller test cell and 2 hrs in case of bigger test cell. At the end of each run, the unsolidified molten wax was drained out through the outlet. The solidified wax was then taken out for subsequent runs, by cutting it into pieces with a sharp knife.

The experiments were performed for different superheats of the molten wax and for different aspect ratios of the test cell.

5.4 RESULTS:

5.4.1 Two Dimensional Experiments: The variations of temperature with time measured by different thermocouples, for the molten wax poured at superheats (θ) of 0.32, 0.61 and 0.83 are shown in Figures 5.3, 5.4 and 5.5 respectively. The plots are drawn for only selected thermocouples out of a total of eighteen for clarity. The thick lines show the results from analytical study described in Chapter 4. For the computations of the Eqs.(4.2.15) to (4.2.23) the physical properties of wax are chosen at a temperature of 62°C . Since the variation of thermal diffusivity α , with the temperature is very little, the constant property assumption is valid for comparison of the analytical results with the experimental results. The parameters y/Y_0 and x/L show the horizontal and vertical positions of the thermocouples from the center and bottom of the test cell respectively. From the figures it is evident that the solidification takes place at a constant temperature and the slopes of the curves change at the solidification point. The curves lying above the solidification point represent the temperature distribution in the melt whereas those lying below the solidification point represent the temperature distribution in the solid. Figures 5.3 - 5.5, show that the experimental points fall reasonably well within the theoretical range, except during the initial stages of solidification. Ramachandran, Gupta and Jaluria (1981d) have discussed that the deviation at the initial stages may be due to the turbulence created by pouring the molten wax into the set up, which takes certain time to subside.

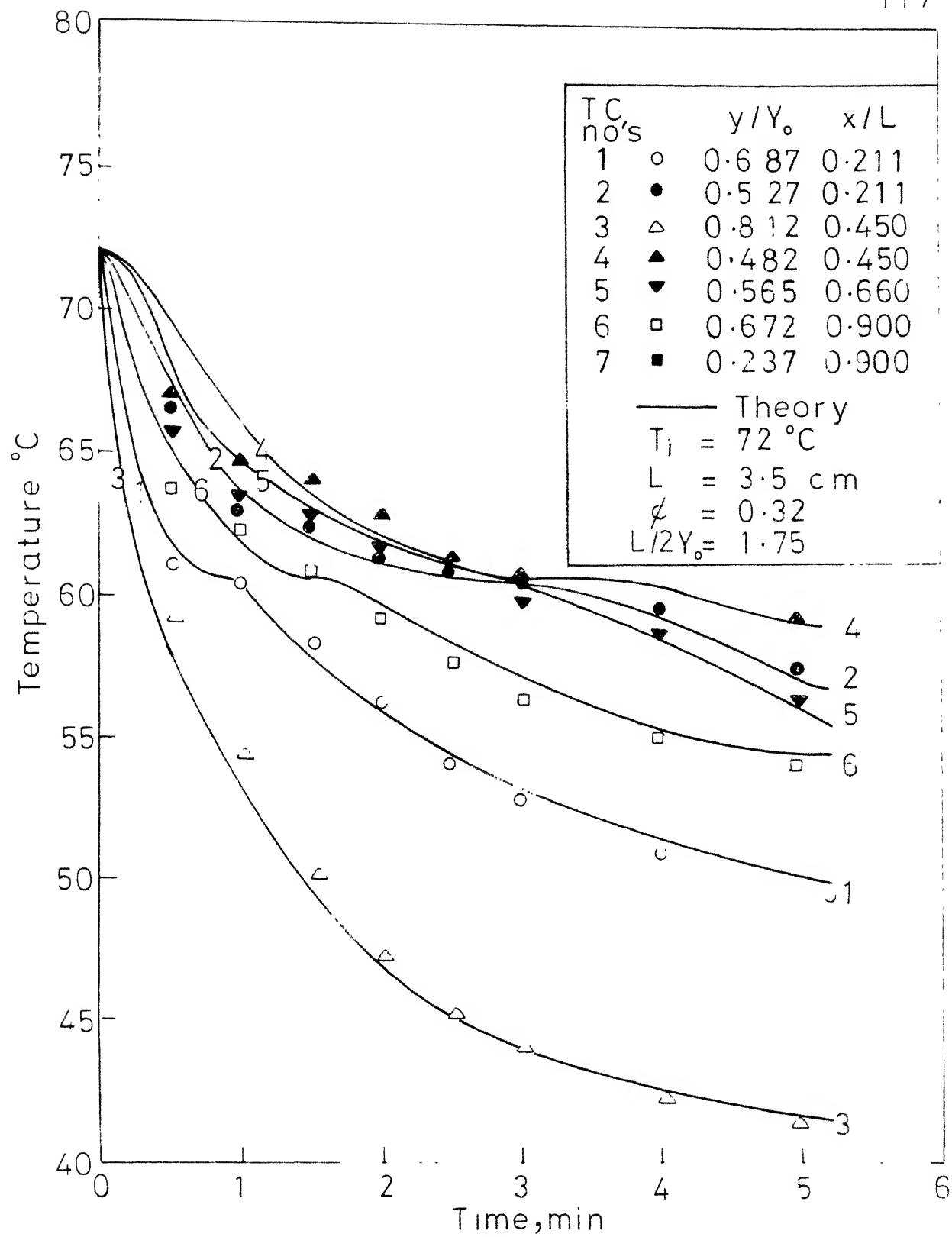


Fig. 5.3 Variation of temperature with time for initial temperature 72°C and height 3.5 cm

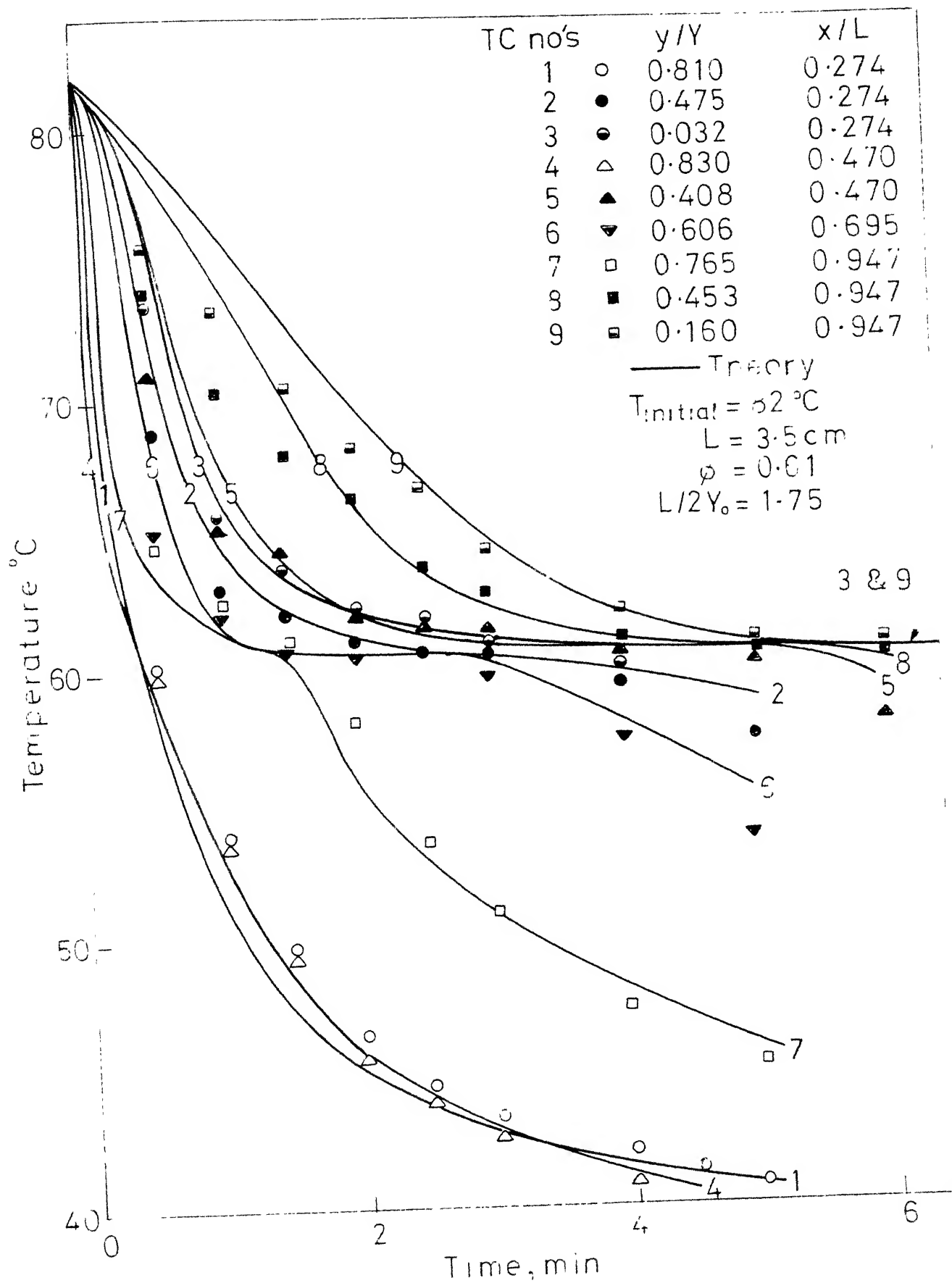


Fig. 5.4 Variation of temperature with time for initial temperature 82°C and height 3.5 cm

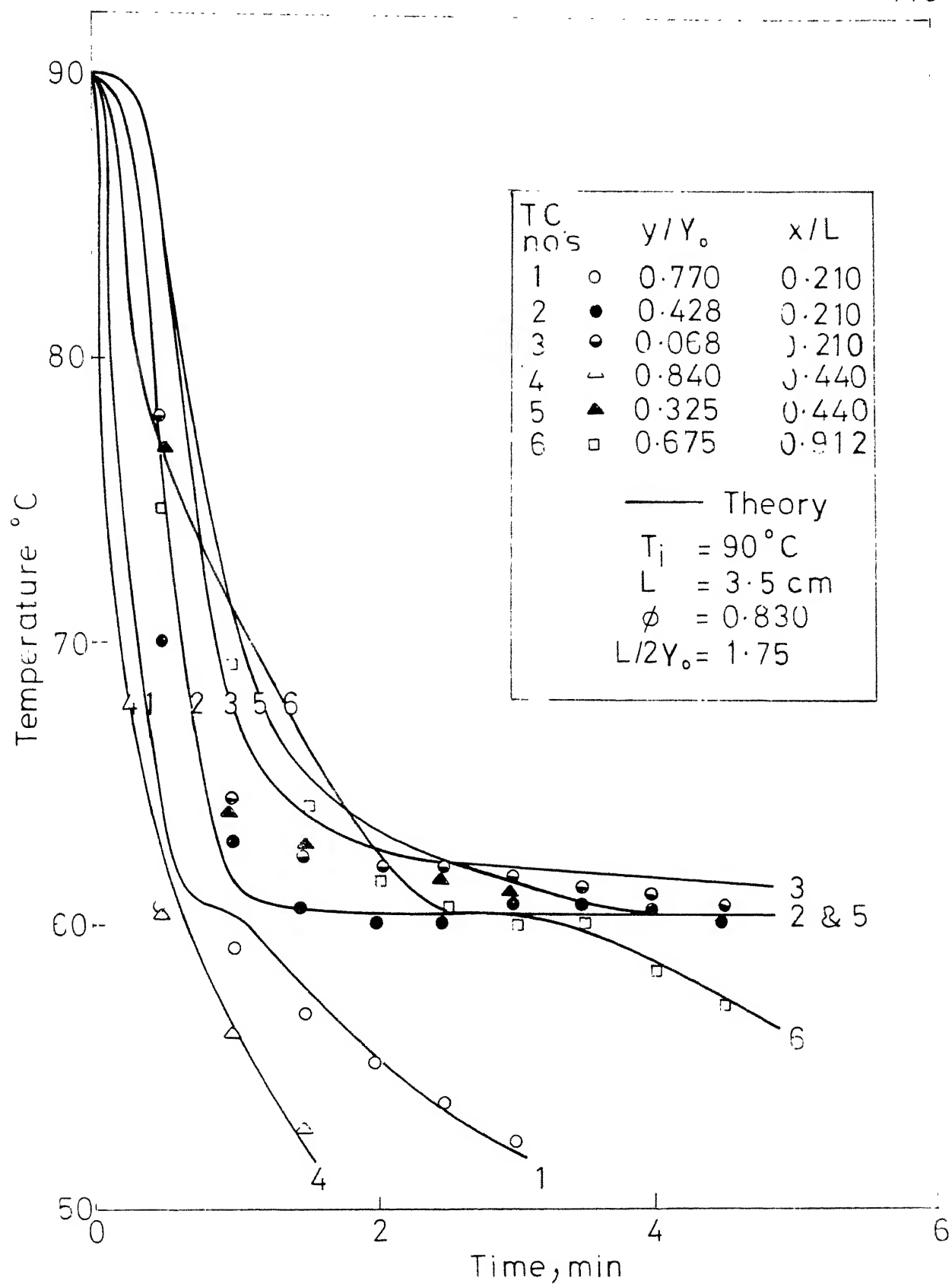


Fig. 5.5 Variation of temperature with time for initial temperature 30°C and height 3.5 cm.

From the temperature vs time plots (Figures 5.3 to 5.5), the time at which the interface touches a particular thermocouple can be easily found out. Since the positions of the thermocouples are predetermined, the thickness of the solid formed at different times are interpolated. Figures 5.6-5.8 show the interpolated experimental results of the variation of solid thickness with time at different x/L values, and for the superheats of 0.32, 0.61 and 0.83 respectively. The thick lines show the analytical results for comparison computed by Eqn.(4.2.21d) of Chapter 4. The rate of solidification decreases with x/L due to the presence of natural convection in the melt. The figures show that the experimental points match well with the analytical solutions. A comparison of Figures 5.6, 5.7 and 5.8 shows that the rate of solidification decreases with increasing superheat which is reasonable as explained in Chapters (3 and 4). The experimental results are compared only to a limited theoretical range due to enormous computation time required (a CPU time > 45 min) to solve the problem numerically for complete solidification.

Figures 5.9 and 5.10 show the theoretical as well as the experimental temperature vs time relationship for a superheat of 0.66, the height L of the enclosure being 5.6cm ($L/2Y_0=2.5, 3.0$) respectively. Similar to the previous cases, the agreement between the theory and the experiments is fairly good. Figure 5.11 shows the variation of the solid

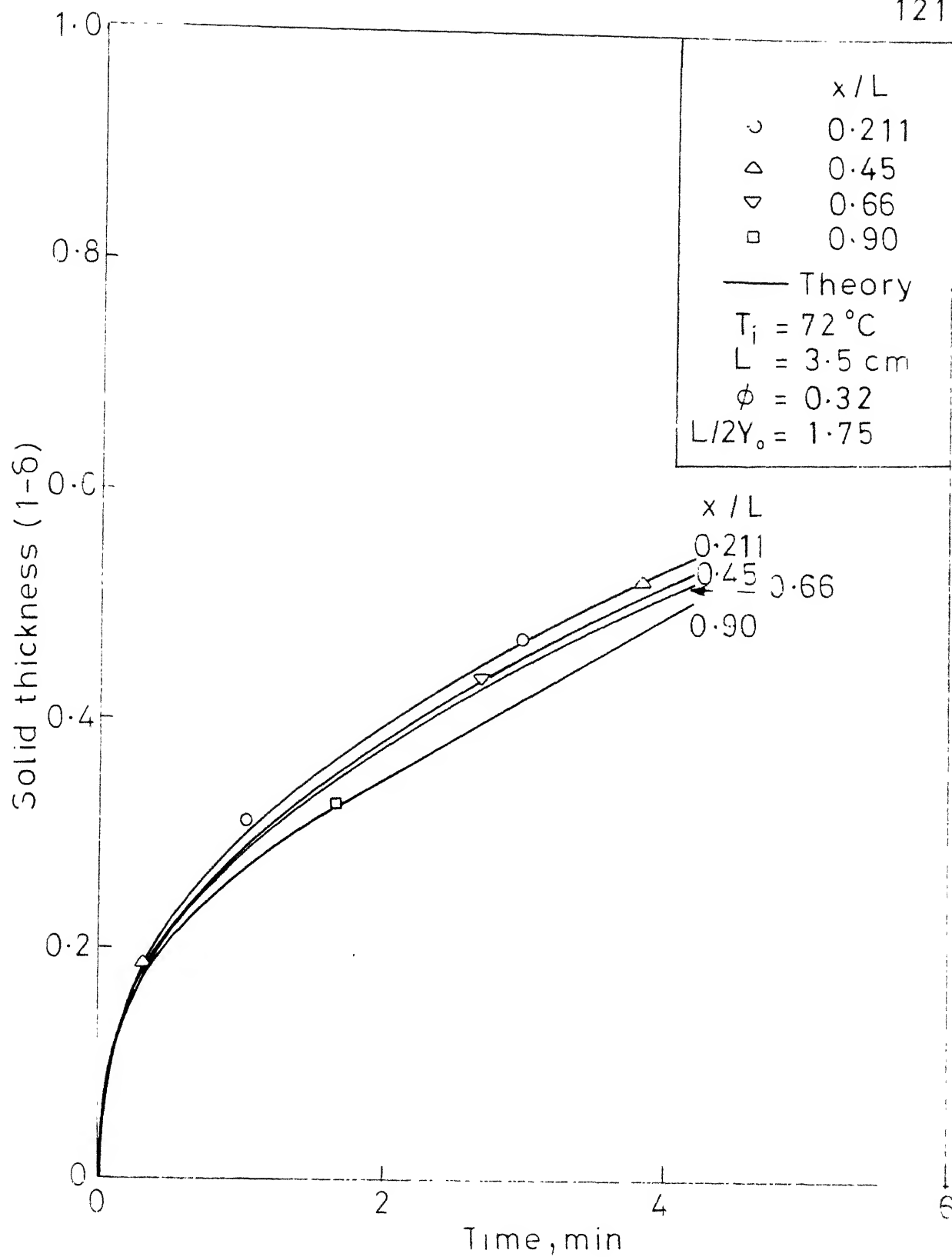


Fig.5-6 Variation of solid thickness with time
initial temperature 72°C and height
3.5 cm

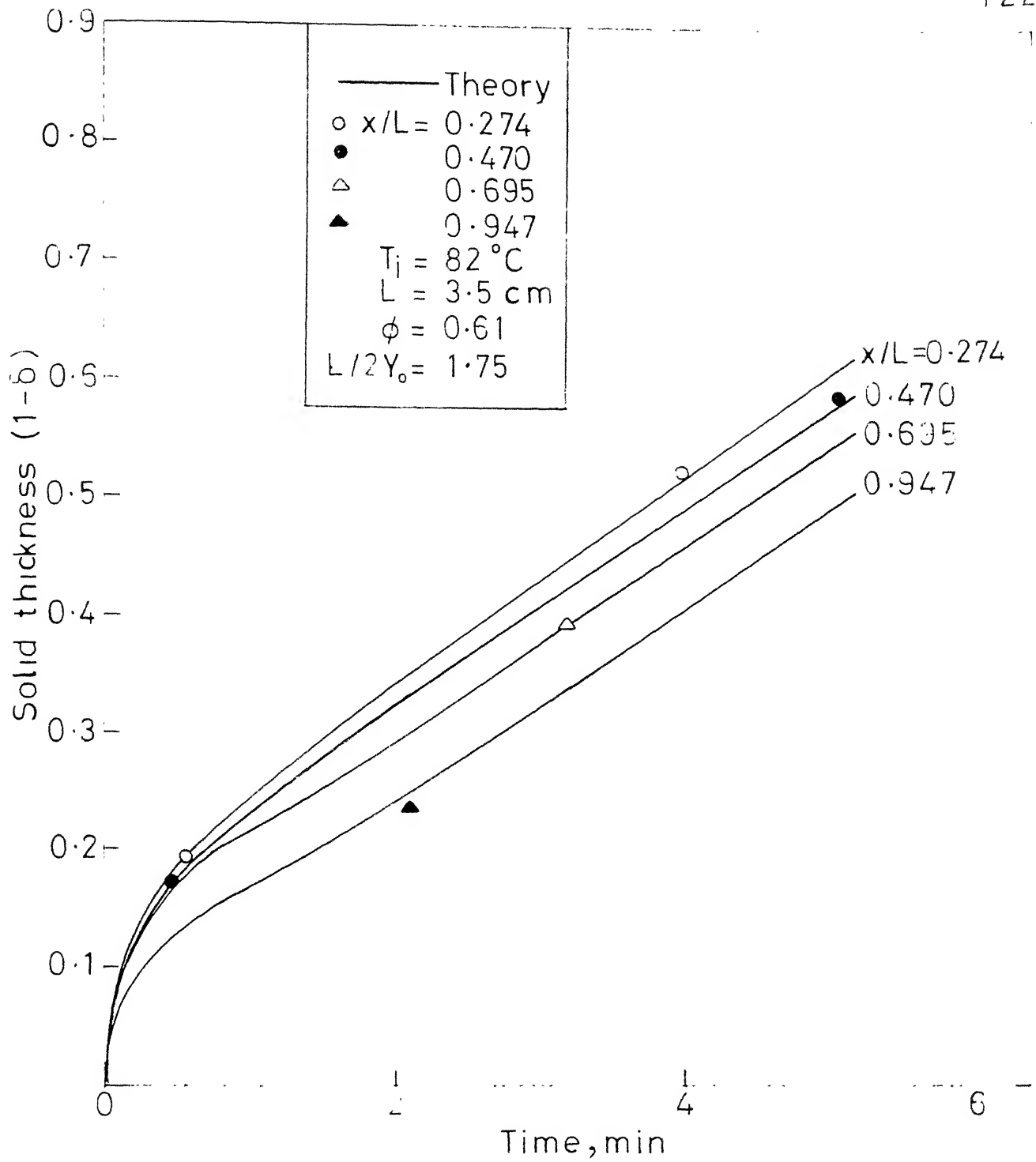


Fig. 5-7 Variation of solid thickness with time for initial temperature 82°C and height 3.5 cm

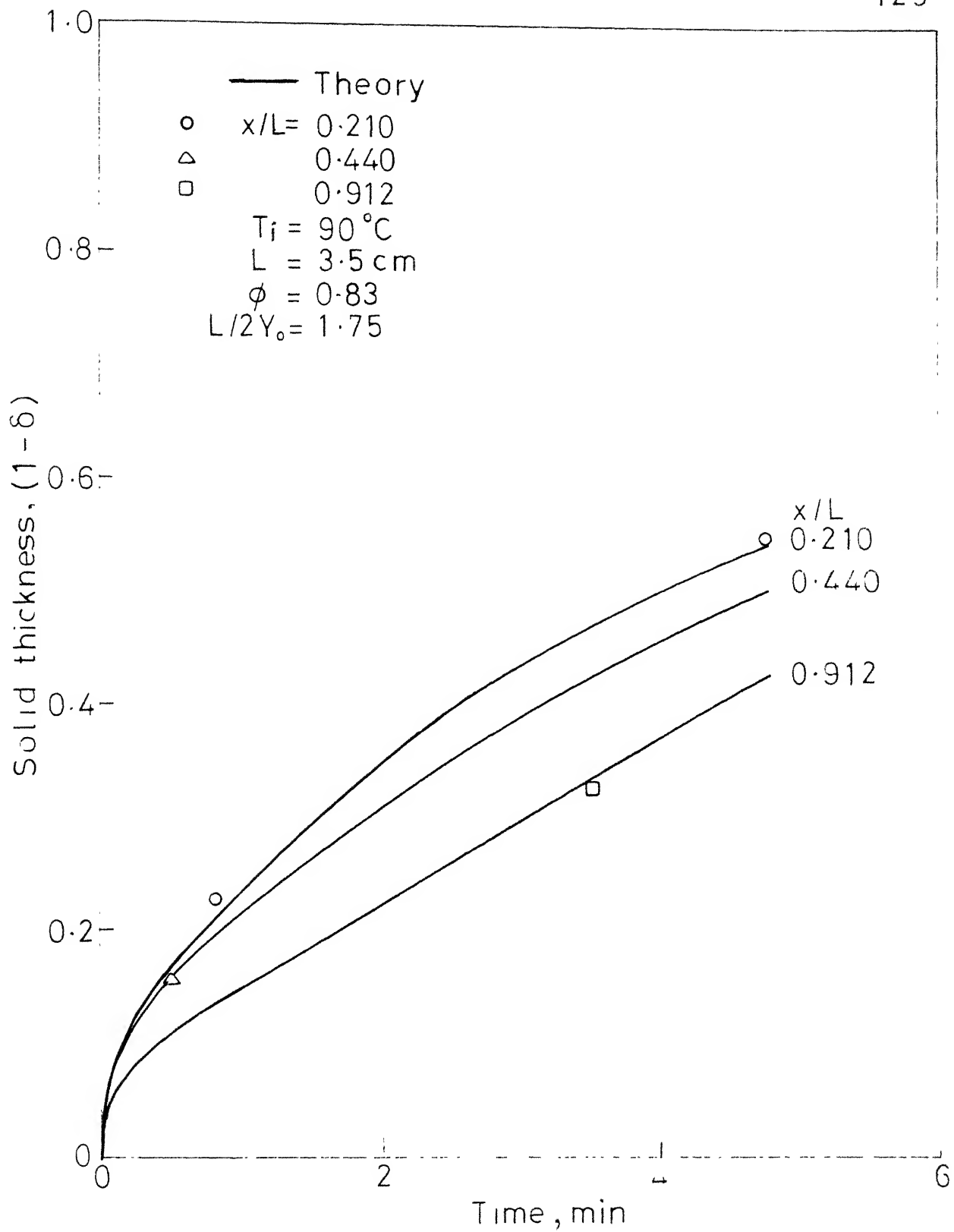


Fig.5.8 Variation of solid thickness with time for initial temperature 90°C and height 3.5 cm

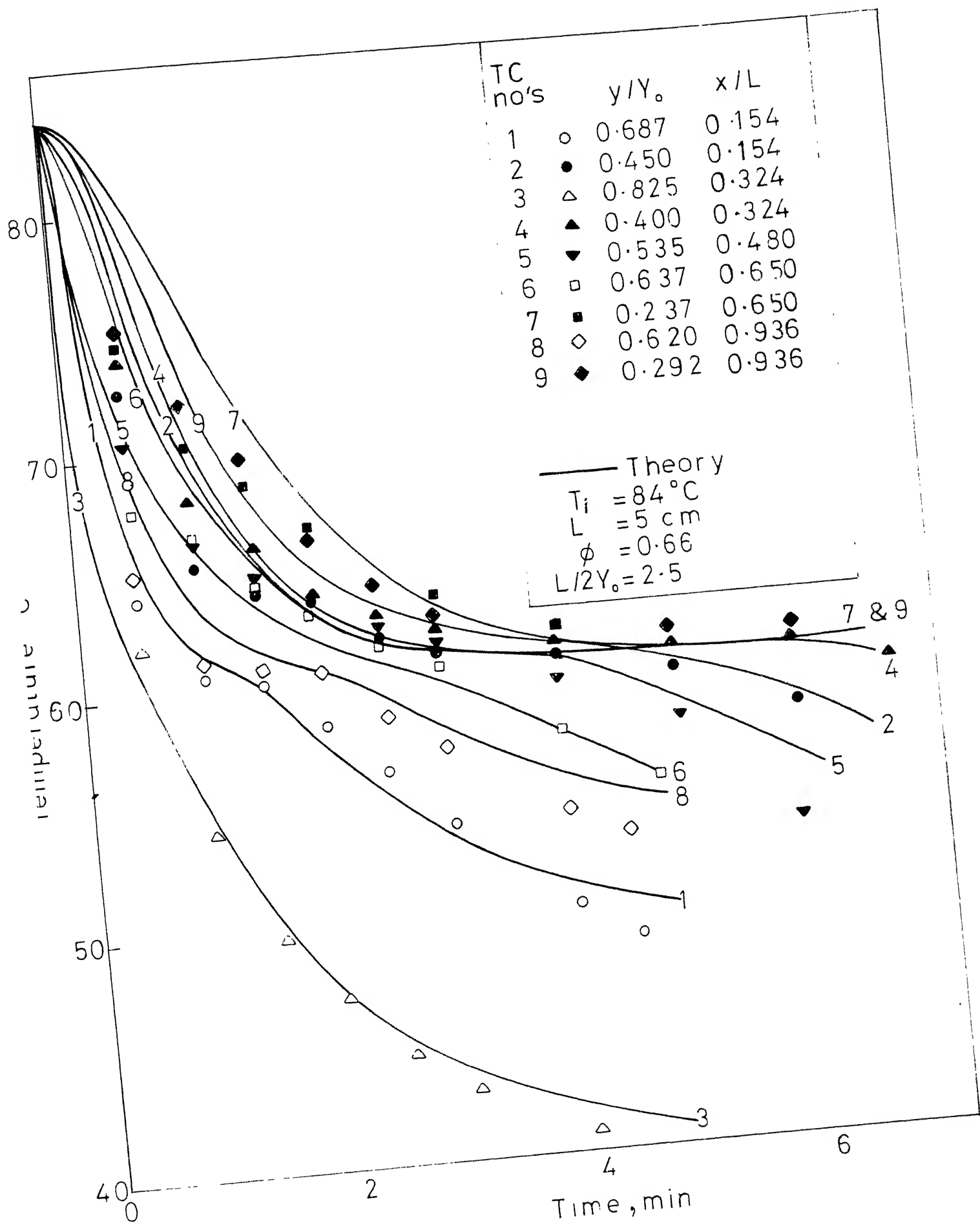


Fig.5.9 Variation of temperature with time for initial temperature 84°C and height 5 cm

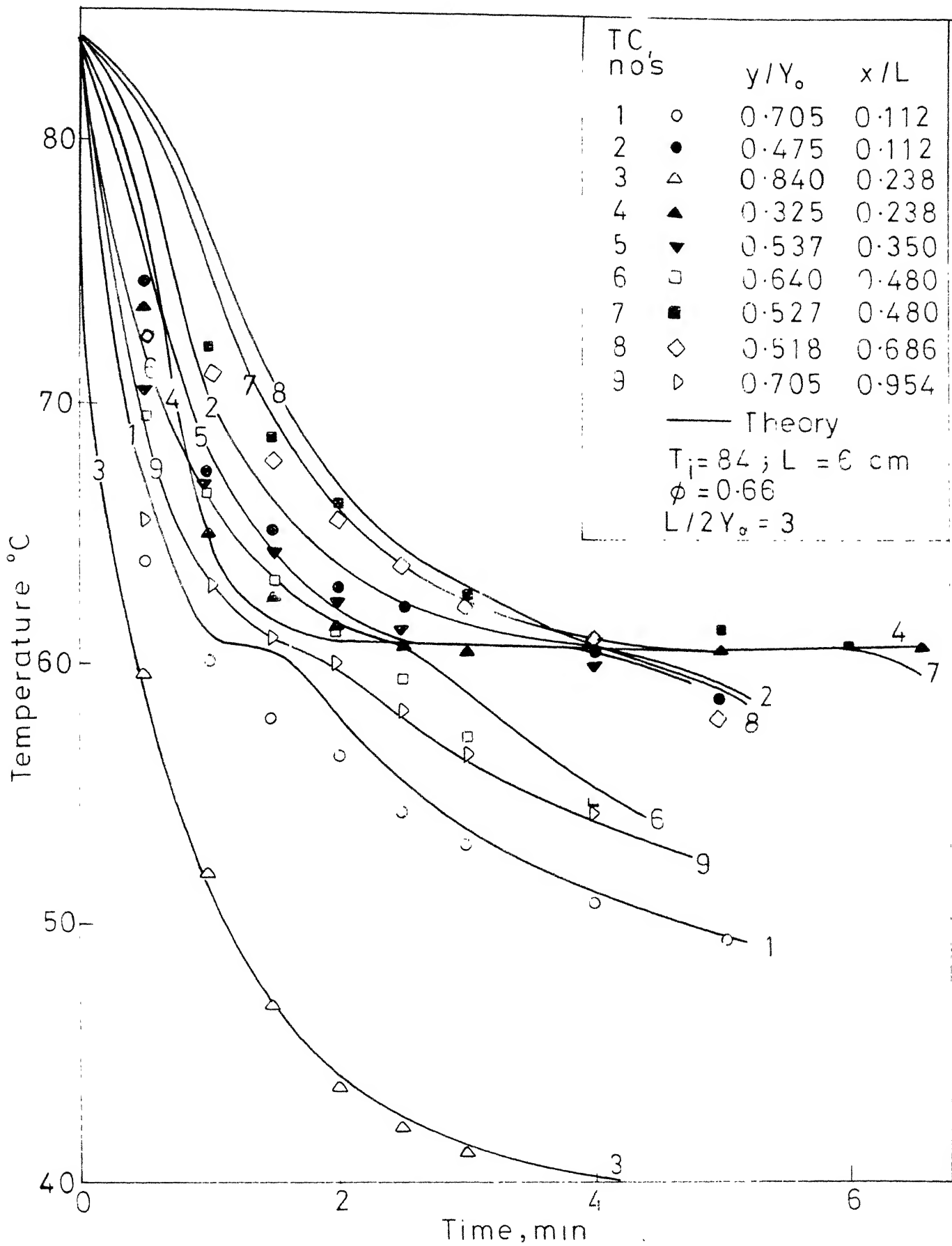


Fig. 5-10 Variation of temperature with time for initial temperature 84 °C and height 6 cm

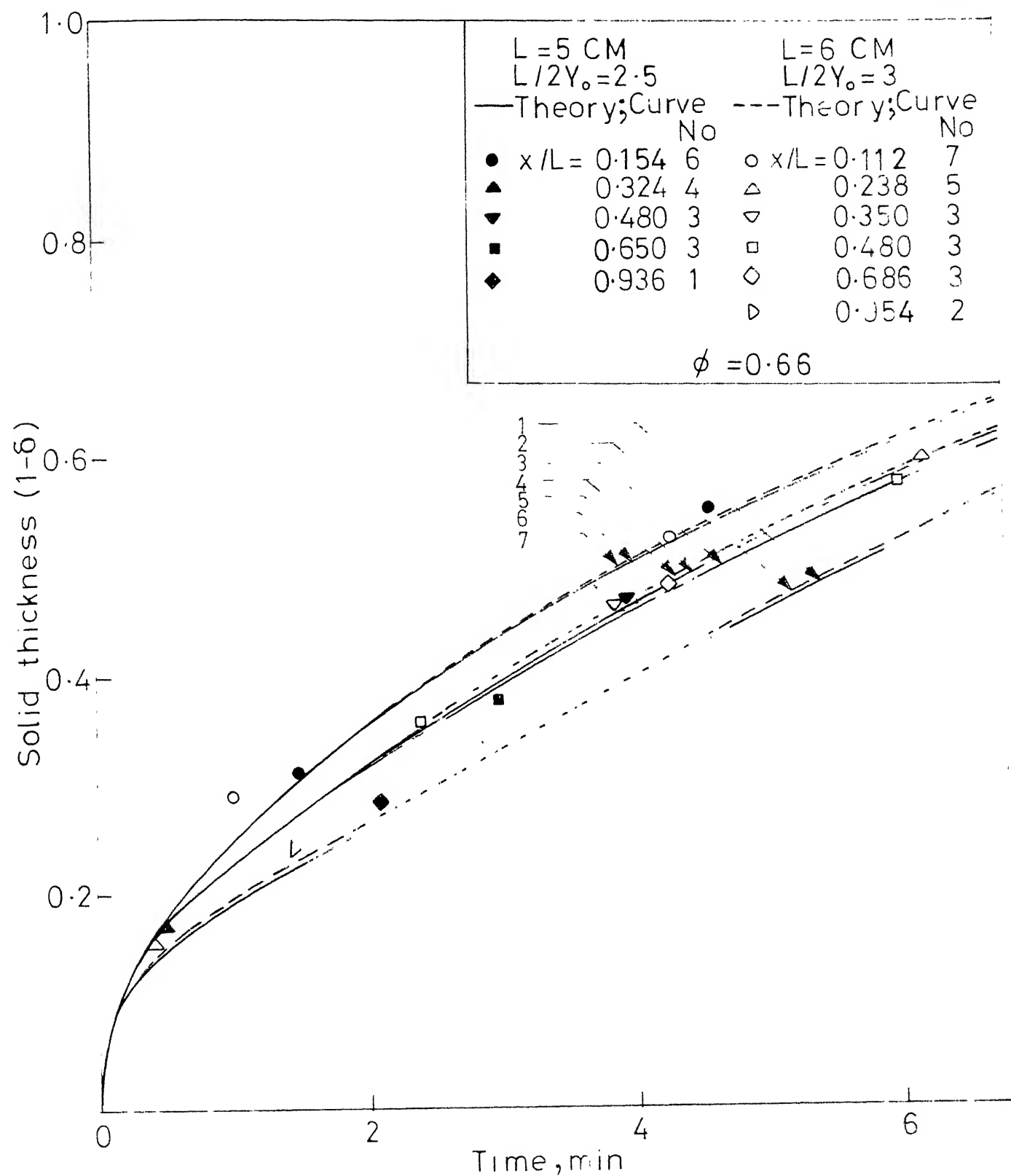


Fig.5-11 Variation of solid thickness with time for initial temperature 84°C and heights 5 cm and 6 cm

thickness with time, interpolated for both the cases (i.e. $L/2Y_0=2.5$ and 3.0). From the figure it is seen that there is very little variation in the thickness of the solid formed at all heights, $0.35 < x/L < 0.9$. This suggests that one can assume the solidification to be one dimensional if the aspect ratio is high.

5.4.2 One Dimensional Case: The results of the experiments conducted in the bigger test cell for the aspect ratio of 4.7 are compared with the theoretical results computed by one dimensional analysis discussed by Ramachandran, Jaluria and Gupta (1981a). The theoretical and experimental values of temperatures measured by different thermocouples at various times, for the superheats of 0.18, 0.35 and 0.6 are shown in Figures 5.12-5.14 respectively. Figures 5.15-5.17 show the thickness of the solid formed at various time for the superheats of 0.16, 0.35 and 0.6. In all these cases the agreement between the theory and experiments is quite good during the initial stages of solidification. As solidification progresses the gap between theory and experiments increases since the two dimensional effects come in. The results are not compared with the two dimensional analysis as the theory developed in Chapter 4 is valid only for the laminar range ($Ra \leq 10^6$), whereas in case of the bigger test cell the Rayleigh number is greater than 10^8 which lies in the turbulent zone. The

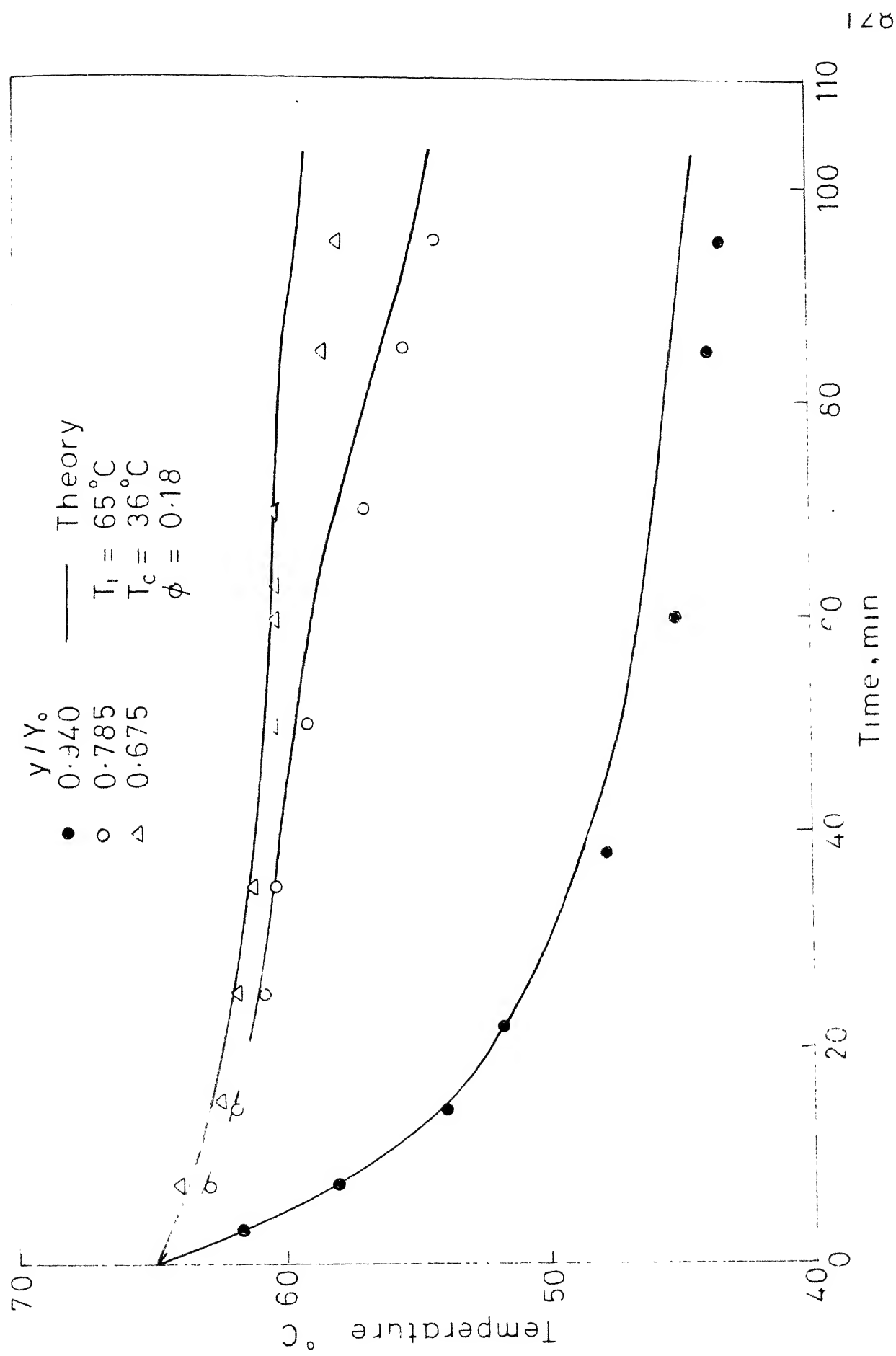


Fig. 5-12 Variation of temperature with time for one dimensional case, initial temperature of wax 65°C

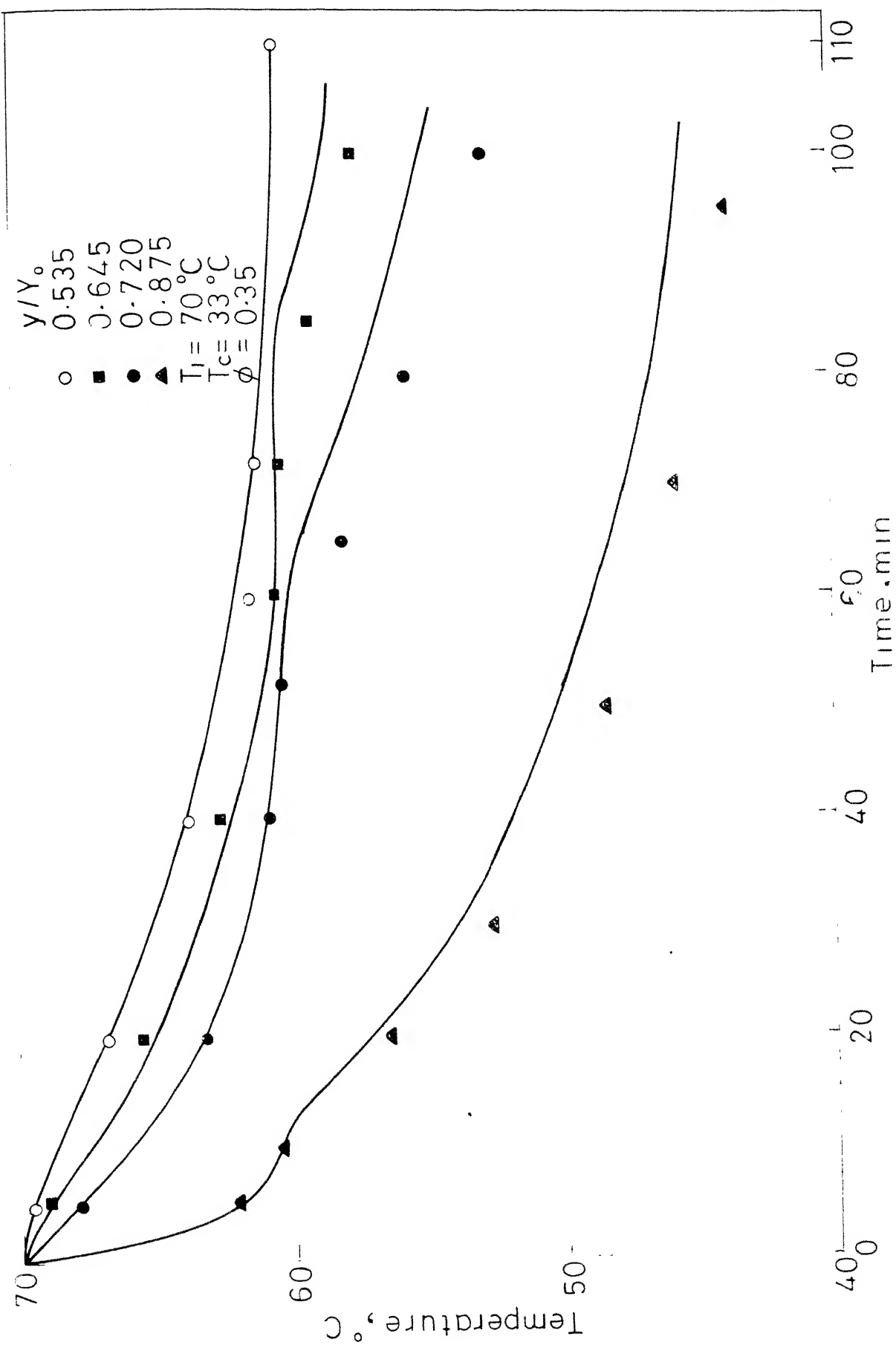


Fig. 5.13 Variation of temperature with time for one dimensional case, initial temperature 70°C

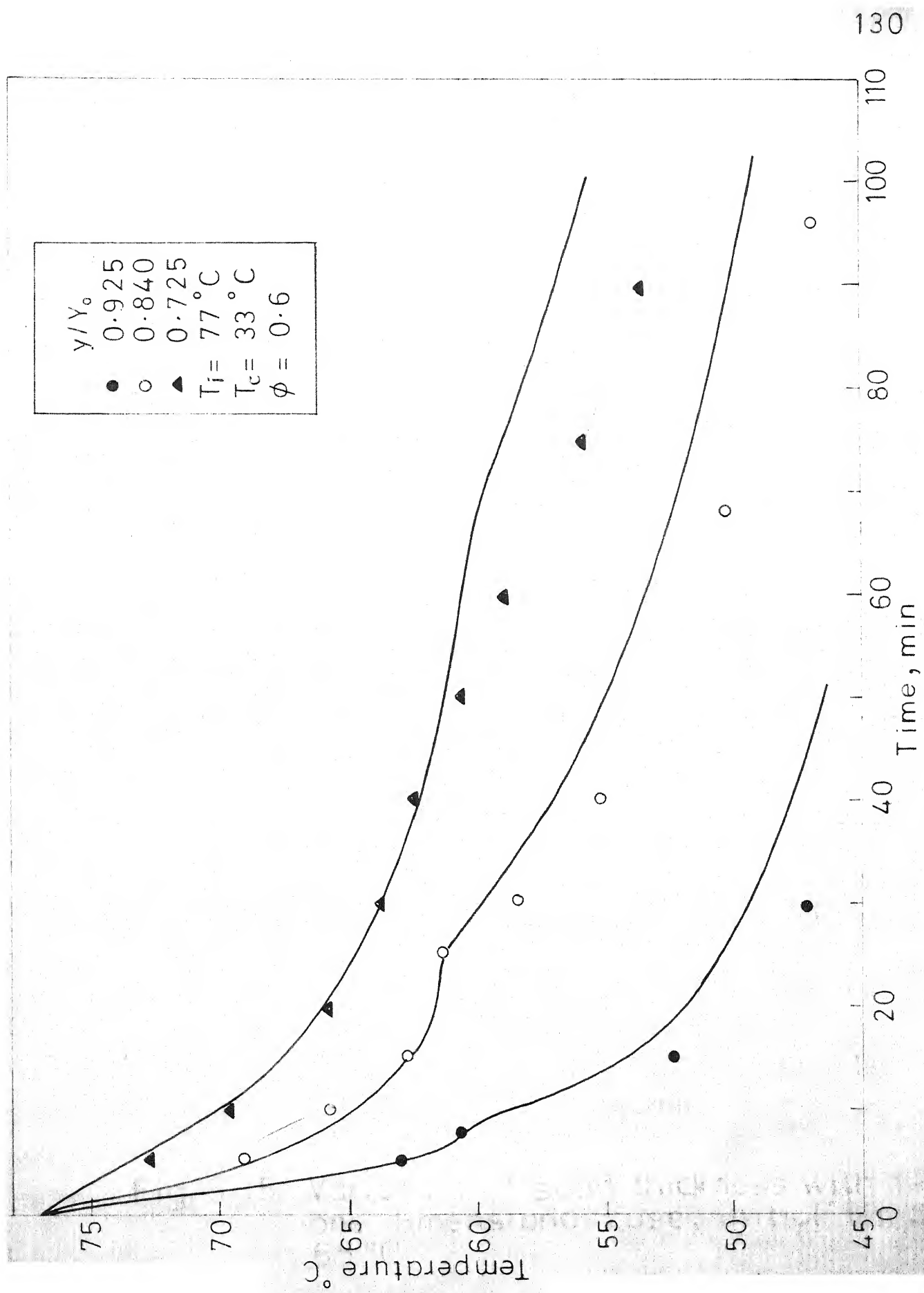


Fig. 5.14 Variation of temperature with time for one dimensional case, initial temperature 77°C

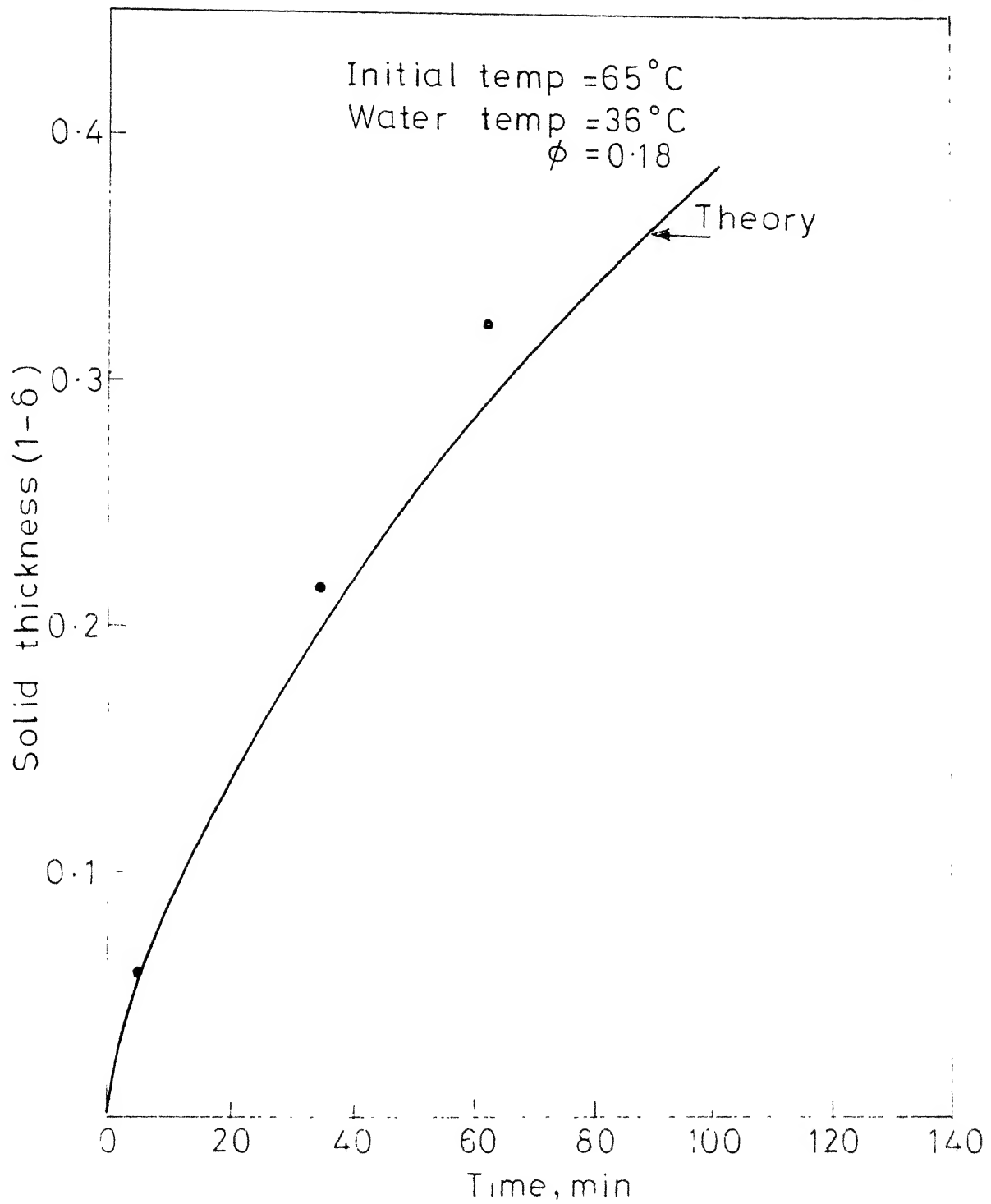


Fig. 5-15 Variation of solid thickness with time for one dimensional case, initial temperature 65°C

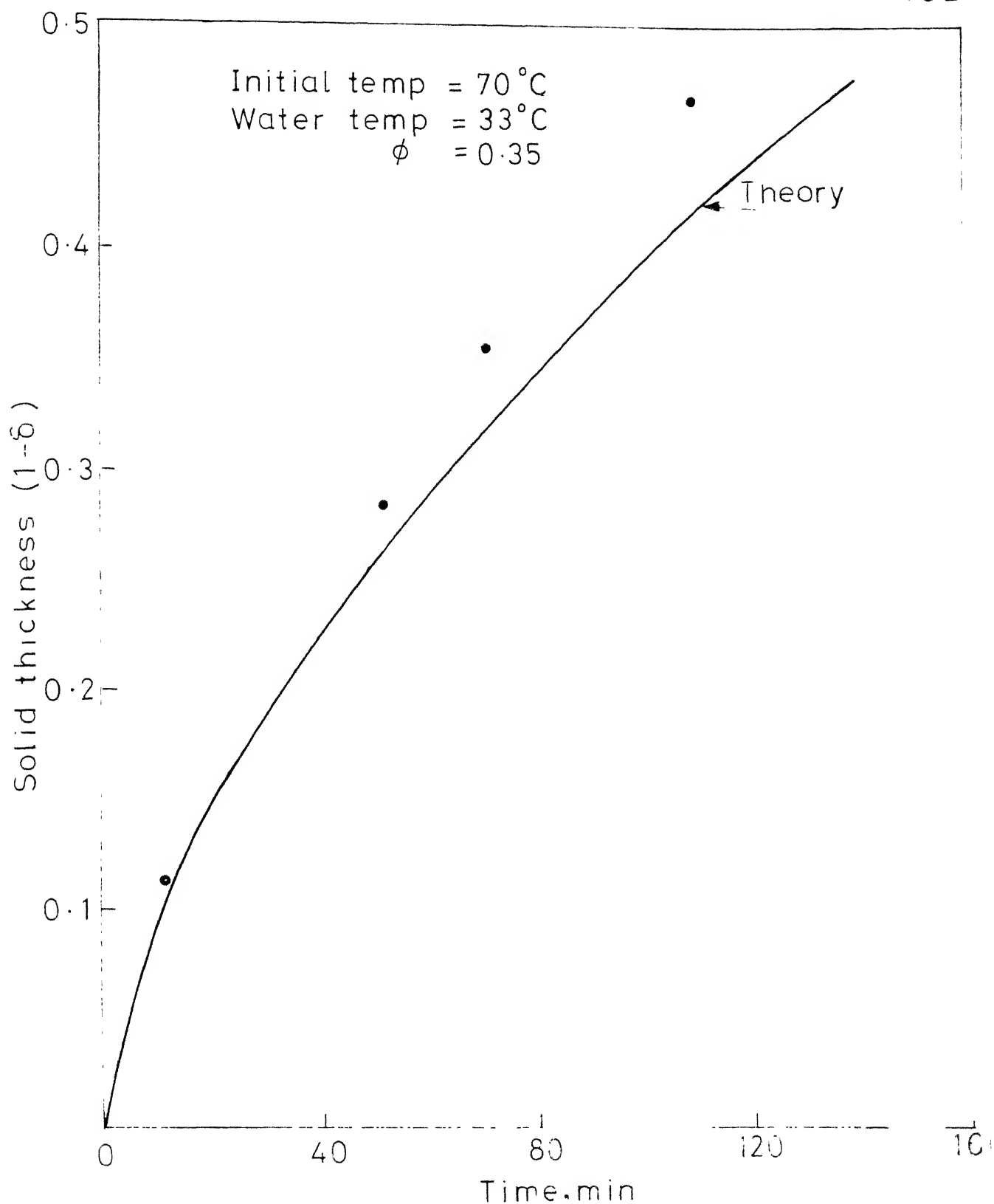


Fig.5-16 Variation of solid thickness with time for one dimensional case, initial temperature 70 °C

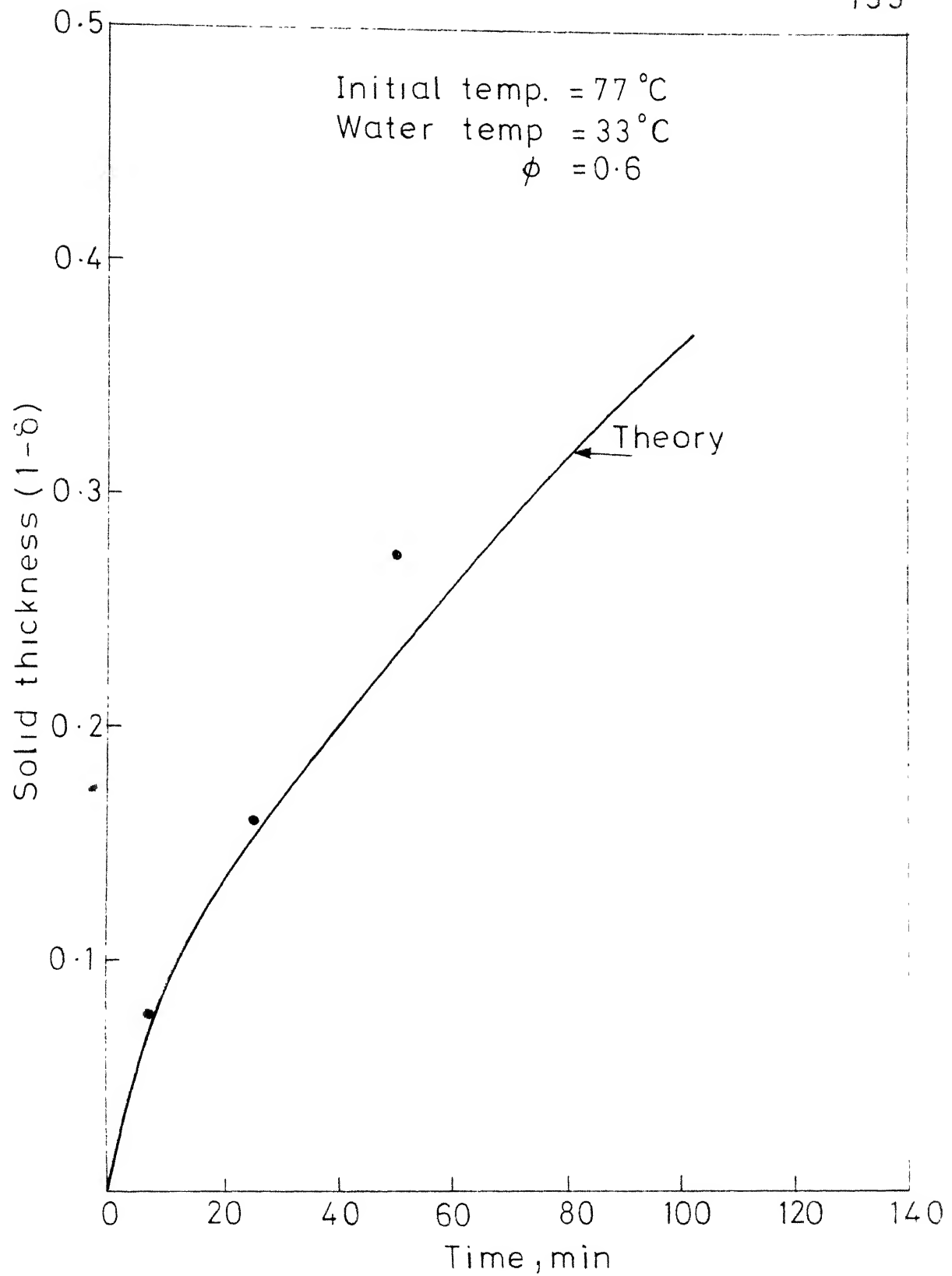


Fig.5.17 Variation of solid thickness with time for one dimensional case, initial temperature 77 °C

turbulent analysis will include the use of time averaging terms and terms related to random fluctuations in the three dimensions. Hence both the analysis and the solution methodology will be quite complex and involved, compared to the laminar analysis.

5.5 CONCLUSION:

Experiments were conducted to find the rate of interface movement and the temperature distribution in the melt and the solid during solidification using paraffin wax as solidifying material. The temperature of the solidifying wax was measured with Iron-Constantan thermocouples fixed inside the test cell. The temperatures were recorded using a high speed Data Acquisition System.

The experiments were conducted for different superheats and aspect ratios. The measured temperatures and the thickness of the solid formed at different times were compared with the theory. The agreement between the theory and experiments was found to be reasonably good.

CHAPTER 6

CONCLUSIONS AND RECOMTEENDATIONS

6.1 SUMMARY AND CONCLUSIONS:

An investigation has been made to study the thermal and fluid flow effects during solidification in an enclosed region. The study has been divided into three sections:

- (i) Computations of solidification inside one dimensional vertical slot and vertical cylinder.
- (ii) Computations of two dimensional solidification in a rectangular enclosure with natural convection in the melt.
- (iii) Experinental verification of the theoretical results obtained via steps (i) and (ii).

In the one dimensional problem, equations were written describing the heat transfer in the melt, the solid and the mold. Consideration has also been given to the natural convection in the melt. The momentum and energy equations were uncoupled and solved separately. At the outer surface of the mold, boundary conditions of first, third and fourth kinds were considered. The governing equations were non-dimensionalized and solved using implicit finite-difference technique, for various non-dimensional parameters such as the Prandtl number, Stefan number, Biot number etc.

The temperature distribution in the melt, the solid and the mold, and the velocity distribution in the melt were plotted. It has been found that value of the Grashof number is quite significant in determining the magnitude of natural convection in the melt. In case of low Prandtl number fluids, appreciable fluid motion persisted even after the removal of all the superheat. The magnitude of the fluid motion, produced by natural convection was found to be quite appreciable and comparable to the terminal rising velocities of typical non-metallic inclusions of liquid metals. The effect of various non-dimensional parameters on solidification has also been studied by plotting the rate of interface movement for them. The rate of solidification of molten steel computed through present work, was compared with the work reported in the literature and the agreement was found to be good.

In case of two dimensional analysis, the thermal and fluid motion that arise due to temperature gradients during solidification in a rectangular enclosure were considered. The equations were first solved without considering the solidification in order to have a check on the numerical scheme and later, solidification was included. The equations of continuity and momentum in the melt were combined and written in terms of vorticity and stream function. These equations along with the energy equations in the melt, the

solid and the mold were non-dimensionalized and solved for the following boundary conditions:

- (i) The top and bottom surfaces of the enclosure were kept adiabatic whereas the outer surfaces of the mold were kept at a constant temperature.
- (ii) The top and bottom surfaces of the enclosure were adiabatic, while the mold outer surfaces exchanged energy with the surroundings by convection and radiation.
- (iii) The top surface and the mold outer surfaces exchanged energy by radiation and convection, the bottom surface being kept adiabatic.

The vorticity and energy equations were solved using Alternating Direction Implicit technique. The elliptic stream function equation was solved using Successive Over-Relaxation method. The steps involved in the computation have been discussed in Section 4.3.6 of Chapter 4. The dependence of the interface movement on various non-dimensional parameters such as Rayleigh number, Prandtl number, Stefan number, aspect ratio, superheat, Biot number and Radiation constant was considered. Streamlines and isotherms were plotted for different Rayleigh numbers.

It has been found that the shape of the melt region obtained, with natural convection in the melt, is markedly different from the pure conduction solution. When the top and bottom surfaces of the enclosure were kept adiabatic,

the thickness of the melt region varied along the length of the enclosure, the thickness being the smallest at the bottom and greatest at the top.

The inclusion of natural convection in the analysis increased the heat transferred at the interface. This has been shown by plotting the ratio of the heat transferred at the interface with natural convection in the melt to the heat transferred at the interface without natural convection, at various times. The results were computed for different Rayleigh numbers and compared. The computation made to study the effect of Prandtl number on the interface motion indicated that $Pr \geq 10$ does not have any effect on the rate of movement of the interface and an asymptotic solution was reached. A comparison of the thickness of the interface at different times and different aspect ratios indicated that the solution approaches the one dimensional case when the aspect ratio is high ($L/2Y_0 \simeq 5$).

Experiments were performed in rectangular test cells using paraffin wax as the solidifying material. The paraffin wax was chosen due to its low melting and easy handling nature. The temperature of the solidifying wax was measured with Iron-Constantan thermocouples kept at predetermined levels inside the test cells and recorded with the help of a Hewlett Packard advanced Data Acquisition system. From the temperature vs time plot, the position

of the interface was found at different times. The experimental results were compared with the theoretical solutions.

In the case of comparison between the measured and computed temperatures, the agreement was found to be reasonably good except during the initial stages of solidification due to turbulence created in pouring the wax into the test cells. The difference in thickness of the wax solidified, measured at different heights of the solidifying wax was found to be negligible in the case of high aspect ratios. Similar results were obtained for the experiments conducted for one dimensional case. Thus the results obtained through the experiments confirmed the conclusion arrived through the two dimensional analysis that the solution for the rate of solidification approaches one dimensional case when the aspect ratio is high.

6.2 RECOMMENDATIONS:

In the present work, the computational program for two dimensional solidification, became unstable for $Ra > 10^5$ and $Pr > 1$. Modifications can be made incorporating better numerical techniques such as upwind differencing scheme, so that the computer program works for higher Rayleigh number. In the case of $Ra > 10^8$, which signifies the natural convection in turbulent region, analysis may be made as discussed by Jin and Churchill (1978). This is quite essential

because in case of ingot solidification of metals, the Rayleigh number calculated for a mold of dimensions found in typical ingot casting is of the order of 10^{12} which is in highly developed turbulent natural convection region.

The computational analysis made for rectangular enclosure can be easily extended to two dimensional solidification problem for cylindrical enclosure. This can be made without changing the main structure of the program written for rectangular enclosure as the only change in the governing equations, Eqs (4.2.5) -(4.2.10), is the additional convection terms due to the introduction of r-coordinate as shown below:

Energy equation in melt:

$$\frac{\partial T_1}{\partial t} + u \frac{\partial T_1}{\partial x} + v \frac{\partial T_1}{\partial r} = \alpha_1 \left(\frac{1}{r} \frac{\partial}{\partial r} \left(r \frac{\partial T_1}{\partial r} \right) + \frac{\partial^2 T_1}{\partial x^2} \right) \quad (6.2.1)$$

Vorticity:

$$\frac{\partial \omega}{\partial t} + u \frac{\partial \omega}{\partial x} + v \frac{\partial \omega}{\partial r} - v \frac{\omega}{r} = \nu \left(\nabla_r^2 \omega - \frac{\omega}{r^2} \right) - g\beta \frac{\partial T_1}{\partial r} \quad (6.2.2)$$

where ∇_r^2 is the Laplace operator in cylindrical coordinates.

Stream function:

$$\omega = -\frac{1}{r} \left(\frac{\partial^2 \psi}{\partial r^2} + \frac{1}{r} \frac{\partial \psi}{\partial r} + \frac{\partial^2 \psi}{\partial x^2} \right) \quad (6.2.3)$$

Velocity:

$$u = -\frac{1}{r} \frac{\partial \psi}{\partial r}; \quad v = \frac{1}{r} \frac{\partial \psi}{\partial x} \quad (6.2.4)$$

Energy equation in solid:

$$-\frac{\partial T_s}{\partial t} = \alpha_s \left(\frac{1}{r} \frac{\partial}{\partial r} \left(r \frac{\partial T_s}{\partial r} \right) + \frac{\partial^2 T_s}{\partial x^2} \right) \quad (6.2.5)$$

Energy equation in mold:

$$-\frac{\partial T_m}{\partial t} = \alpha_m \left(\frac{1}{r} \frac{\partial}{\partial r} \left(r \frac{\partial T_m}{\partial r} \right) + \frac{\partial^2 T_m}{\partial x^2} \right) \quad (6.2.6)$$

The analysis for the two dimensional solidification may be further extended to alloy systems. This would find a direct application in most of the metallurgical industries, where the melt solidifies over a range of temperature. In case of alloys, separate momentum and energy equations will have to be written for the mushy zone apart from the existing equations for the melt, the solid and the mold. This part can also be introduced in the existing computer program without any major change in the program structure.

Finally, the analysis can be extended to three dimensional solidification. The introduction of the third dimension complicates the solution methodology and special methods are to be looked into to solve the three dimensional parabolic equations.

In the case of experiments, apart from the temperature measurements, the flow developed in the melt can be studied

with the help of tracer particles and optical methods as discussed by Szekely and Jassal (1978). This is possible only if the solidification occurs below room temperature, so that the material does not solidify on the Perspex walls of the test cell, immediately after pouring the melt and thereby obstructing the view for any optical measurement. For this purpose any low melting n-paraffin between $C_{14}H_{30}$ and $C_{19}H_{40}$ may be used. The flow developed in the melt can be observed using Schlieren photographic technique and the interface movement can be photographed. For experiments to study the solidification of binary alloy systems, a solution of ammonium chloride in water can be used as the solidifying material with methanol circulated in the jacket of the test cell as coolant. Experiments may also be conducted for other boundary conditions described in Chapters 3 and 4.

REFERENCES

1. Batchelor, G.K., Quart J. Appl. Math., 12, p.209 (1954).
2. Bennett, H., 'Commercial Waxes', 2nd ed., Chemical Publishing Co., Inc., New York, (1959).
3. Boley, B.A., Quart J. Mech. Appl. Math., 17, p.253(1964).
4. Carnahan, B., Luther, H.A., and Wilkes, J.O., 'Applied numerical methods', John Wiley and Sons, Inc., New York, (1969).
5. Carslaw, H.S., and Jaeger, J.C., 'Conduction of heat in solids', 2nd ed., Clarendon Press, Oxford (1959).
6. Chiesa, F.H., and Guthrie, R.I.L., J. Heat Transfer, Trans. ASME, Series C, 96, p.377 (1974).
7. Cole, G.S., 'Solidification', Paper presented at a Seminar of the Am.Soc. for Metals, Metals Park, Ohio (1969).
8. Cole, G.S., and Bolling, G.F., Trans. TMS-AIME, 233, p.1568 (1965).
9. De Vahl Davis, G., Int. J. Heat Mass Transfer, 11, p.1675 (1968).
10. Dix, R.C., and Cizek, J., Paper presented at the IVth International Heat Transfer Conference at Paris, Vol. I, Elsevier Publishing Co., Amsterdam, (1970).
11. Eckert, E.R.G., and Carlson, W.O., Int. J. Heat Mass Transfer, 2, p.106 (1961).
12. Elder, J.W., J. Fluid Mech., 23, part 1, p.77 (1965).

13. Elder, J.W., J. Fluid Mech., 24, part 4, p.823(1966).
14. Elliott, J.F., and Gleiser, H., 'Thermochemistry for Steelmaking', Vol.1, Addison-Wesley Publishing Co., Inc., London, (1960).
15. Forsythe, G.E., and Wasow, W., 'Finite difference methods for partial differential equations', Wiley, New York (1960).
16. Garcia, A., and Prates, M., Met. Trans. B, 9B, p. 449 (1978).
17. Goodling, J.S., and Khader, H.S., J. Heat Transfer, Trans. ASME, 96, p.114 (1974).
18. Goodman, T.R., Trans. ASME, 80, p.335 (1958).
19. Hamil, T.D., and Bankoff, S.G., AIChE J., 9, p.741 (1963).
20. Heertjes, P.M., Jongenelen, J.A., and de Leeuw den Bouter, J.A., Chemical Engineering Science, 25, p. 1881 (1970).
21. Hills, A.W.D., and Moore, H.K., 'Heat and Mass Transfer in Process Metallurgy', Inst. Mining Met., London, (1967).
22. Hrycak, P., AIChE J, 9, p. 585 (1963).
23. Jaluria, Y., 'Natural convection heat and mass transfer', Pergamon Press, Oxford (1980).
24. Kosky, P.G., Letters in Heat Mass Transfer, 2, p.339 (1975).
25. Lin, S.J., and Churchill, S.W., Numerical Heat Transfer, 1, p.129 (1978).

- 147
26. Hegerlin, F., *Forsch. Ing.-Wes.*, 34, p.40 (1968)
(as referred to in Ref.22).
 27. Nelson, W.L., 'Petroleum refinery engineering', 4th ed.,
McGraw-Hill, New York (1958).
 28. Nowell, M.E., and Schmidt, F.W., *J. Heat Transfer, Trans.*
ASME, 92, p.159 (1970).
 29. Ostrach, S., and Kroger, P.G., *Int. J. Heat Mass Transfer*,
17, p.1191 (1974).
 30. Özisik, H.N., and Nody, K.J., *Letters in Heat Mass*
Transfer, 2, p.487 (1975).
 31. Paschkis, V., *Trans. AFS*, 53, p.90 (1945).
 32. Patankar, S.V., and Spalding, D.B., *Int. J. Heat Mass*
Transfer, 10, p.1389 (1967).
 33. Patel, P.D., *AIAA J.*, 6, p.2454 (1968).
 34. Peaceman, D.W., and Rachford, H.H., Jr., *J.Soc. Indust.*
Applied Mathematics, 3, p.28 (1955).
 35. Ramachandran, N., Jaluria, Y. and Gupta, J.P., *Letters*
in Heat Mass Transfer, (1981a) (accepted for publication).
 36. Ramachandran, N., Gupta, J.P., and Jaluria, Y., *Int. J.*
Heat Mass Transfer, (1981b) (communicated).
 37. Ramachandran, N., Gupta, J.P., and Jaluria, Y., *Numerical*
Heat Transfer, (1981c) (in preparation).
 38. Ramachandran, N., Gupta, J.P., and Jaluria, Y., *Int.*
J. Heat Mass Transfer, (1981d) (in preparation).
 39. Riemann, W., 'Die partiellen differentialgleichungen
der mathematischen physik' Vol.2, 5th ed., (1912) (as
referred to in Ref.5).

40. Roache, P.J., 'Computational fluid dynamics', Hermosa, Albuquerque, New Mexico, (1976).
41. Ruddle, R.W., 'The Solidification of Casting', Inst. Metals Monograph No.7, London, (1957).
42. Samuels, H.R., and Churchill, S.W., AICHE J., 13 p.77 (1967).
43. Sarjant, R.J., and Slack, M.R., J. Iron Steel Inst., 177, p.428 (1954).
44. Schlichting, H., 'Boundary Layer Theory', 6th ed., McGraw-Hill Book Co., New York (1969).
45. Schwartz, C., Z. Angew Math Mech, 13, p.202 (1933).
(as referred to in Ref.39).
46. Seki, N., Fukusako, S., and Sugawara, H., J. Heat Transfer, Trans. ASME, 99, p. 92 (1977).
47. Spalding, D.B., 'GENHEX - A General computer program for two dimensional parabolic phenomena', Pergamon Press, Oxford (1977).
48. Sparrow, E.M., Patankar, S.V., Ramadhyani, S., J. Heat Transfer, Trans. ASME, 99, p.520 (1977).
49. Sparrow, E.M., Ramsey, J.W., J. Heat Transfer, Trans. ASME, 100, p.368 (1978).
50. Sparrow, E.M., Ramsey, J.W., Kemink, R.G., J. Heat Transfer, Trans. ASME, 101, p.578 (1979).
51. Sparrow, E.M., Shamsundar, H., J. Heat Transfer, Trans. ASME., 96, p.541 (1974).

52. Szekely, J., and Chhabra, P.S., Met. Trans., 1, p.1195 (1970).
53. Szekely, J., and Ludley, J.H., J. Iron Steel Inst., 204, p.12 (1966).
54. Szekely, J., and Stanek, V., Met. Trans. 1, p.2243 (1970).
55. Szekely, J., and Todd, H.R., Int. J. Heat Mass Transfer, 14, p.467 (1971).
56. Szekely, J., and Jassal, A.S., Met. Trans.B., 9B, p.389 (1978).
57. Tien, R.H., Trans. TMS-AIME, 233, p.1837 (1965).
58. Tiller, W.A., Trans. TMS-AIME, 224, p.448 (1962).
59. Torrance, K.E., Rockett, J.A., J. Fluid Mech., 36, Part 1, p.33 (1969).
60. Wilkes, J.O., and Churchill, S.W., AIChE J., 12, p.161 (1966).

APPENDIX I

SIMPLIFICATION OF MOMENTUM EQUATION

The momentum equation for the u-component is written as

$$\rho \cdot \frac{\partial u}{\partial t} = \mu \frac{\partial^2 u}{\partial y^2} - \rho g - \frac{\partial p}{\partial x} \quad (I.1)$$

The pressure term appearing in the RHS may be broken into two terms; one due to hydrostatic pressure p_a and the other due to motion of fluid. The variation of p_a along x-direction is neglected, because of the one dimensional assumption. Since the gravitational force is acting on the x-direction, the hydrostatic pressure term p_a can be written as:

$$\frac{\partial p_a}{\partial x} = - \rho_{sat} g \quad (I.2)$$

Substituting (I.2) in (I.1)

$$\rho \frac{\partial u}{\partial t} = \mu \frac{\partial^2 u}{\partial y^2} + g (\rho_{sat} - \rho) \quad (I.3)$$

The densities appearing in Eqn.(I.3) can be related to the temperature through the Boussinesq approximation, discussed by Jaluria (1980).

According to Boussinesq approximation, density variations are considered only insofar as they contribute

to buoyancy, but otherwise neglected. If \bar{T} is the average temperature of the fluid and ρ_{sat} is the corresponding density, then,

$$\rho = \rho_{\text{sat}} - \beta \rho (T - \bar{T}) \quad (\text{I.4})$$

where β = temperature coefficient of cubic expansion.

Thus the Eqn.(I.1) becomes,

$$\frac{\partial u}{\partial t} = \nu \frac{\partial^2 u}{\partial y^2} + g\beta (T - \bar{T}) \quad (\text{I.5})$$

APPENDIX II

RADIATIVE BOUNDARY CONDITION

From the Eqn.(3.2.15i), the radiative boundary condition is written as,

$$\frac{\partial T_m^*}{\partial y_m^*} = - Rc_1 [(T_c^* + T_m^*)^4 - T_c^{*4}] \quad (II.1)$$

This can be simplified to:

$$\frac{\partial T_m^*}{\partial y_m^*} = - Rc_1 (T_t^{*2} + T_c^{*2}) (T_t^* + T_c^*) T_m^* \quad (II.2)$$

where $T_t^* = T_c^* + T_m^*$

In finite-difference form, the above equation may be written as,

$$\frac{T_{m,j,n+1}^* - T_{m,j-1,n+1}^*}{\Delta y_m^*} = -T_{m,j,n+1}^* Rc_1 (T_{t,j,n}^{*2} + T_c^{*2}) (T_{t,j,n}^* + T_c^*) \quad (II.3)$$

Since $T_{t,j,n}^*$ is known from the previous time step, Eqn.(II.3) can be simplified to:

$$(1 + K_c) T_{m,j,n+1}^* - T_{m,j-1,n+1}^* = 0 \quad (II.4)$$

where $K_c = Rc_1 (T_{t,j,n}^{*2} + T_c^{*2}) (T_{t,j,n}^* + T_c^*)$

Eqn.(II.4) is linear and can be solved along with the other equations formed by implicit, finite-difference method.

APPENDIX IIIPROPERTIES OF STEEL

From Elliott and Gleason (1960), the following properties are taken:

$$\text{Specific heat } C_p = 6.3 \times 10^2 \text{ J/Kg } ^\circ\text{K}$$

$$\text{Density } \rho = 7.1 \times 10^3 \text{ Kg/m}^3$$

$$\text{Kinematic viscosity } \nu = 9.4 \times 10^{-7} \text{ m}^2/\text{s}$$

$$\text{Prandtl number } Pr = 0.15$$

$$\text{Latent heat } L_q = 226 \times 10^3 \text{ J/Kg}$$

$$\text{Thermal conductivity } k_1 = 0.464 \text{ J/s m } ^\circ\text{K}$$

$$\text{Thermal diffusivity } \alpha_1 = 6.27 \times 10^{-6} \text{ m}^2/\text{s}$$

$$\begin{aligned} \text{Coefficient of cubical} \\ \text{expansion } \beta &= 1.3 \times 10^{-4} \text{ } ^\circ\text{K}^{-1} \end{aligned}$$

APPENDIX IV

MOVING BOUNDARY EQUATION

The energy balance at the melt-solid interface is written as,

$$k_s \frac{\partial T_s}{\partial n} - k_l \frac{\partial T_l}{\partial n} = \rho L_q v_n \quad (\text{IV.1})$$

where n = outward normal to the interface (i.e. into the melt)

v_n = velocity of the interface in the normal direction

Since the interface is an isotherm the following condition is written,

$$T_l = T_{\text{sat}} = T_s \quad (\text{IV.2})$$

The interface position can be defined by the following equation

$$f'(x, y, z, t) = 0 \quad (\text{IV.3})$$

In the case of two dimensional solidification only the effect of x and y directions is considered. Moreover, the temperature gradients at the interface in the x -direction can be expressed in terms of gradients in y -direction by the differentiation of Eqs (IV.2) and (IV.3) as

$$\frac{\partial T_l}{\partial x} = \frac{\partial f' / \partial x}{\partial f' / \partial y} \frac{\partial T_l}{\partial y} \quad (\text{IV.4})$$

and,

$$\frac{\partial T_S}{\partial x} = \frac{\partial f' / \partial x}{\partial f' / \partial y} \frac{\partial T_S}{\partial y} \quad (\text{IV.5})$$

Equation (IV.1) can be expressed in the following form as discussed by Patel (1968).

$$k_S \nabla T_S \nabla f' - k_L \nabla T_L \nabla f' = - \rho L_q \left(\frac{\partial f'}{\partial t} \right) \quad (\text{IV.6})$$

Substitution of Eqs.(IV.4) and (IV.5) into Eqn.(IV.6) results in the following expression

$$\left[1 + \left(\frac{\partial f' / \partial x}{\partial f' / \partial y} \right)^2 \right] \left[k_S \frac{\partial T_S}{\partial y} - k_L \frac{\partial T_L}{\partial y} \right] = - \rho L_q \frac{\partial f' / \partial t}{\partial f' / \partial y} \quad (\text{IV.7})$$

If $f'(x, y, t) = y - Y'(x, t) = 0$, Eqn.(IV.7) reduces to

$$\left(k_S \frac{\partial T_S}{\partial y} - k_L \frac{\partial T_L}{\partial y} \right) \left(1 + \left(\frac{\partial Y'}{\partial x} \right)^2 \right) = \rho L_q \frac{\partial Y'}{\partial t} \quad (\text{IV.8})$$

APPENDIX V

COORDINATE TRANSFORMATION

The original variables x , y and t can be replaced by the transformed variables x^* , y^* and t^* , applying the non-dimensional parameters described in Chapter 4 (Eqn. (4.2.14)).

Thus,

For melt:

$$\frac{\partial}{\partial t} = \frac{\alpha_1}{D^2} \frac{\partial}{\partial t^*} - \frac{y_1^*}{Y_1} \frac{\partial Y_1}{\partial t^*} \frac{\partial}{\partial y_1^*} \quad (V.1a)$$

$$\frac{\partial}{\partial x} = \frac{1}{L} \frac{\partial}{\partial x^*} - \frac{Y_1^*}{Y_1} \frac{\partial Y_1}{\partial x^*} \frac{\partial}{\partial y_1^*} \quad (V.1b)$$

$$\frac{\partial}{\partial y} = \frac{1}{Y_1} \frac{\partial}{\partial y_1^*} \quad (V.1c)$$

For solid:

$$\frac{\partial}{\partial t} = \frac{\alpha_1}{D^2} \frac{\partial}{\partial t^*} + \left(\frac{y_S^*}{Y_0} - \frac{1}{Y_1} \right) \frac{\partial Y_1}{\partial t^*} \frac{\partial}{\partial y_S^*} \quad (V.2a)$$

$$\frac{\partial}{\partial x} = \frac{1}{L} \frac{\partial}{\partial x^*} + \left(\frac{y_S^*}{Y_0} - \frac{1}{Y_1} \right) \frac{\partial Y_1}{\partial x^*} \frac{\partial}{\partial y_S^*} \quad (V.2b)$$

$$\frac{\partial}{\partial y} = \left(\frac{1}{Y_0} - \frac{1}{Y_1} \right) \frac{\partial}{\partial y_S^*} \quad (V.2c)$$

Applying Eqs (V-1a) - (V-2c) to Eqs (4.2.5)-(4.2.10) of Chapter 4, the following transformed equations are obtained:

$$\begin{aligned}
& \frac{\partial T_1^*}{\partial t^*} + u^* \frac{\partial T_1^*}{\partial x^*} + \left(\frac{D}{Y_1}\right) v^* \frac{\partial T_1^*}{\partial y_1^*} - \frac{y_1^*}{\delta} \frac{\partial \delta}{\partial t^*} \frac{\partial T_1^*}{\partial y_1^*} \\
& = \left(\frac{D}{L}\right)^2 \frac{\partial^2 T_1^*}{\partial x^{*2}} + \left(\frac{D}{Y_1}\right)^2 \frac{\partial^2 T_1^*}{\partial y_1^{*2}} - \left(\frac{D}{L}\right)^2 \left\{ \frac{y_1^*}{\delta} \frac{\partial^2 \delta}{\partial x^{*2}} \frac{\partial T_1^*}{\partial y_1^*} \right. \\
& \quad \left. - \frac{y_1^*}{\delta^2} \left(\frac{\partial \delta}{\partial x^*}\right)^2 \frac{\partial T_1^*}{\partial y_1^*} + \frac{y_1^*}{\delta} \frac{\partial \delta}{\partial x^*} \frac{\partial^2 T_1^*}{\partial x^* \partial y_1^*} + \frac{1}{\delta} \frac{\partial \delta}{\partial x^*} \frac{\partial T_1^*}{\partial y_1^*} \frac{\partial y_1^*}{\partial x^*} \right\} \\
& \quad + u^* \frac{y_1^*}{\delta} \frac{\partial \delta}{\partial x^*} \frac{\partial T_1^*}{\partial y_1^*} \tag{V.3}
\end{aligned}$$

$$\begin{aligned}
& \frac{\partial \omega^*}{\partial t^*} + u^* \frac{\partial \omega^*}{\partial x^*} + v^* \left(\frac{D}{Y_1}\right) \frac{\partial \omega^*}{\partial y_1^*} - \frac{y_1^*}{\delta} \frac{\partial \delta}{\partial t^*} \frac{\partial \omega^*}{\partial y_1^*} \\
& = - \text{Ra} \cdot \text{Pr} \left(\frac{D}{L}\right) \left(\frac{D}{Y_1}\right) \left(\frac{D}{Y_0}\right)^3 \frac{\partial T_1^*}{\partial y_1^*} + \text{Pr} \left(\frac{D}{L}\right)^2 \frac{\partial^2 \omega^*}{\partial x^{*2}} + \text{Pr} \left(\frac{D}{Y_1}\right)^2 \frac{\partial^2 \omega^*}{\partial y_1^{*2}} \\
& \quad - \text{Pr} \left(\frac{D}{L}\right)^2 \left\{ \frac{y_1^*}{\delta} \frac{\partial \omega^*}{\partial y_1^*} \frac{\partial^2 \delta}{\partial x^{*2}} - \frac{y_1^*}{\delta^2} \left(\frac{\partial \delta}{\partial x^*}\right)^2 \frac{\partial \omega^*}{\partial y_1^*} \right. \\
& \quad \left. + \frac{y_1^*}{\delta} \frac{\partial \delta}{\partial x^*} \frac{\partial^2 \omega^*}{\partial x^* \partial y_1^*} + \frac{1}{\delta} \frac{\partial \delta}{\partial x^*} \frac{\partial \omega^*}{\partial y_1^*} \frac{\partial y_1^*}{\partial x^*} \right\} \\
& \quad + u^* \frac{y_1^*}{\delta} \frac{\partial \delta}{\partial x^*} \frac{\partial \omega^*}{\partial y_1^*} \tag{V.4}
\end{aligned}$$

$$\begin{aligned}
\omega^* & = - \left(\frac{D}{Y_1}\right)^2 \frac{\partial^2 \psi^*}{\partial y_1^{*2}} - \left(\frac{D}{L}\right)^2 \frac{\partial^2 \psi^*}{\partial x^{*2}} + \left(\frac{D}{L}\right)^2 \left\{ \frac{y_1^*}{\delta} \frac{\partial \psi^*}{\partial y_1^*} \frac{\partial^2 \delta}{\partial x^{*2}} \right. \\
& \quad \left. - \frac{y_1^*}{\delta^2} \left(\frac{\partial \delta}{\partial x^*}\right)^2 \frac{\partial \psi^*}{\partial y_1^*} + \frac{y_1^*}{\delta} \frac{\partial \delta}{\partial x^*} \frac{\partial^2 \psi^*}{\partial x^* \partial y_1^*} + \frac{1}{\delta} \frac{\partial \delta}{\partial x^*} \frac{\partial \psi^*}{\partial y_1^*} \frac{\partial y_1^*}{\partial x^*} \right\} \\
& \tag{V.5}
\end{aligned}$$

$$u^* = \left(\frac{D}{Y_1}\right) \frac{\partial \psi^*}{\partial y_1^*}; \quad v^* = -\left(\frac{\partial \psi^*}{\partial x^*} - \frac{y_1^*}{\delta} \frac{\partial \delta}{\partial x^*} \frac{\partial \psi^*}{\partial y_1^*}\right) \quad (V.6)$$

$$\begin{aligned} \frac{\partial T_s^*}{\partial t^*} + \left(\frac{y_s^* - 1}{1 - \delta}\right) \frac{\partial \delta}{\partial t^*} \frac{\partial T_s^*}{\partial y_s^*} &= \frac{\alpha_s}{\alpha_1} \left[\left(\frac{D}{L}\right)^2 \frac{\partial^2 T_s^*}{\partial x^{*2}} + \left(\frac{D}{Y_0 - Y_1}\right)^2 \frac{\partial^2 T_s^*}{\partial y_s^{*2}} \right. \\ &+ \left(\frac{D}{L}\right)^2 \left\{ \left(\frac{y_s^* - 1}{1 - \delta}\right) \frac{\partial \delta}{\partial x^*} \frac{\partial^2 T_s^*}{\partial x^* \partial y_s^*} + \left(\frac{y_s^* - 1}{1 - \delta}\right) \frac{\partial^2 \delta}{\partial x^{*2}} \frac{\partial T_s^*}{\partial y_s^*} \right. \\ &+ \left. \left. \frac{y_s^* - 1}{(1 - \delta)^2} \left(\frac{\partial \delta}{\partial x^*}\right)^2 \frac{\partial T_s^*}{\partial y_s^*} + \frac{1}{(1 - \delta)} \frac{\partial \delta}{\partial x^*} \frac{\partial T_s^*}{\partial y_s^*} \frac{\partial y_s^*}{\partial x^*} \right\} \right] \quad (V.7) \end{aligned}$$

$$\frac{\partial T_m^*}{\partial t^*} = \frac{\alpha_m}{\alpha_1} \left[\left(\frac{D}{L}\right)^2 \frac{\partial^2 T_m^*}{\partial x^{*2}} + \left(\frac{D}{D - Y_0}\right)^2 \frac{\partial^2 T_m^*}{\partial y_m^{*2}} \right] \quad (V.8)$$

The Eqs(V.3)-(V.8) are quite complex and difficult to solve even with a numerical scheme as the convergence of the iterative scheme is quite likely to be affected. In the actual formulation it has been assumed that the interface remains stationary for the period in which heat is transferred across it. During this period, the equations describing the momentum and energy of the melt and the energy equations of the solid and mold are solved assuming pseudo-steady state as discussed at great length by Sparrow, Patankar and Ramadhyani (1977). Because of this assumption, the term containing $\partial \delta / \partial t^*$ in the LHS of Eqs (V.3), (V.4) and (V.7) can be neglected. Further, it has also been assumed that the thickness of the melt region δ varies

slowly with x^* so that the terms involving $\partial\delta/\partial x^*$ and $\partial^2\delta/\partial x^{*2}$ appearing in the RHS of Eqs.(V.3) to (V.7) are neglected. Sparrow, Patankar and Ramachyani (1977) have discussed that in the case of two dimensional solidification, this assumption is quite valid as a first approximation in most cases of phase change problems with natural convection in the melt.

Because of these assumptions Eqs.(V.3) - (V.8) are simplified to Eqs. (4.2.15) to (4.2.20) given in Chapter 4.

APPENDIX VI

SECOND UPWIND DIFFERENCING METHOD

The vorticity equation is written as,

$$\begin{aligned} \frac{\partial \omega^*}{\partial t^*} + u^* \frac{\partial \omega^*}{\partial x^*} + v^* \left(\frac{D}{Y_1} \right) \frac{\partial \omega^*}{\partial y_1^*} = - \left(\frac{D}{L} \right) \left(\frac{D}{Y_1} \right) \left(\frac{D}{Y_0} \right)^3 Ra Pr \frac{\partial T_1^*}{\partial y_1^*} \\ + \left(\frac{D}{L} \right)^2 Pr \frac{\partial^2 \omega^*}{\partial x^{*2}} + \left(\frac{D}{Y_1} \right)^2 Pr \frac{\partial^2 \omega^*}{\partial y_1^{*2}} \end{aligned} \quad (VI.1)$$

The second upwind differencing scheme is used to write the convective terms appearing in LHS of Eqn.(VI.1) in finite-difference form. Thus, for example, $u^* \frac{\partial \omega^*}{\partial x^*}$ is written as,

$$u^* \frac{\partial \omega^*}{\partial x^*} = \frac{u_R^* \omega_R^* - u_L^* \omega_L^*}{\Delta x^*} \quad (VI.2)$$

where $u_R^* = \frac{1}{2} (u_{i+1}^* + u_i^*) \quad (VI.3)$

$$u_L^* = \frac{1}{2} (u_i^* + u_{i-1}^*) \quad (VI.4)$$

and

$$\omega_R^* = \omega_i^*, \quad \text{for } u_R^* > 0 \quad (VI.5)$$

$$\omega_R^* = \omega_{i+1}^*, \quad \text{for } u_R^* < 0 \quad (VI.6)$$

$$\omega_L^* = \omega_{i-1}^*, \quad \text{for } u_L^* > 0 \quad (VI.7)$$

$$\omega_L^* = \omega_i^*, \quad \text{for } u_L^* < 0 \quad (VI.8)$$

APPENDIX VII

ADI ALGORITHM FOR VORTICITY EQUATION

The vorticity equation is written as

$$\begin{aligned} \frac{\partial \omega^*}{\partial t^*} + u^* \frac{\partial \omega^*}{\partial x^*} + v^* \left(\frac{D}{Y^*}\right) \frac{\partial \omega^*}{\partial y_1^*} = - \left(\frac{D}{L}\right) \left(\frac{D}{Y^*}\right) \left(\frac{D}{Y_0}\right)^3 Ra Pr \frac{\partial T_1^*}{\partial y_1^*} \\ + \left(\frac{D}{L}\right)^2 Pr \frac{\partial^2 \omega^*}{\partial x^{*2}} + \left(\frac{D}{Y^*}\right)^2 Pr \frac{\partial^2 \omega^*}{\partial y_1^{*2}} \quad (VII.1) \end{aligned}$$

In the first half of the time step, Eqn.(VII.1) is written as,

$$\begin{aligned} \frac{\omega_{i,j,2}^* - \omega_{i,j,1}^*}{\Delta t^*/2} = - \left(\frac{D}{L}\right) \left(\frac{D}{Y^*}\right) \left(\frac{D}{Y_0}\right)^3 Ra Pr \frac{T_{1,i,j+1,2}^* - T_{1,i,j-1,2}^*}{2(\Delta y^*)} \\ + \left(\frac{D}{L}\right)^2 Pr \left(\frac{\omega_{i-1,j,1}^* - 2\omega_{i,j,1}^* + \omega_{i+1,j,1}^*}{(\Delta x^*)^2} \right) \\ + \left(\frac{D}{Y^*}\right)^2 Pr \left(\frac{\omega_{i,j-1,2}^* - 2\omega_{i,j,2}^* + \omega_{i,j+1,2}^*}{(\Delta y^*)^2} \right) \\ - \frac{(u_{i+1,j,1}^* \omega_{i+1,j,1}^* - u_{i-1,j,1}^* \omega_{i-1,j,1}^*)}{2(\Delta x^*)} \\ - \left(\frac{D}{Y^*}\right) \left(\frac{v_{i,j+1,1}^* \omega_{i,j+1,2}^* - v_{i,j-1,1}^* \omega_{i,j-1,2}^*}{2(\Delta y^*)} \right) \quad (VII.2) \end{aligned}$$

This can be simplified to,

$$\begin{aligned} - \omega_{i,j-1,2}^* (E1 + E2) + \omega_{i,j,2}^* (1+E3) - \omega_{i,j+1,2}^* (E1-E4) \\ = \omega_{i-1,j,1}^* (E5+E6) + \omega_{i,j,1}^* (1-E7) + \omega_{i+1,j,1}^* (E5 - E8) \\ + E9 \quad (VII.3) \end{aligned}$$

$$\text{where } E1 = \frac{Pr}{2} \left(\frac{\Delta t^*}{\Delta y^*} \right) \left(\frac{D}{Y_1} \right)^2$$

$$E2 = \frac{v_{i,j-1,1}^*}{4} \left(\frac{\Delta t^*}{\Delta y^*} \right) \left(\frac{D}{Y_1} \right)$$

$$E3 = 2E1$$

$$E4 = \left(\frac{v_{i,j+1,1}^*}{4} \right) \left(\frac{\Delta t^*}{\Delta y^*} \right) \left(\frac{D}{Y_1} \right)$$

$$E5 = \left(\frac{Pr}{2} \right) \left(\frac{\Delta t^*}{\Delta x^*} \right) \left(\frac{D}{L} \right)^2$$

$$E6 = \left(\frac{u_{i-1,j,1}^*}{4} \right) \left(\frac{\Delta t^*}{\Delta x^*} \right)$$

$$E7 = 2E5$$

$$E8 = \left(\frac{u_{i+1,j,1}^*}{4} \right) \left(\frac{\Delta t^*}{\Delta x^*} \right)$$

$$E9 = -\left(\frac{D}{L} \right) \left(\frac{D}{Y_1} \right) \left(\frac{D}{Y_0} \right)^3 \left(\frac{Ra \cdot Pr}{4} \right) \left(\frac{\Delta t^*}{\Delta y^*} \right) (T_{1,i,j+1,2}^* - T_{1,i,j-1,2}^*)$$

Similarly for the second half of the time step, Eqn.(VII.1) can be simplified to:

$$\begin{aligned} & -\omega_{i-1,j,3}^* (E5+E6) + \omega_{i,j,3}^* (1+E7) - \omega_{i+1,j,3}^* (E5-E8) \\ & = \omega_{i,j-1,2}^* (E1+E2) + \omega_{i,j,2}^* (1-E3) + \omega_{i,j+1,2}^* (E1-E4) + E10 \end{aligned}$$

(VII.4)

$$\text{where } E10 = -\left(\frac{D}{L} \right) \left(\frac{D}{Y_1} \right) \left(\frac{D}{Y_0} \right)^3 \left(\frac{Ra \cdot Pr}{4} \right) \left(\frac{\Delta t^*}{\Delta y^*} \right) (T_{1,i,j+1,3}^* - T_{1,i,j-1,3}^*)$$

The subscripts 1,2,3 appearing in Eqns.(VII.2) - (VII.4) are the variables at the beginning, first half and end of the time step, respectively.

APPENDIX VIIIPROPERTIES OF PARAFFIN WAX

From Bennett (1959) and Nelson (1958), the following properties are taken:

$$\text{Specific heat } C_p = 2.29 \times 10^3 \text{ J/Kg } ^\circ\text{K}$$

$$\text{Density } \rho = 7.8 \times 10^2 \text{ Kg/m}^3$$

$$\text{Kinematic viscosity } \nu = 3.1 \times 10^{-6} \text{ m}^2/\text{s}$$

$$\text{Latent heat } L_q = 222 \text{ KJ/Kg}$$

$$\text{Thermal conductivity } k_1 = 3.8 \times 10^{-3} \text{ J/s m } ^\circ\text{K}$$

$$\text{Thermal diffusivity } \alpha_1 = 2.0 \times 10^{-6} \text{ m}^2/\text{sec}$$

$$\begin{aligned} \text{Coefficient of cubical} \\ \text{expansion } \beta &= 1.15 \times 10^{-5} \text{ } ^\circ\text{K}^{-1} \end{aligned}$$